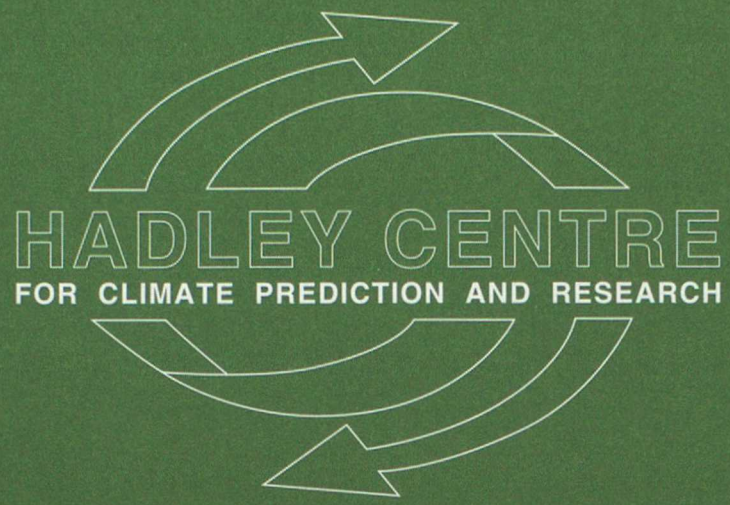

Palaeoclimate Modelling Intercomparison : UKMO GCM simulations for 6kBP and 21kBP

by

C D Hewitt and J F B Mitchell

CRTN 72

July 1996

CLIMATE
RESEARCH
TECHNICAL
NOTE

Hadley Centre
Meteorological Office
London Road
Bracknell
Berkshire RG12 2SY

CLIMATE RESEARCH TECHNICAL NOTE NO. 72

Palaeoclimate Modelling Intercomparison : UKMO GCM simulations for 6kBP and 21kBP

by

C. D. Hewitt and J.F.B. Mitchell

Hadley Centre for Climate Prediction and Research,
Meteorological Office,
London Road,
Bracknell,
Berkshire RG12 2SY
United Kingdom.

NOTE: This paper has not been published. Permission to quote from it should be obtained from the director of the Hadley Centre.

Final Report for the CEC Paleoclimate Modelling Intercomparison contract EV5V-CT94-0457

Contribution of the U.K. Meteorological Office

C. D. Hewitt and J.F.B. Mitchell

Hadley Centre for Climate Prediction and Research,
Meteorological Office, Bracknell, United Kingdom.

Contents **Page**

1. Introduction 2

2. GCM simulations of the climate of 6kBP : mean changes and inter-decadal variability 4

3. Simulation of the climate of the Last Glacial Maximum at 21kBP using the UKMO coupled atmosphere - mixed layer ocean model 35

Chapter 1

Introduction

C. D. Hewitt

This report describes research carried out at the Hadley Centre in the U.K. Meteorological Office under CEC contract EV5V-CT94-0457 on paleoclimate modelling intercomparison. The contract is the European contribution to the Paleoclimate Modelling Intercomparison Project (PMIP), an international project which is coordinating modelling and data reconstruction efforts on two specific snapshots - 6,000 years before present (6kBP) during the Mid-Holocene and the last glacial maximum at 21kBP. The PMIP project involves model-model and model-data intercomparison. Here, we report on experiments carried out using the U.K. Meteorological Office's (UKMO) climate model.

In chapter 2 we describe results from the UKMO general circulation model (GCM) simulation for 6kBP. Our multi-decadal simulation allows us to study inter-decadal variability and to asses the suitability of the PMIP recommended 10 year averaging period. We also describe the mean changes in climate simulated at 6kBP, discussing seasonal temperature changes, changes in hydrological cycle, and cloud and cloud radiative forcing. The Northern hemisphere winter storm tracks were also analysed, but there were no majors changes simulated at 6kBP. In section 4 of chapter 2 a brief model-data comparison is made. Elsewhere in this report Lund University describe a biome model used as a diagnostic tool to compare model results from the four GCMs used in this contract.

In chapter 3 we describe results from the UKMO atmosphere - mixed layer ocean GCM simulation for 21kBP. The sea surface temperature (SST) and sea-ice extents are compared to the only global palaeoclimatic reconstruction available, that of the CLIMAP project. This reconstruction is the subject of considerable debate, but it still remains the best available dataset - the main regions of uncertainty are mentioned in the text. A model-model comparison of the four GCM's climate sensitivity, as measured by changes in surface air temperature, is made using experiments with CLIMAP SSTs and computed SSTs.

Chapter 2

GCM simulations of the climate of 6kBP : mean changes and inter-decadal variability.

C.D. Hewitt and J.F.B. Mitchell.

Hadley Centre for Climate Prediction and Research,

Meteorological Office, Bracknell, United Kingdom.

Accepted for publication by *Journal of Climate*.

Abstract

A simulation of the climate for 6kBP, using the Hadley Centre's atmospheric GCM with prescribed SSTs is described. The control simulation successfully reproduces the large-scale features of the present day climate, and has realistic atmospheric inter-annual variability. The anomaly simulation for 6kBP produces a climate with an enhanced Northern hemisphere seasonal cycle, and in particular a strengthened African-Asian summer monsoon. Integrated over the full annual cycle the land surface of the southern tropics dries while the northern tropics get wetter, and the high northern latitudes also dry. The model simulates large regional inter-decadal differences in the response at 6kBP highlighting the need to allow for and account for variability on long, i.e. at least decadal, time-scales. We describe the consequences of part of the experimental design we have employed, whereby the SSTs for the 6kBP simulation are the same as in the control as recommended by the Paleoclimate Modelling Intercomparison Project (PMIP), in particular the potential importance of ocean and sea-ice feedbacks.

1. Introduction

General circulation models (GCMs) are being used to predict how the earth's climate may respond to anthropogenic activities, in particular to the large increase in industrial emissions of greenhouse gases that has taken place since the 18th Century (for example, Houghton *et al.* 1990, 1992). These models may reproduce the present day climate, but there is no guarantee that they are capable of realistically simulating a perturbed climate, as for example that due to increasing greenhouse gas concentrations. Past climates may provide a useful test for GCMs by enabling a comparison between model simulations and palaeoclimatic reconstructions, and thereby providing a means of assessing their capability to simulate changes of climate.

The Mid-Holocene is a period that has numerous well-dated proxy records indicating a climate that differed, at least regionally and seasonally, from today's. Variations in the earth's orbital parameters, as determined by Milankovitch theory (Berger 1978), lead to changes in the seasonal and latitudinal distribution of incoming solar radiation at the top of the earth's atmosphere (insolation), and the differences between the Mid-Holocene climate and the present climate are believed to be largely attributable to these insolation changes. The geologic record indicates that the the Mid-Holocene ice sheet

distributions, natural aerosol concentrations, topographic heights, and continental positions were similar to those of the present (see, for example, COHMAP 1988), as was the global mean annual sea surface temperature (SST).

Previous simulations for the Middle Holocene have been completed for both 9000 years before present (9kBP) and 6kBP (see review by Mitchell 1993). Early simulations used prescribed present day SSTs (Kutzbach and Otto-Bliesner 1982; Kutzbach and Guetter 1986). Later studies used atmospheric models coupled to a simple mixed layer ocean (Kutzbach and Gallimore 1988; Mitchell *et al.* 1988) which allow ocean and sea-ice feedbacks to be represented. Other studies have demonstrated the potential importance of vegetation albedo feedbacks (Street-Perrott *et al.* 1990; Foley *et al.* 1994).

The task of simulating palaeoclimates with GCMs and comparing the model simulated climates with climate reconstructions from the geologic record is the aim of the Paleoclimate Modelling Intercomparison Project (PMIP, Joussaume and Taylor 1995). PMIP is coordinating modelling and data reconstruction efforts on two time periods - 6kBP during the Mid-Holocene, which is the subject of this paper, and the last glacial maximum at 21kBP. The GCM simulations will have the same experimental design, boundary conditions and forcing for each time period. It should be noted that one of the specifications of the PMIP programme is that the modelling groups involved should perform the experiments with the versions of their GCMs that are being used to predict the future climate.

The period 6kBP was chosen as it is believed the changes in boundary conditions were relatively small (Kutzbach and Street Perrott 1985). Changes in orbital forcing and reductions in CO_2 concentrations are believed to have been the principal contributors to the differences in forcing. The major continental ice sheets were similar to present. Also, there has been a concerted effort to produce a global palaeoclimatic data base for the period (for example, COHMAP 1988) allowing a good opportunity for model data comparisons.

Numerical model experiments are restricted in their design by the availability of computer power - this limits the horizontal and vertical resolution of the model, the processes and components of the climate system that are represented, and the length of the model integration. In the first phase of the PMIP 6kBP experiments, it was decided to prescribe sea surface temperatures at present day values in order to avoid the computer time required to bring an ocean model to equilibrium. The reconstructions of sea temperatures for 6kBP suggest that changes from present were patchy and relatively small (Ruddiman and Mix 1993; Morley and Dworetzky 1993), and as a result there is no universally accepted SST and sea-ice data set for 6kBP. Changing orbital parameters in models with a simple interactive ocean produces generally small changes in temperature,

except near the northern sea-ice margins (Kutzbach and Gallimore 1988; Mitchell *et al* 1988). Furthermore, the change in CO_2 concentrations used in the PMIP experiments may be unrealistically large as discussed later. The use of prescribed sea temperatures means that it is effectively the atmospheric components of climate models which are being compared. This may help with the comparison between different models, as only one component is allowed to vary, but the climate sensitivity to lowering CO_2 and changing insolation may be underestimated which would reduce the usefulness of the comparison with palaeodata.

The atmospheric model used in this study is of a higher horizontal resolution than used in most studies to date. It is important to include the diurnal and annual cycles and to have a simulation long enough to allow statistics to be formed that can account for inter-annual variability. Initial GCM palaeoclimate experiments were limited to simulating less than one season, but, with the increases in computer power, experiments are now carried out to simulate decades with diurnal and annual cycles being represented. The PMIP experimental design recommends that simulations should be of 10 years to account for inter-annual variability. The multi-decadal simulations described in this paper provide a longer time-series for the study of atmospheric inter-annual and inter-decadal variability, and the suitability of the recommended 10-year averaging period is assessed.

The aim of this paper is to describe the model's response to the 6kBP insolation forcing, highlighting the necessity to take into account the model's atmospheric variability. The following section outlines the GCM used in this study and the design of the experiments. Section 3 describes the results of the experiments and emphasises some points that need to be taken into consideration when comparing GCM simulations to palaeoclimatic data :-

- does the model have a realistic simulation of the present day climate when compared to the observed climate (§3.1)?
- what features of the response simulated at 6kBP are consistent from decade to decade, and statistically significant (§3.2 and §3.3)?
- and what are the potential shortcomings of the experimental design, in particular, what further feedbacks might be important (§3.4)?

The GCM response is compared with palaeoclimatic data reconstructions in section 4.

2. The atmospheric model and experimental design

a. The model

The GCM (HADAM2) is the atmospheric component of the coupled atmosphere/ocean model (HADCM2) used by the Hadley Centre at the United Kingdom Meteorological Office (UKMO). This coupled model has been used to predict the climate response to a gradual increase in greenhouse gases and sulphate aerosols in to the next century (Mitchell *et al.* 1995).

The model is a hydrostatic primitive equation grid-point model with a horizontal resolution of 2.5° by 3.75° and 19 levels on hybrid vertical coordinates (Simmons and Burridge 1981), the bottom level being at about 50 metres, and the top level at about 0.5 mb. The hybrid coordinate system has terrain-following σ coordinates (σ = pressure/surface pressure) in the bottom four layers, pressure coordinates for the top three layers, and a linear combination for the intermediate 12 layers. The model has a 360 day year and uses a fourth-order split-explicit integration scheme (Cullen and Davies 1991) with a half hour time step.

The model has an annual and diurnal cycle for insolation and the shortwave and longwave radiative fluxes depend on temperature, water vapour, clouds, CO_2 and O_3. The shortwave scheme uses four spectral bands as defined in Slingo (1989), and the longwave scheme uses six spectral bands as described in Slingo and Wilderspin (1986). Interactive cloud optical properties are computed from the derived cloud water and ice contents (Slingo 1989).

The penetrative convection scheme (Gregory and Rowntree 1990) includes an explicit downdraught (Gregory and Allen 1991), and the calculation of the convective mass flux in the updraught is based on parcel theory modified by entrainment and detrainment. Convective cloud amounts are calculated from total cloud condensate. The large scale cloud and precipitation scheme is formulated in terms of a total water variable q_T and liquid water temperature T_L (Smith 1990).

A parameterization of sub-grid scale gravity wave drag based on Palmer *et al* (1986) is included. The land surface albedo is a function of snow depth, and vegetation and soil type. As the surface temperature increases above -2°C the albedo of snow reduces linearly, until melting point is reached, to take account of the snow ageing. A similar method is used for the albedo of sea-ice. The fluxes of heat, moisture and momentum from the surface are dependent on stability, based on Monin-Obukhov similarity theory. The atmospheric boundary layer is allowed to occupy up to five model layers, depending on the

position of the lowest inversion. A four layer soil model is used in the land surface temperature scheme. The hydrology scheme allows for surface runoff and soil drainage based on a single moist layer - a vegetation canopy is represented to allow for canopy evaporation and interception, and evaporation from the land surface is restricted by a prescribed stomatal resistance (Warrilow *et al.* 1986). The land surface characteristics are a function of soil and vegetation types which are prescribed from climatology.

This atmospheric model and its performance when coupled to a dynamical ocean model are described in more detail in Johns *et al* (1996).

b. Experimental design

A 51 year control simulation for the present day climate and 31 year anomaly simulation for the climate of 6kBP were performed. The first year of each run was ignored to allow the model to come to quasi-equilibrium (a reasonable time-scale since the SSTs and sea-ice are fixed), and multi-annual means were constructed covering the final 50 and 30 years of the two integrations, respectively. The studies on inter-decadal variability in the palaeoclimate simulation were made by splitting the 30 year period in to three consecutive 10 year meaning periods. Differences between the simulated climates were constructed as anomaly minus control (past climate minus present climate).

The anomaly run differs from the control run in only two ways :-

1) CO_2 was reduced by a multiplying factor of 0.81 from the control run concentration giving a concentration of about 262 ppmv. This factor was chosen so that all of the PMIP GCM experiments would have the same change in radiative forcing at the tropopause, ΔF, as detailed in the IPCC report (Houghton *et al.* 1990):

$$\Delta F = 6.3 \ln C/C_o$$

where $C_o = 323$ ppmv in the control simulation, giving a radiative forcing of -1.3 W m^{-2} on reducing CO_2. However, if one allows for the thermal adjustment of the stratosphere (Schneider 1975), the actual forcing is closer to -1.1 W m^{-2} . The full effect of the change in CO_2 will not be realised because the SSTs are prescribed and hence can not respond. It is also worth noting here that the current climate and the modern vegetation have most likely not come into equilibrium with the recent rapid rise in CO_2 , and so this decrease at 6kBP in CO_2 in the model experiments may be larger than that seen over the period of the data reconstructions.

2) The insolation forcing was changed by modifying the orbital parameters (Table 1) as derived from Berger (1978), fixing the Vernal equinox at noon on March 21st.

All of the other boundary conditions are unchanged. This keeps the experimental design relatively simple which aids the intercomparison between different model simulations. Reconstructions of other boundary conditions are not global, and most of the estimated changes lie within the error of reconstructed data. Hence, the sea surface temperature and sea-ice boundaries are specified as present day seasonally varying climatological values.

A further experiment was performed with the change in insolation forcing only, to isolate the effect of the orbital forcing from the CO_2 forcing. This experiment was run for 11 years, with data analysed from the final 10 years of the integration.

3. Results

a. Control simulation (present day climate)

A necessary condition for a reliable GCM prediction of regional climate change is that the control simulation should be realistic - if features are positioned incorrectly, then any simulated shifts in these features may also be in the wrong position. Here the control simulation is assessed by comparison with climatological data. Climatological estimates are subject to error due, for example, to inadequate temporal or spatial sampling, observational error, and different periods of observation, and so there may be substantial differences between climatologies, particularly in data sparse regions.

1) MEAN SEA LEVEL PRESSURE

The model successfully reproduces the main features of the atmospheric low-level circulation (see for example, Schutz and Gates 1971), but there are errors in detail. In December-January-February (DJF, figure 1a) the Icelandic low is not deep enough and the associated trough does not extend far enough east-northeastwards due to excessive pressure over the Arctic. The Azores high is not intense enough over the eastern Atlantic and the ridge extends too far westwards across into the United States. This results in the gradient being too slack across the mid-latitude Atlantic and northern Eurasia. The Aleutian low is displaced slightly eastwards and, in the Southern hemisphere, the circumpolar trough is deeper than observed leading to excessively zonal surface winds.

In June-July-August (JJA, figure 1b) the model produces anomalously low pressure over much of Asia, and the Asian monsoon trough extends too far into the West Pacific and the Bay of Bengal. The pressure is too high over Africa which prevents the African monsoon trough from extending far enough over the Sahara/Sahel region. In the Southern hemisphere the pressure is too high in the sub-tropics , and too low in mid-latitudes, again leading to excessively zonal low-level winds. The low-level flow is generally well reproduced over Europe and North America.

2) TEMPERATURE

The surface temperature of the control simulation (not shown) is within one or two degrees of observational climatologies (for example, Legates and Willmott 1990a) over most of the globe, but there are some regions where the differences exceed 4°C. The largest discrepancies are in the regions of high orography such as the Tibetan plateau, the Andes, Greenland, and Antarctica. Legates and Willmott (1990a) note that no climatology perfectly represents the true air temperature field and other climatologies (for example the RAND climatology, Schutz and Gates 1971, 1972) differ greatly in these mountainous regions. In the winter, much of northern Asia is also too cold in the model, consistent with the lack of westerly flow in to this region discussed previously.

3) PRECIPITATION

Precipitation is highly variable both spatially and temporally, and it is difficult to obtain homogeneous measurements globally, especially over the oceans. Precipitation is heaviest along the Inter-Tropical Convergence Zone (ITCZ), over warm oceanic regions and in monsoonal areas (see for example, Legates and Willmott 1990b). Arid regions tend to occur in regions of descending air, and in polar regions, where the cold air also reduces the capacity of the atmosphere to hold moisture.

The GCM reproduces the main synoptic scale precipitation patterns (figures 2a and 2b) including those associated with the mid-latitude storm tracks and the continental monsoons. In JJA, the South China Sea and the Bay of Bengal receive too much precipitation, and the western Sahel receives too little. These discrepancies are largely a consequence of the circulation problems discussed above - the trough extending over the western Pacific, the monsoon low too deep and too far south over the Bay of Bengal, and a weaker than observed monsoonal trough over northern Africa.

4) INTER-ANNUAL VARIABILITY

We have described aspects of the mean state of the atmosphere, but also of interest is how well the model reproduces the climate's internal year to year variability. The variability of the model's surface air temperature is compared here to observations covering the period 1950 - 1990 (derived from data held in a combined land surface and sea surface temperature data bank - Parker *et al.* 1994). Standard deviations have been computed for seasonal (DJF and JJA) and annual mean surface air temperature in order to study atmospheric variability. It should be noted that the inter-annual variability of air temperature over the oceans in this model will be lower than that in the observations since the SSTs are prescribed and do not vary from year to year; however, when this model is coupled to an ocean GCM much of the observed variability over the oceans is simulated (Tett *et al.* 1995).

The model simulates the observed inter-annual variability of annual mean temperature reasonably well (not shown), although in the tropics the model tends to underestimate the variability, while in the extra-tropics it tends to be overestimated, in particular over the eastern United States, Europe and south-east Asia as found in the study by Tett *et al* (1995). A 500-year integration using a fixed SST configuration of the GFDL model produced similar variability (Manabe and Stouffer 1996).

The observations indicate that the variability is greatest in the winter hemispheres, particularly in the Northern hemisphere high-latitudes, although unfortunately the Southern hemisphere high latitudes are data sparse, especially in winter. The model simulates these seasonal changes to the variability, particularly the high standard deviations in the Northern hemisphere in DJF (compare figures 3a and 3b), and even manages to capture some of the observed variability over the North Atlantic in DJF. In JJA however, the variability is far too high over large regions of the Northern hemisphere, by more than a factor of two (compare figures 3c and 3d). Delworth and Manabe (1989) found that the variability of summer surface air temperature is strongly influenced by the variability of soil moisture. Soil moisture is highly variable in the model, especially over the eastern United States, Europe and western Asia (figure 4) in JJA, the regions that portray unrealistically high standard deviations of surface air temperature. The radiative effects of clouds also has an influence on the surface temperature, and cloud cover over the south-eastern United States, Europe and south-eastern Asia is highly variable in the model in JJA as well (not shown). Unfortunately, there are not yet any sufficiently reliable global data sets of soil moisture and cloud cover to validate the model against.

b. Mid-Holocene experiment (6kBP)

Since models, like the real atmosphere, generate substantial internal variability, one must examine the possibility that some of the differences between the anomaly and control simulations have arisen by chance. A two-tailed Student's *t*-test has been performed on the individual seasonal (for surface air temperature) and annual (for soil moisture content) mean model data to deduce whether any increases or decreases of the long-term mean changes can be described as significant at and above the 95% level of confidence. The significance levels should only be regarded as approximate since meteorological variables are correlated in time and space, and the *t*-test will tend to overestimate the significance (Zwiers and von Storch 1995).

1) ZONAL MEAN CHANGES

The effect of changing the earth's orbital parameters as detailed in Table 1 is to cause a latitudinal and seasonal redistribution of the incoming solar radiation at the top of the earth's atmosphere (figure 5a) - the latitudinal changes are caused by the increased tilt of the earth's axis (obliquity), and the seasonal redistribution results from the precessional shifting of the date of perihelion from January at present to September at 6kBP. The seasonal cycle is enhanced in the Northern hemisphere and reduced in the Southern hemisphere.

The incoming short-wave radiation is modified by the earth's atmosphere, by reflection from clouds and atmospheric absorption and scattering, so the change in shortwave flux at the top of the atmosphere is reduced, by roughly a factor of two, at the earth's surface (figure 5b). The short-wave radiation changes drive the surface temperature response shown in figure 5c (over land only). Since the sea surface temperature is kept the same in the anomaly experiment the main changes to the surface air temperature are over land and sea-ice. The Northern hemisphere continents generally warm throughout the summer and cool from October through to May (figure 5c). The Southern hemisphere continents warm later, in phase with the insolation forcing.

The temperature response is generally consistent with the sign of the insolation forcing, although there are three areas of exception - a cooling throughout July-August-September at about 15°N (also reported in the 9kBP simulation of Mitchell *et al.* 1988) which we attribute to a strengthening of the summer monsoon and a resulting increase in cloud (figure 5d), a warming in February-March at 18°S which we attribute to a weakening of the winter monsoons and a subsequent decrease in cloud (figure 5d), and a

warming in January located around 80°N which we attribute to changes in the low level circulation. The magnitude of the temperature change is not as consistent with the insolation changes - the Southern hemisphere temperature response is smaller than the Northern hemisphere response due in part to the greater influence of the oceans where the surface temperature is prescribed.

2) SEASONAL TEMPERATURE RESPONSE

In JJA there is a warming over much of the continental land-masses (figure 6a), consistent with previous GCM studies (see for example, Kutzbach and Guetter 1986; Mitchell 1993; Liao 1991; Hall and Valdes 1996). The warming exceeds 1°C over large parts of North America, Greenland, North Africa, Eastern Europe and Asia with a maximum warming exceeding 2°C over eastern Asia, and is generally significant at the 99% confidence level (figure 6b. Note that the statistically significant 1.5m temperature changes evident over the tropical Pacific Ocean arise as a result of small temperature changes occurring in a region of extremely low variability). The warming is smaller than the 3-4°C maximum over Asia reported by Mitchell (1993) and Liao (1991). There are two factors which could contribute to this discrepancy. First, these two studies, and other palaeoclimate simulations, are for experiments of the order of one decade, and the multi-decadal simulation described here tends to smooth out the maxima and minima. It will be shown below that analysis of decadal means does lead to larger changes locally than with longer term means, as might be expected. Second, the earlier studies used a different cloud parameterization which may give a stronger cloud feedback over land.

Another significant feature of the temperature response in JJA is the cooling throughout the monsoon regions of Africa and India. This is due to an increase in cloud cover (figure 6c), and an associated increase in precipitation (figure 6d) which leads to an increase in ground wetness and evaporation, and hence an increase in the evaporational cooling. These changes are consistent with a strengthening of the summer monsoon as described in the following section.

The reduced insolation in DJF leads to a cooling over almost all of the land masses, exceeding 2°C throughout a large part of eastern Asia (figure 7a). There is a warming exceeding 0.5°C over the Canadian archipelago, western Greenland and the extreme northeastern region of Asia which are all associated with the advection of warm maritime air (figure 7f) as a consequence of low-level circulation changes. The temperature changes generally are not statistically significant at the 95% confidence level throughout the northern mid- and high-latitudes (figure 7b), as these are regions of high natural variability

(figure 3a).

3) MONSOON RESPONSE

The increase in surface temperature in JJA over the Northern hemisphere continents leads to a reduction of the surface pressure over the continents and a compensatory increase in pressure over the oceanic regions (figure 6e). The increased land-ocean pressure gradient strengthens the low-level convergence and upward motion throughout the African-Asian monsoon region which results in an enhancement of the low-level monsoon winds (figure 6f) - strengthened south-westerly winds over West Africa, greater penetration of the monsoon over East Africa, and enhanced westerly flow in to northern India. These stronger moisture-laden winds, combined with enhanced ascent, produce a band of increased precipitation (figure 6d) stretching from West Africa, across the Sahel, East Africa, southern Arabia, India and the Himalayan region over to China. There is also evidence from the precipitation changes of a northward migration of the ITCZ across the Sahel and southern India, and the monsoon precipitation influencing a wider area, consistent with previous GCM results (see for example, Kutzbach and Guetter 1986; Mitchell 1993; Liao 1991).

In DJF, however, the large-scale cooling of the continents leads to an increase in the mean sea level pressure over Asia, Africa, Australasia and South America (figure 7e). The Southern hemisphere monsoons show signs of weakening with less precipitation over the Amazon Basin, Central Africa and Indonesia (figure 7d) and an associated decrease in cloud cover in these regions (figure 7c), resulting in regions of reduced cooling or even slight warming.

The strengthened mid-Holocene Northern hemisphere summer monsoon and weakened Southern hemisphere summer monsoon are summarised in table 2. An increase (decrease) in insolation leads to an increase (decrease) in surface air temperature, the changes being larger over land than over the oceans, since the SSTs are fixed, which results in a larger (smaller) land-ocean pressure gradient, and hence a stronger (weaker) Northern (Southern) hemisphere summer monsoon producing wetter (drier) conditions over the continents. However, the insolation forcing may also produce seasonal changes to the SSTs, if they weren't prescribed, which could create important feedbacks affecting the monsoon response.

The total effect of the seasonal hydrologic changes can be summarised by looking at the annual mean changes in the model's soil moisture content (figure 8a), a measure of

the annual mean ground wetness. There is a drying of much of the tropical rain forest region of Africa, southern Africa, northern Asia, the Amazon Basin, the continental interior of North America, Scandinavia and central Europe, although only small areas have changes significant at the 95% level (figure 8b), due to the high variability of surface hydrologic conditions discussed previously. There is a moistening of the Sahel region, East Africa, northern India, Morocco, southern Spain, and the southwest corner of North America, as well as a moistening of much of China, Indonesia, and the northwest and northeast regions of North America, although the changes that are statistically significant are patchy in extent.

Two questions arise from the annual mean changes in soil moisture. First, why do the northern tropics moisten whereas the southern tropics dry out? The increase in insolation occurs in the north during summer when the prevailing low level circulation is convergent and precipitation is high. The enhanced convergence and ascent discussed above occurs in a moist unstable atmosphere and thus is particularly effective in enhancing precipitation (figure 9a). The increase in evaporation is smaller, partly because of local increases in cloud which tend to reduce the radiative energy available for evaporation. This can be seen in the changes in cloud radiative forcing (CRF) at the top of the atmosphere (figure 10a). This is conventionally defined as the outgoing radiative flux minus the clear-sky outgoing radiative flux. However, at 6kBP, there are changes in incoming solar radiation (see figure 5a) which would give a change in CRF as defined here, even if clouds did not change. Hence, in figure 10a, we have normalised the insolation changes at 6kBP, S_{6k} , by the 0kBP radiation S_{0k} (after Liao 1991), i.e., the change in short-wave CRF at the top of the atmosphere at 6kBP is

$$\Delta SCF = SCF_{6k} - (S_{6k} / S_{0k}) \, SCF_{0k}$$

This ensures that the changes in solar CRF are primarily due to changes in cloud. The changes to the long-wave cloud forcing are much smaller, of the order of 1 W m^{-2} . In the northern tropics the CRF is increased (becomes more negative) due to cloud increases, and so there is less radiative energy available for evaporation. Overall, evaporation increases less than precipitation and soil moisture is increased through the summer. In the northern tropics in winter, precipitation is much smaller due to lower temperatures and a less favourable circulation, so the winter reduction in insolation is less effective in reducing precipitation. Evaporation decreases are also small, of similar magnitude to the precipitation reductions, and there are smaller changes in cloud and short-wave cloud forcing (figure 10b). The net decrease in P–E and soil moisture is smaller than in summer, so the annual means of these quantities increase. In the southern tropics, insolation increases in JJA, when the low level circulation is divergent, and hence increases in precipitation are smaller than during the wet season (DJF) when the changes in insolation

are most effective, giving large net reductions in precipitation (figure 9b). This is the reverse of the seasonal changes in the Northern hemisphere - hence the annual mean P, P–E and soil moisture decrease.

Second, why do the high northern latitudes dry whereas the northern tropics become moister? The moisture convergence at low levels is enhanced in the tropics due to the increased land-sea temperature contrast, so precipitation increases faster than evaporation. In the extratropics, the westerly flow which transports moist air over land is, if anything, weakened,especially over Eurasia in summer (figure 6f). In addition, there is a net annual increase in insolation at the top of the atmosphere in high latitudes to drive increases in evaporation (figure 9c. Note that the scale is larger compared to 9a and 9b), whereas, the net insolation in the tropics is reduced . Finally, summer temperature decreases over much of the northern tropics because of increased cloud associated with a stronger monsoon noted above, whereas in high latitudes, temperatures increase. All other things being equal, evaporation will increase with temperature at the expense of sensible heat over a moist surface. Increased temperatures also increase snow melt, but this is compensated for by increases in runoff. These factors combine to produce a net drying in high northern latitudes. A similar contrast between low and high latitudes was noted by Mitchell (1990) in a 9kBP experiment.

The contrast between the response to increased insolation in the tropics and extratropics is consistent with the findings of Lofgren (1995) who investigated the effects of reducing surface albedo. Reducing surface albedo is a similar radiative perturbation to increasing insolation - both primarily increase solar heating at the surface. Lofgren (1995) found that increasing surface heating in the tropics in the summer hemisphere led to increased vertical motion and low level convergence and a marked increase in precipitation. Evaporation also increased, but not as much as precipitation, giving a net increase in soil moisture. In contrast, the increased surface heating in the extratropics produced a direct increase in evaporation, but changes in precipitation were less marked because there was little effect on circulation. (In high latitudes, the Coriolis effect tends to weaken thermally direct driven vertical circulations). As a result, Lofgren (1995) found soil moisture levels drop more rapidly through the summer with reduced surface albedo.

c. Inter-decadal variability of 1.5 metre temperature

Having described the model's multi-decadal mean response at 6kBP we now consider the response at 6kBP simulated in three individual consecutive decades - a decade being the typical length of current GCM simulations for the mid-Holocene. A two-sided

Student's *t*-test has been used to test the statistical significance of changes in surface air temperature for the 10 seasonal means for each decade of the anomaly experiment compared to the 50 seasonal means of the control experiment, and an F-test has been used to test the significance of any change in the variance of surface air temperature over the 30 years of the anomaly compared to the 50 years from the control.

In JJA in all three individual decades, and in the 30 year average, there is a global mean warming at 6kBP of between 0.23 and 0.26°C when compared to the 50 year control simulation (the warming averaged over land points only ranges between 0.69 and 0.77°C). However, on a regional scale there are some large differences between each of the three decades and the 50 year average of the control (figure 11). The greatest variability is seen in the Northern hemisphere in the regions where the control simulation has also been shown to be highly variable. For example, over much of Europe there is a warming of over 1°C in the second and third decades, while in the first decade there is a cooling over much of the U.K. and neighbouring continental Europe (although this is not significant at the 95% confidence level). These changes are mainly due to variations in the cloud cover, with warm events corresponding to a decrease in cloud cover, but variations in the low-level circulation are also important, with, for example, a reduction in surface pressure in the first decade over Scandinavia at 6kBP drawing cold Arctic air into the region. Note also that the magnitude of the warming over Asia in the first decade, exceeding 2°C over large parts of Russia, is comparable to that found in earlier, shorter, GCM integrations (see, for example, Mitchell 1990; Liao 1991).

The climate response of the Southern hemisphere is generally less variable, since it is influenced to a much greater extent by the oceans. The Antarctic winter, however, shows large variability, although most of the temperature changes are not statistically significant at the 95% level, and, again, the observations indicate that the control simulation may be too variable in this region.

It is instructive to consider what one gains by extending the original PMIP specification of 10 year simulations to 50 and 30 years in the control and anomaly respectively. With all the data, 60% of land grid points show a significant change in temperature in JJA at the 95% level of confidence (table 3). If one considers the control and anomaly simulations as a series of consecutive 10 year experiments (5 in the control, 3 in the anomaly)) and average over all 15 possible combinations of control and anomaly decades, the percentage of significant points fall to 39%. Thus, a fourfold increase in computing time increases the number of points with significant change by half. One can also determine the number of points where changes are deemed to be significant using decadal means, but not using the longer simulations - what one might refer to as "false alarms". On average, about 6% of points are deemed significant using decadal means but

not significant with the full data (table 3). Of course, even using the full data there are likely to be some "false alarms" - the above calculation is illustrative rather than definitive.

In DJF the interdecadal variations are of similar magnitude (not shown) with a global mean cooling of between 0.24 and 0.27°C and large differences are evident over Alaska, Greenland and northern Asia, regions where the winter surface circulation patterns vary.

One consequence of this simulated interdecadal variability is that long averaging periods are required to produce an accurate estimate of the model's response at a regional level. It is particularly important to bear this in mind when comparing palaeoclimatic reconstructions with simulated changes. This uncertainty is over and above that due to the use of different models.

There is little change in the standard deviation of the annual mean grid-point values at 6kBP compared to 0kBP (not shown), but there are large changes in the winter mean values in some regions (figure 12a). In DJF the inter-annual variability is reduced at 6kBP over most of northern Asia, Eastern Europe and Scandinavia, and is increased over much of Canada (figure 12a) with significant changes indicated (by the F-test, figure 12b) over Russia and the Canadian archipelago. Reductions in the soil moisture content over Russia (not shown) lead to reduced variability (c.f. section 3.1), and increases in temperature over the Canadian archipelago reduces the snow cover which increases the variability significantly. The changes simulated in JJA are less dramatic (not shown), although there is a significant increase in variability over Russia and eastern Scandinavia.

In general, bigger samples are required to show that changes in variance, rather than mean, are significant (compare the extent of the significant areas in figures 12b and 7b). Longer simulations than those conducted here would be necessary to confirm the changes in variability outlined above, and to elucidate the mechanisms responsible.

The changes that are consistently simulated for all three decades are a warming of the continents, particularly Greenland and the Northern hemisphere extra-tropics including the U.S.A., North Africa, the Middle East and central and eastern Asia, a smaller warming of South America, southern Africa and Australia, and a region of cooling in the tropical monsoon regions. All of these changes are statistically significant for the 30 year mean at the 99% level of confidence (figure 6b), but not necessarily as significant for each individual decade. The response over Antarctica is highly variable.

d. Sensitivity experiment with present day CO_2

The experiment with present day atmospheric CO_2 concentrations and

mid-Holocene insolation (called 6kINS hereafter) allows an investigation in to the effect of the separate forcings to be carried out. Over the annual cycle the nature of the two forcings is different - the solar forcing varies seasonally and latitudinally and has a large amplitude, whereas the CO_2 forcing is small and varies little. This was one of the reasons why Mitchell (1990) concluded that the mid-Holocene was not a good analogue for future greenhouse gas induced climate change. The 6kINS experiment was run for only 11 years with differences relative to the 50 year control (0kBP) experiment. We will not describe regional changes in the 6kINS experiment since the previous section has highlighted the consideration that a 10 year simulation may not be long enough for such a detailed study.

The global annual mean land surface temperature cooled by 0.10 K in the first decade of the 6kBP experiment, compared to the 0kBP experiment, and the 6kINS experiment produced a negligible temperature response (a warming of 0.005 K), implying that the 19% decrease in CO_2 concentrations produced a cooling of 0.1 K. By way of comparison, this model when coupled to a full ocean model (Johns *et al.* 1996) produces a global mean warming of about 3.3°C on doubling CO_2 (Senior, pers. comm.). The change in radiative forcing at the tropopause, ΔF, for $2\times CO_2$ experiments is about 4 W m^{-2} which would imply a cooling of 1.1°C for the -1.3 W m^{-2} forcing due to lowering CO_2 by 19%. An experiment simulating the climate of 6kBP with a 19% reduction to CO_2 concentrations using this coupled model has produced a cooling of about 0.7°C, although this simulation was not long enough for the deep ocean to have reached equilibrium.

The model's (global mean) sensitivity to lowering CO_2 concentrations is therefore, not surprisingly, severely restricted by fixing the SSTs, and the near-surface response over the oceans is obviously unrealistically damped. Experiments modelling the atmospheric response to a doubling of CO_2 are performed with an interactive ocean, and this sensitivity study implies that it would be of great interest for performing palaeoclimatic experiments with altered CO_2 concentrations to include an interactive ocean. However, the response of the 6kINS experiment is qualitatively similar to the 6kBP experiment with the same enhanced seasonal cycle of insolation producing temperature increases over land in JJA and decreases in DJF, which then produces an enhanced summer monsoon (stronger in the 6kINS experiment than in the 6kBP one), and weakened winter monsoon (compare table 4 to table 2).

4. Comparison with palaeoclimatic data

Data output from the GCM is located evenly on a latitude-longitude grid and interpolation between grid-points gives a continuous domain over the whole globe. The interpolation technique used for the data presented in this paper does not take into account sub-gridscale features such as actual topographic heights and local surface characteristics. The geologic data is distributed unevenly at specific sampling sites with a regional picture reconstructed from data that may have recorded local events. With these limitations in mind the following section will attempt to compare model results with palaeoclimatic reconstructions concentrating on surface temperature and effective moisture for Europe, North America and Africa - the regions and atmospheric quantities that have a relative wealth of published data from proxy records. The broad patterns are compared, rather than individual data sites which may not be representative of the surrounding region, and the results of section 3 describing which features are statistically significant and consistent from decade to decade should be borne in mind in this intercomparison. Model results are from the 6kBP and 0kBP experiments and anomalies are for the mid-Holocene climate compared to the present day climate, i.e., 6kBP - 0kBP.

Recall that the effects of changes in sea surface temperature, sea ice and vegetative cover, which are ignored in the model, may have contributed to the reconstructed changes in temperature and precipitation. An otherwise perfect model would not necessarily reproduce all the "observed" changes, and discrepancies between the simulated and reconstructed data cannot necessarily be attributed to errors in the atmospheric model.

a. Temperature

The model produces a warming in summer over most of continental Europe, with a slight cooling over the Mediterranean Sea (figure 6a). This is largely consistent with the reconstructions from pollen data of Huntley and Prentice (1988, 1993) although they indicate that the maximum warming exceeds 4°C, and in particular there is no maxima produced over the Alps in the GCM simulation, even in the decadal means (cf. figure 11). Over eastern North America a reconstruction of July temperatures (Webb *et al.* 1993 from pollen data) indicates a cooling of up to 2°C over Quebec, and a slight warming over the rest of the eastern side of the continent, apart from a slight cooling along the coast and the Great Lakes region. The model, however, produces a significant warming of over 1°C over nearly all of the North American continent, consistent over the three decades (figure 6a).

Huntley and Prentice (1993) also formed a reconstruction of January temperature

anomalies for Europe, showing a warming over Scandinavia and the Baltic States exceeding 2°C, and a cooling elsewhere. The model's response is in agreement with the reconstructed cooling over western, central and northern Europe, but the simulated cooling over Scandinavia and slight warming over Eastern Europe and the eastern Mediterranean region (figure 7a) are in disagreement with the reconstruction, although this response is not statistically significant (cf. figure 7b). Over northeastern U.S.A. and eastern Canada pollen data indicates a warming exceeding 4°C (Webb *et al.* 1993), while the GCM simulates a cooling exceeding 1°C (figure 7a). These model results are qualitatively, but not quantitatively, similar to those from the CCM reported in Webb *et al* (1993) and the UGAMP model (Hall and Valdes 1996). However, these models do not explicitly calculate the extent of sea-ice. The sea-ice feedback may be important in this region and could lead to a high-latitude warming, as found in simulations for 9kBP using mixed-layer ocean models (for example, Mitchell *et al.* 1988).

For the annual mean temperature response the model simulates a cooling of about 0.5°C over the northern half of Europe, and a similar magnitude warming over the southern half (figure 13). These changes are not statistically significant, except for the warming over south-eastern Europe. The reconstruction by Guiot *et al* (1993) using pollen data constrained by lake-level data differs, implying a warming over most of Europe and of about 2°C over Finland, the Baltic states, central Europe and the former Yugoslavia, which does not agree with the model results.

b. Precipitation minus evaporation (effective moisture)

Analysis of the change in the level of lakes provides information on hydrological changes and can be compared to model simulated changes in precipitation minus evaporation. The largest changes in this 'effective moisture' simulated by the model are seen in the Tropics and over the Pacific Ocean (figure 14).

Street-Perrott and Perrott (1993) describe Holocene climatic reconstructions for Africa using pollen and lake-level data, extracted from the Oxford lake-level data bank. The data indicates higher lake levels and wetter conditions at the data sites in North Africa, the Sahara, and along the East African Rift Valley, with smaller anomalies in the Southern hemisphere. The pollen data indicates drier conditions in South Africa and possibly the southern West African coast. The model's northward shift of the ITCZ and greater penetration of the monsoon precipitation described previously produce a moistening of the Sahel region, and East Africa, a small moistening over the Sahara and North Africa, and a drying of the southern West African coast, all of which are consistent with the geologic

evidence. Southern Africa up to Kenya and the Tanzanian coast experiences a drying, which is not supported by the lake level data, but does not contradict the pollen data. This response is consistently simulated for each of the individual decades as well as for the multi-decadal mean.

In Europe the model simulates wetter conditions over Spain and the Mediterranean region in agreement with lake-level data (Huntley and Prentice 1993; Harrison and Digerfeldt 1993; Harrison *et al.* 1993), and a slight drying of parts of Scandinavia, for example Finland which is consistent with lake-level and pollen data (Huntley and Prentice 1993; Guiot *et al.* 1993). Again, this model response is consistent for each decade and the long-term mean.

Webb *et al* (1993) show drier conditions for the region stretching from New England across the great Lakes to the Missouri River, and also Florida. The model produces a drying of Florida but no clear signal in the belt in the northeast of the United States.

5. Summary and concluding remarks

The GCM produces a realistic simulation of the present day climate, as determined from observational climatological data sets, managing to reproduce the main low-level circulation features, precipitation and temperature patterns. There are shortcomings, however, which are of similar magnitude to other GCM simulations at comparable resolution.

By altering the orbital parameters and reducing the atmospheric carbon dioxide concentrations to values appropriate for the mid-Holocene the model's seasonal cycle is enhanced over the Northern hemisphere continents, which strengthens the African-Asian summer monsoon. There is considerable evidence from proxy records to support this strengthened mid-Holocene summer monsoon climate and the model simulated surface hydrologic quantities are generally consistent with the palaeoclimatic data.

Continental proxy records, mainly from pollen data, indicate that in the mid-Holocene the Boreal summer was generally warmer and the Boreal winter was generally cooler, but there were variations to this overall pattern with regions of summertime cooling and wintertime warming - these anomalies are of the opposite sign to the insolation forcing indicating the importance of circulation changes in influencing the surface temperature response. The model produces a response qualitatively similar to the

data with a general boreal summer warming and boreal winter cooling and also produces regional variations from this overall structure. There are differences between the palaeoclimatic GCM simulation and the palaeoclimatic data, as well as differences with other GCM simulations - it will be interesting, in the PMIP framework, to see if these discrepancies are systematic or model dependent.

Also of interest is the net annual drying of the Northern hemisphere extra-tropics and Southern hemisphere tropics, while the Northern hemisphere tropics get moister. These hydrologic patterns arise from the seasonal nature of the insolation forcing. The Northern hemisphere tropical response is dominated by summer increases in precipitation resulting from increases in insolation and a strengthened monsoon with evaporation changes damped by the larger shortwave cloud forcing. The Southern hemisphere tropical response is dominated by reductions in summer monsoon precipitation resulting from decreases in insolation. The Northern hemisphere extra-tropical response is dominated by increases in evaporation in summer driven by insolation increases.

The GCM manages to realistically simulate much of the observed variability of the present day climate but is too variable over large regions of the Northern hemisphere in summer, and at 6kBP the model simulates some changes to this variability, in particular a reduction of variability over north-western Asia in winter and an increase in summer. The large regional differences seen between the three successive decades indicates that, for this model at least, the PMIP proposed 10 year integration is not long enough to account for significant atmospheric variability, and, not surprisingly, a larger area of the globe is seen to have a statistically significant response for the multi-decadal mean than the individual decades. Care should be taken when comparing 'short' integrations (i.e., of the order of one decade) with palaeoclimatic data - some measure of the model's interannual variability should be taken into account.

The assumption that the sea surface temperatures in the mid-Holocene were similar to present day allows for the simplification to the (PMIP) experimental design in these GCM experiments, but the model can not represent any changes in the ocean or the sea-ice, both of which may produce important feedbacks, and the present day atmospheric variability over the equatorial Pacific (figures 3b and 3d) is not captured. For example, changes in the El Niño Southern Oscillation may lead to large regional atmospheric anomalies. Rowell *et al* (1995) discuss the importance of SST anomalies on summer rainfall in Tropical North Africa, and the impact of possible mid-Holocene El Niño anomalies, and the resulting interaction with the African-Asian monsoon climate in

particular, would be worthy of investigation. The sensitivity experiment with present day CO_2 concentrations and 6kBP insolation (6kINS) reinforces the need to allow the SSTs to vary by including some form of interactive ocean.

A mixed layer ocean model coupled to the atmospheric model would calculate the SSTs and the sea-ice thickness and extents but would not compute changes in the ocean's circulation. A full three-dimensional ocean model coupled to the atmospheric model would calculate changes to the ocean circulation allowing for feedbacks between the atmosphere, ocean and sea-ice. Fully coupled atmosphere-ocean GCMs are computationally expensive and are limited to relatively short integrations. The deep ocean may take several hundred years to reach equilibrium ("spin-up"), but the oceanic mixed layer would spin up more quickly.

Liao *et al* (1994) performed an experiment for 6kBP with an earlier version of the UKMO atmospheric model coupled to a mixed layer ocean model, using present day CO_2 concentrations for 6kBP. The main difference between their results and those presented here is a cooling over most of the ocean and some of the continents south of the Tropic of Cancer in July.

It is clear that future phases of the PMIP 6kBP project should allow for changes in sea surface temperature and sea-ice if model-palaeodata comparisons are to have real value. A choice may have to be made between using a simple mixed layer ocean which requires a relatively short time to come to equilibrium, allowing more centres to participate but ignoring possible changes in ocean circulation, or to promote studies with full ocean-atmosphere models, with the attendant problems bringing the deep ocean to equilibrium.

As noted in the introduction, changes in vegetation also have the potential to feedback on climate, particularly through the associated changes in surface albedo. This too needs to be considered in the next stage of PMIP if model-data comparisons are to be of maximum benefit. Initially, it would be simpler to impose the reconstructed changes in vegetation, as few centres have developed and validated interactive models of vegetation In the longer term, one could include an interactive representation of vegetation. It may be preferable to add these additional features sequentially if one is to understand and interpret the results.

Finally, as more geologic data becomes available the spatial coverage and spatial resolution of palaeoclimatic reconstructions will increase which will prove invaluable for data-model intercomparisons and for evaluating future finer resolution models. Greater temporal resolution records would also be of great interest for assessing the climatic variability of past climates, be it inter-annual, inter-decadal or longer time-scales.

We feel that the next generation of palaeoclimatic GCM experiments should couple an interactive ocean model to an atmospheric GCM, and should simulate many decades in an attempt to account for and investigate inter-annual variability, both of the atmosphere, and, in the first instance, the surface mixed-layer of the ocean.

Acknowledgements. We would like to thank Catherine Senior, Simon Tett, Chris Folland, Sylvie Joussaume, Tony Broccoli, and an anonymous reviewer for many helpful comments on improving this manuscript. This work was partially supported by the CEC under Contract EV5V-CT94-0457 .

References

Berger, A.L., 1978: Long-term variations of daily insolation and Quaternary climatic changes. *J. Atmos. Sci*, **35**, 2362-2367.

COHMAP members, 1988: Climatic changes of the last 18,000 years: Observations and model simulations. *Science*, **241**, 1043-1052.

Cullen, M.J.P., and T.R. Davies, 1991: A conservative split-explicit integration scheme with fourth order advection. *Quart. J. Roy. Meteor. Soc.*, **117**, 993-1002.

Delworth, T.L., and S. Manabe, 1989: The influence of soil wetness on near-surface atmospheric variability. *J. Climate*, **2**, 1447-1462.

Foley, J.A., J.E. Kutzbach, M.T. Coe, and S. Lewis, 1994: Feedbacks between climate and boreal forests during the Holocene epoch. *Nature*, **371**, 52-54.

Gregory, D., and P.R., Rowntree, 1990: A mass flux convection scheme with representation of cloud ensemble characteristics and stability dependent closure. *Mon. Wea. Rev.*, **118**, 1483-1506.

Gregory, D., and S. Allen, 1991: The effect of convective scale downdraughts upon NWP and climate simulations. *9th Conf. on Numerical Weather Prediction*, Denver, Colorado, Amer. Meteor. Soc., 122-123.

Guiot, J., S.P. Harrison, and I.C. Prentice, 1993: Reconstruction of Holocene precipitation patterns in Europe using pollen and lake-level data. *Quat. Res.*, **40**, 139-149.

Hall, N.M.J., and P.J. Valdes, 1996: A GCM simulation of the climate 6000 years ago. *J.Climate*, submitted.

Harrison, S.P., and G. Digerfeldt, 1993: European lakes as palaeohydrological and palaeoclimatic indicators. *Quat. Sci. Rev.*, **12**, 233-248.

Harrison, S.P., I.C. Prentice, and J. Guiot, 1993: Climatic controls on Holocene lake-level changes in Europe. *Climate Dyn.*, **8**, 189-200.

Houghton, J.T., G.J. Jenkins, and J.J. Ephraums, 1990: *Climate Change - The IPCC Scientific Assessment.* Cambridge University Press, Cambridge, 365 pp.

Houghton, J.T., B.A. Callander, and S.K. Varney, 1992: *Climate Change 1992 - The Supplementary Report to the IPCC Scientific Assessment.* Cambridge University Press, Cambridge, 200 pp.

Huntley, B., and I.C. Prentice, 1988: July temperatures in Europe from pollen data, 6000 years before present. *Science*, **241**, 687-690.

Huntley, B., and I.C. Prentice, 1993: Holocene vegetation and climates of Europe. *In Wright et al.*, 136-168.

Johns, T.C., R.E. Carnell, J.F. Crossley, J.M. Gregory, J.F.B. Mitchell, C.A. Senior, S.F.B. Tett, and R.A. Wood, 1996: The Second Hadley Centre Coupled Ocean-Atmosphere GCM: Model Description, Spinup and Validation. *Climate Dyn.*, Submitted.

Joussaume, S. and K.E. Taylor, 1995: Status of the Paleoclimate Modeling Intercomparison Project. *Proceedings of the first international AMIP scientific conference*, Monterrey, USA, WCRP-92, 425-430.

Kutzbach, J.E., and B.L. Otto-Bliesner, 1982: The sensitivity of the African-Asian monsoonal climate to orbital parameter changes for 9000 years B.P. in a low-resolution general circulation model. *J. Atmos. Sci*, **39**, 1177-1188.

Kutzbach, J.E., and F.A. Street-Perrott, 1985: Milankovitch forcing of fluctuations in the level of tropical lakes from 18 to 0 kyr BP. *Nature*, **317**, 130-34.

Kutzbach, J.E., and P.J. Guetter, 1986: The influence of changing orbital parameters and surface boundary conditions on climate simulations for the past 18000 years. *J. Atmos. Sci.*, **43**, 1726-1759.

Kutzbach, J.E., and R.G. Gallimore, 1988: Sensitivity of a coupled atmosphere/mixed layer ocean model to changes in orbital forcing at 9000 years B.P. *J. Geophys. Res.*, **93**, 803-821.

Legates, D.R. and C.J. Willmott, 1990a: Mean seasonal and spatial variability in global surface air temperature. *Theor. Appl. Climatol.*, **41**, 11-21.

Legates, D.R. and C.J. Willmott, 1990b: Mean seasonal and spatial variability in gauge-corrected global precipitation. *Int. J. Climatol.*, **10**, 111-127.

Liao, X., 1991: Two general circulation model experiments for 6000 years B.P.: Analyses and comparisons with palaeoclimatic data. Ph.D. thesis, University of Oxford, 184 pp.

Liao, X., F.A. Street-Perrott, and J.F.B. Mitchell, 1994: GCM experiments with different cloud parameterization: Comparisons with palaeoclimatic reconstructions for 6000 years B.P. *Palaeoclimates*, **1**, 99-123.

Lofgren, B.M., 1995: Sensitivity of land-ocean circulations, precipitation, and soil moisture to perturbed land surface albedo. *J. Climate*, **8**, 2521-2542.

Manabe, S., and R.J. Stouffer, 1996: Low frequency variability of surface air temperature in a 1,000 year integration of a coupled atmosphere-ocean-land surface model. *J. Climate*, **9**, 376-393.

Mitchell, J.F.B., 1990: Greenhouse warming: Is the mid-Holocene a good analogue? *J. Climate*, **3**, 1177-1192.

Mitchell, J.F.B., 1993: Modelling of palaeoclimates : examples from the recent past. *Philos. Trans. Roy. Soc. London*, **341**, 267-275.

Mitchell, J.F.B., N.S. Grahame, and K.J. Needham, 1988: Climate simulations for 9000 years before present: seasonal variations and effect of the Laurentide ice sheet. *J. Geophys. Res.*, **93**, 8283-8308.

Mitchell, J.F.B., T.C. Johns, J. Gregory, and S.F.B. Tett, 1995: Climate response to increasing levels of greenhouse gases and sulphate aerosols. *Nature*, **376**, 501-504.

Morley, J.J., and B.A. Dworetzky, 1993: Holocene temperature patterns in the south Atlantic, southern, and Pacific oceans. *In Wright et al.*, 125-135.

Palmer, T.N., G.J. Shutts, and R. Swinbank, 1986: Alleviation of a systematic westerly bias in general circulation and numerical weather prediction models through an orographic gravity wave drag parameterization. *Quart. J. Roy. Meteor. Soc.*, **112**, 1001-1039.

Parker, D.E., P.D. Jones, C.K. Folland, and A. Bevan, 1994: Interdecadal changes of surface temperature since the late nineteenth century. *J. Geophys. Res.*, **99**, 14373-14399.

Rowell, D.P., C.K. Folland, K. Maskell, and M.N. Ward, 1995: Variability of summer rainfall over tropical North Africa (1906-92) : Observations and modelling. *Quart. J. Roy. Meteor. Soc.*, **121**, 669-704.

Ruddiman, W.F., and A.C. Mix, 1993: The north and equatorial Atlantic at 9000 and 6000 yr B.P. *In Wright et al.*, 94-124.

Schutz, C., and W.L. Gates, 1971: Global climatic data for surface, 800 mb, 400 mb: January. Rand, Santa Monica, R-915-ARPA.

Schutz, C., and W.L. Gates, 1972: Global climatic data for surface, 800 mb, 400 mb: July. Rand, Santa Monica, R-1029-ARPA.

Schneider, S.H., 1975: On the carbon dioxide - climate confusion. *J. Atmos. Sci.*, **32**, 2060-2066.

Simmons, A.J. and D.M. Burridge, 1981: An energy and angular momentum conserving finite difference scheme with hybrid coordinates. *Mon. Wea. Rev.*, **109**, 758-766.

Slingo, A., 1989: A GCM parameterization for the shortwave radiative properties of water clouds. *J. Atmos. Sci.*, **46**, 1419-1427.

Slingo, A. and R.C. Wilderspin, 1986: Development of a revised long wave radiation scheme for an atmospheric general circulation model. *Quart. J. Roy. Meteor. Soc.*, **112**, 371-386.

Smith, R.N.B., 1990: A scheme for predicting layer clouds and their water content in a general circulation model. *Quart. J. Roy. Meteor. Soc.*, **116**, 435-460.

Street-Perrott, F.A., and R.A. Perrott, 1993: Holocene vegetation, lake levels, and climate of Africa. *In Wright et al.*, 318-356.

Street-Perrott, F.A., J.F.B. Mitchell, D.S. Marchand, and J.S. Brunner, 1990: Milankovitch and albedo forcing of the tropical monsoons: a comparison of geological evidence and numerical simulations for 9000 yBP. *Trans. Roy. Soc. Edinb.*, **81**, 407-427.

Tett, S.F.B., T.C. Johns, and J.F.B. Mitchell, 1996: Global and Regional Variability in a coupled AOGCM. Submitted to *Climate Dyn.*

Warrilow, D.A., A.B. Sangster, and A. Slingo, 1986: Modelling of land surface processes and their influence on European climate. *Met O 20 DCTN 38*, Meteorological Office, Bracknell, UK.

Webb, T., P.J. Bartlein, S.P. Harrison, and K.H. Anderson, 1993: Vegetation, lake levels, and climate in eastern North America for the past 18,000 years. *In Wright et al.*, 415-467.

Wright, H.E.,Jr., J.E. Kutzbach, T. Webb, W.F. Ruddiman, F.A. Street-Perrott, and P.J. Bartlein, 1993: *Global Climates since the Last Glacial Maximum.* University of Minnesota Press, 569 pp.

Zwiers, F.W., and H. von Storch, 1995: Taking serial correlation into account in tests of the mean. *J. Climate*, **8**, 336-351.

Figure legends

Figure 1: pressure at mean sea level from the control simulation. Contours every 4 mb (hPa), heavy shading above 1020 mb, light shading below 1000 mb. (a) DJF. (b) JJA.

Figure 2: precipitation from the control simulation. Contours at 0.1, 1, 2, 5, 10, 20 mm day^{-1}, shaded above 5 mm day^{-1}. (a) DJF. (b) JJA.

Figure 3: standard deviation of observed and modelled surface air temperature, contours at 0.5, 1, 1.5, 2, 3, 4, shaded above 1. Missing data in observations masked out. (a) DJF from control simulation. (b) DJF from observations. (c) JJA from control simulation. (d) JJA from observations.

Figure 4: standard deviation of soil moisture content for JJA from the control simulation. Contours at 1, 5, 10, 20, 30 mm, shaded above 5 mm.

Figure 5: time-latitude diagrams (zonal mean of average monthly values) of changes between 6kBP and 0kBP with areas of decrease shaded. Missing data has been masked out. (a) Incoming shortwave radiation at the top of the atmosphere, contours every 10 W m^{-2}. (b) Total downward shortwave radiation at the surface, contours every 10 W m^{-2}. (c) Surface air temperature over land points, contours every 1 K. (d) Cloud amount over land points, contours every 5%.

Figure 6: JJA model differences between 6kBP and 0kBP, areas of decrease stippled. (a) Surface air temperature, contours every 0.5 K. (b) 2-sided Student's t-test on the changes in surface air temperature, contours at the 95% and 99% significance levels. Heavy shading for regions of cooling significant above the 95% confidence level, light shading for regions of significant warming. (c) Total cloud amount, contours every 5%. (d) Total precipitation, contours at 0, $\pm$ 0.5, 1, 2, 5 mm day^{-1}. (e) Mean sea level pressure, contours every 1 mb. (f) Low-level wind (model level 4, $\sigma = 0.8698$), contours every 1 m s^{-1}.

Figure 7: as figure 6 but for DJF.

Figure 8: (a) change in model's annual mean soil moisture content between 6kBP and 0kBP, contours at $\pm$ 1, 5, 10, 20 mm, shaded below -1 mm. (b) Statistical significance of soil moisture changes, with contours at the 95 and 99% level of significance, heavy shading for drier regions, light shading for wetter regions.

Figure 9: Monthly average changes between 6kBP and 0kBP averaged over land points. Dashed line is precipitation, dotted line is evaporation, thick solid line with diamonds is P–E, all in mm day^{-1} . Squares are vertical velocity in cm s^{-1} . Note the change of scale in (c). (a) Northern tropics, Equator to 30°N. (b) Southern tropics, 30°S to equator. (c) Northern high latitudes, 60°N to 90°N.

Figure 10: Zonal average changes, between 6kBP and 0kBP, over land in cloud amount (% of total cover, dashed line) and TOA short-wave cloud forcing (in W m^{-2} , solid line). (a) JJA. (b) DJF.

Figure 11: change in model's surface air temperature between individual decades of 6kBP experiment and 50 years of 0kBP experiment for JJA, contours every 1 K, areas of decrease shaded. (a) 1st decade. (b) 2nd decade. (c) 3rd decade.

Figure 12: standard deviation of DJF surface air temperature from the 6kBP and 0kBP simulations. (a) 6kBP – 0kBP, contours at ± .25, 0.5, 1, heavy shading for lower variability at 6kBP, light shading for higher variability. (b) F-test on the ratio of variances, contours at the 95% and 99% confidence levels, shaded above 95%.

Figure 13: change in model's annual mean surface air temperature between 6kBP and 0kBP, contours every 0.5 K, areas of decrease shaded.

Figure 14: change in model's precipitation-evaporation between 6kBP and 0kBP, contours at ± 0.1, 0.5, 1.0 mm day^{-1} . Heavy shading for drier regions, light shading for wetter regions.

Table 1: Orbital parameters for the control (0kBP) and mid-Holocene (6kBP) experiments derived from Berger (1978)

	0kBP	6kBP
Longitude of perihelion (relative to the vernal equinox)	102.5°	0.9°
Obliquity	23.44°	24.10°
Eccentricity	0.0167	0.0187

Table 2: Comparison of changes between 6kBP and 0kBP averaged separately over land and sea points in the Northern hemisphere tropics (0°–30°N) in JJA and the Southern hemisphere tropics (0°–30°S) in DJF. ΔINS is change in insolation in W m^{-2}, ΔT is change in surface air temperature in K, Δpmsl is change in mean sea level pressure in mb (hPa), Δsmc is change in soil moisture content in mm, Δtppn is change in precipitation in mm day^{-1}, and Δ(P–E) is change in (precipitation minus evaporation) in mm day^{-1}.

	JJA, 0°–30°N		DJF, 0°–30°S	
	Land	Ocean	Land	Ocean
ΔINS	19.60	19.19	-20.02	-20.02
ΔT	0.39	0.07	-0.38	-0.08
Δpmsl	-0.48	0.25	0.72	0.13
Δsmc	0.73	–	-2.76	–
Δtppn	0.27	-0.30	-0.47	0.23
Δ(P–E)	0.18	-0.17	-0.35	0.11

Table 3: Number of land grid-points showing a significant change in 1.5 m temperature in JJA between 6kBP and 0kBP, expressed as a percentage of total number of land grid-points (see text). Column A compares 30 years of the anomaly experiment to 50 years of the control. Column B concerns all 15 combinations of comparing 1 decade of the anomaly against 1 decade of the control.

	A	B		
		Mean	Min	Max
% points significant at 95% level	60	39	32	47
% points significant in B but not A (Estimate of "false alarms")	0	6	1	15

Table 4: As table 2 but for changes between 6kBPINS and 0kBP experiments.

	JJA, 0°–30°N		DJF, 0°–30°S	
	Land	Ocean	Land	Ocean
ΔINS	19.60	19.19	-20.02	-20.02
ΔT	0.45	0.06	-0.18	-0.05
Δpmsl	-0.45	0.45	0.70	0.14
Δsmc	2.35	–	-1.08	–
Δtppn	0.33	-0.44	-0.49	0.25
Δ(P–E)	0.23	-0.20	-0.35	0.16

Figure 1a

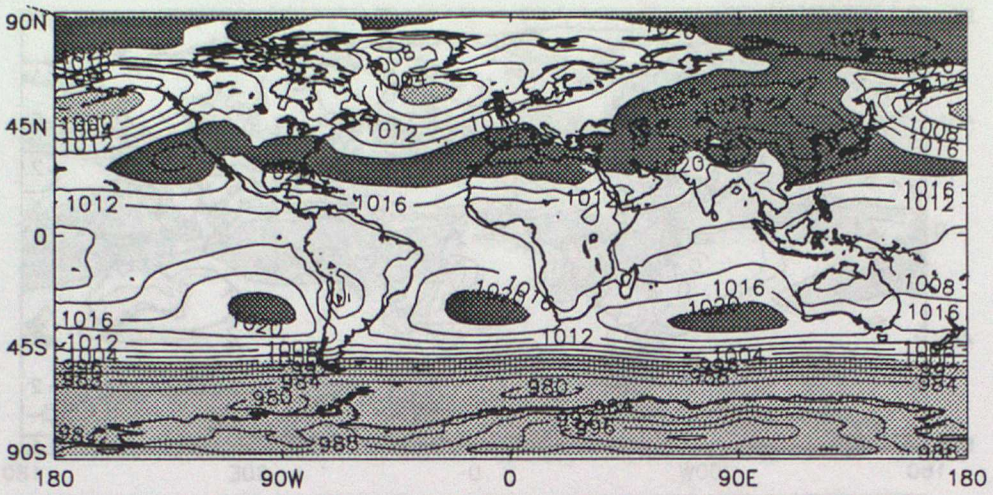

Figure 1b

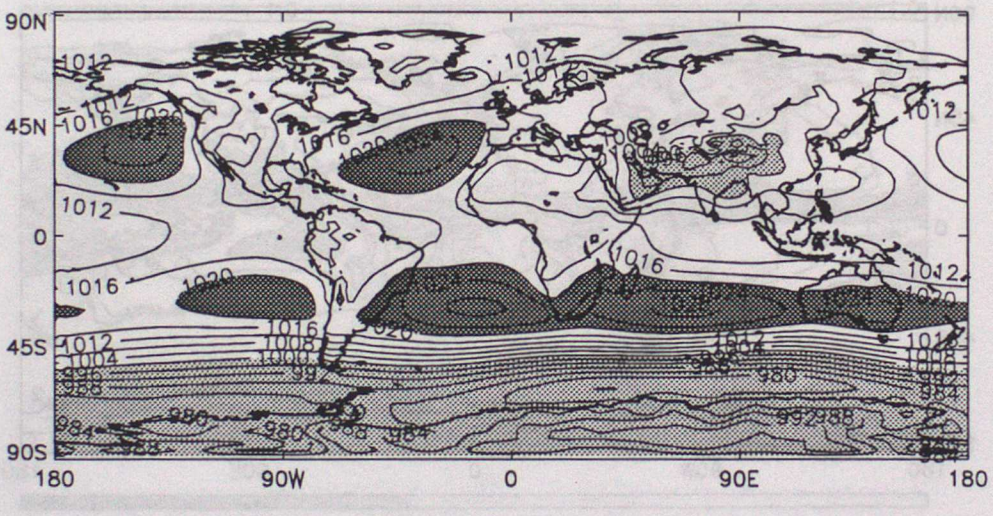

Figure 2a

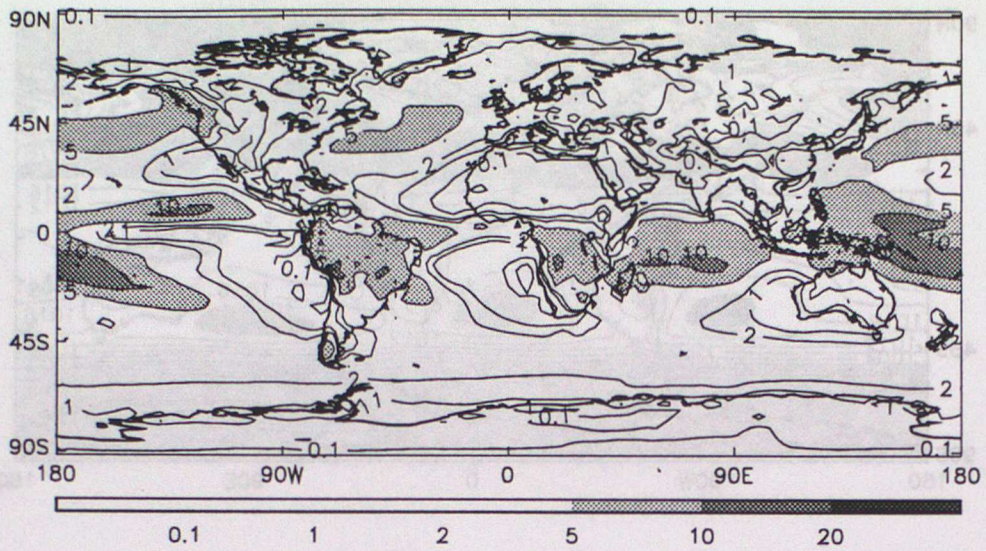

Figure 2b

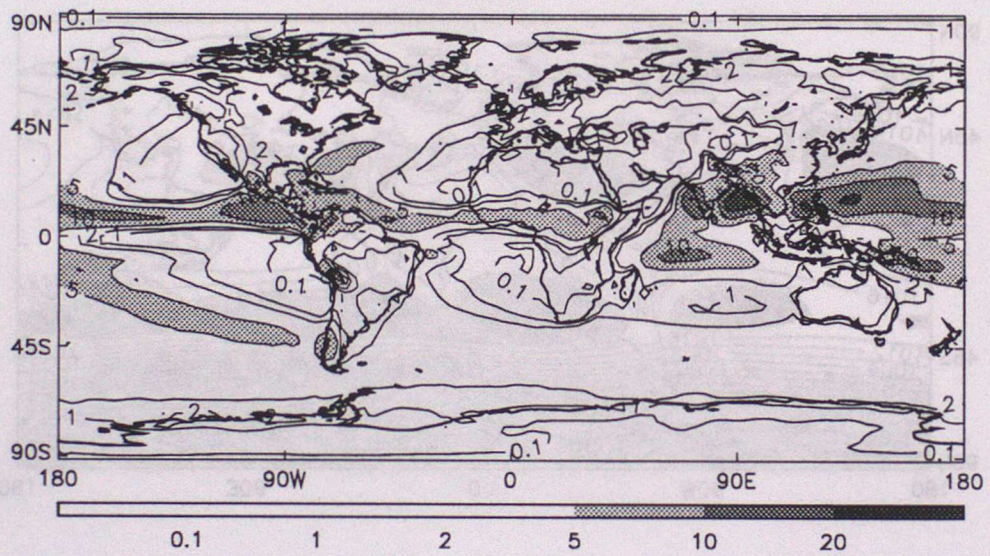

Figure 3a

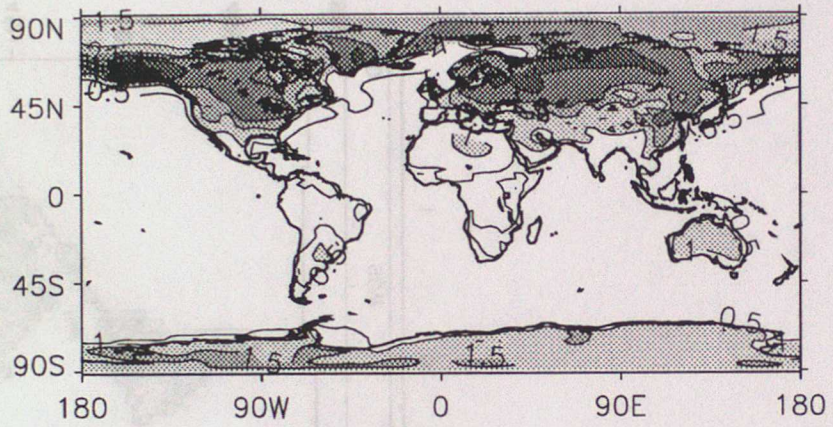

Figure 3b

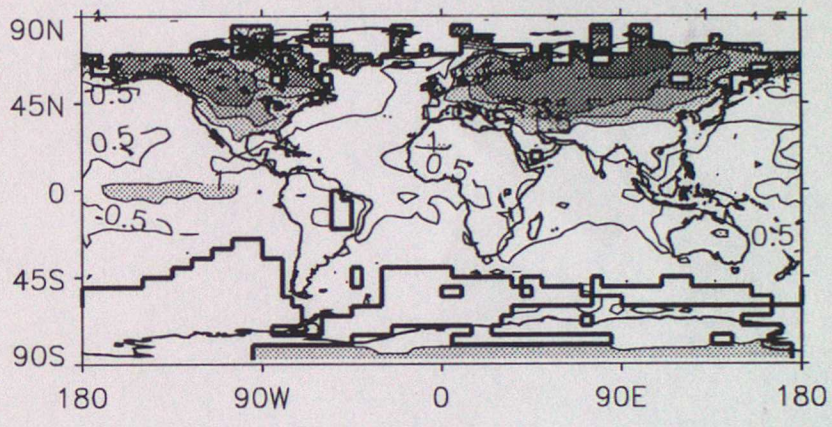

Figure 3c

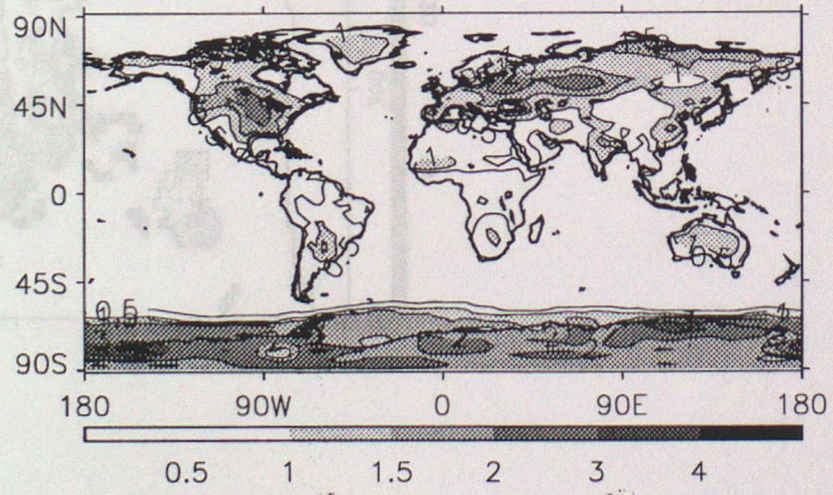

Figure 3d

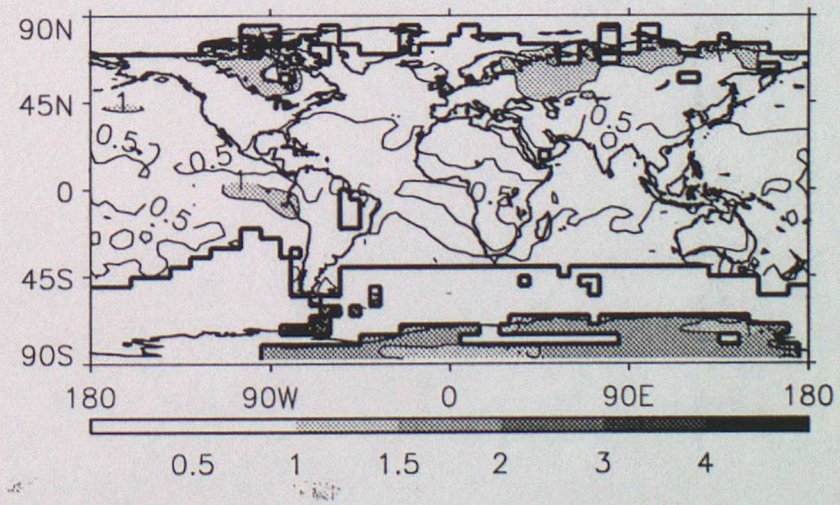

Figure 4

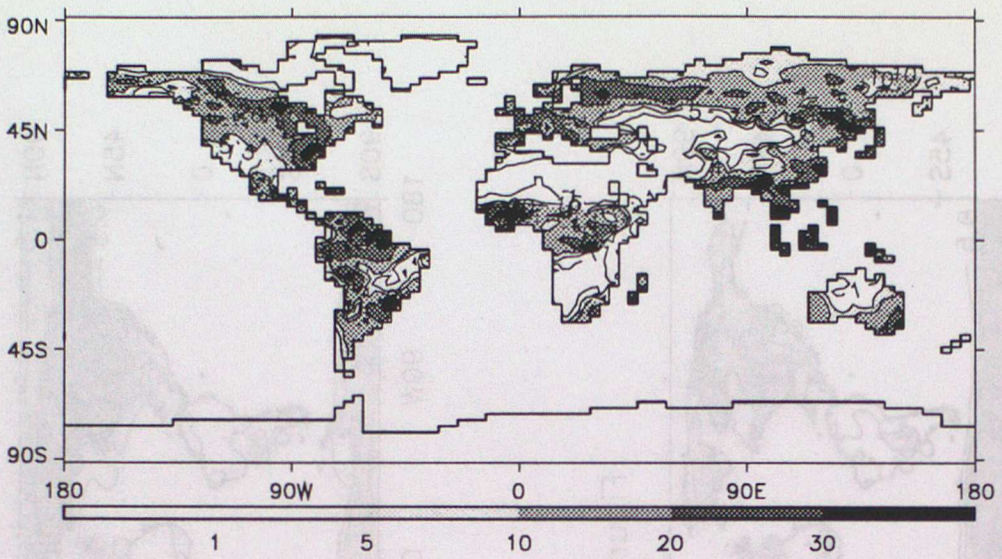

Figure 5a

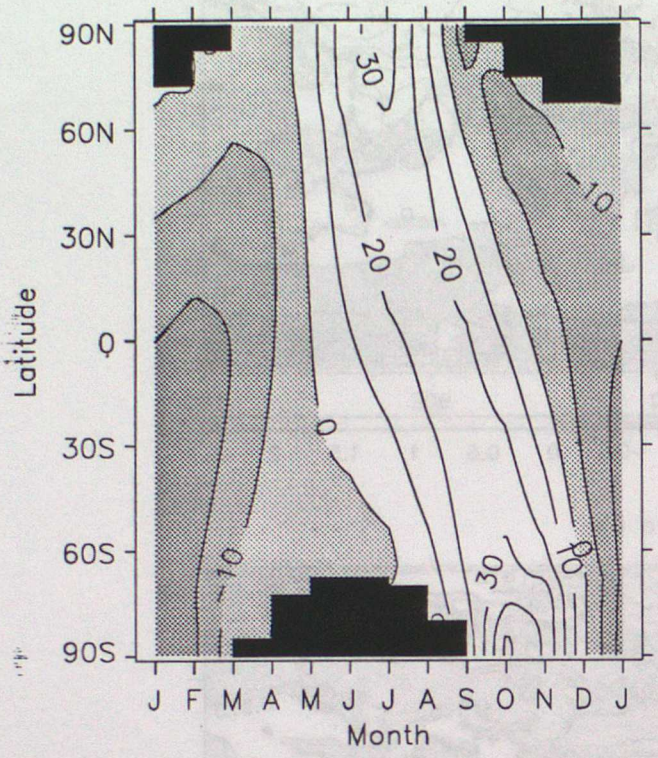

Figure 5b

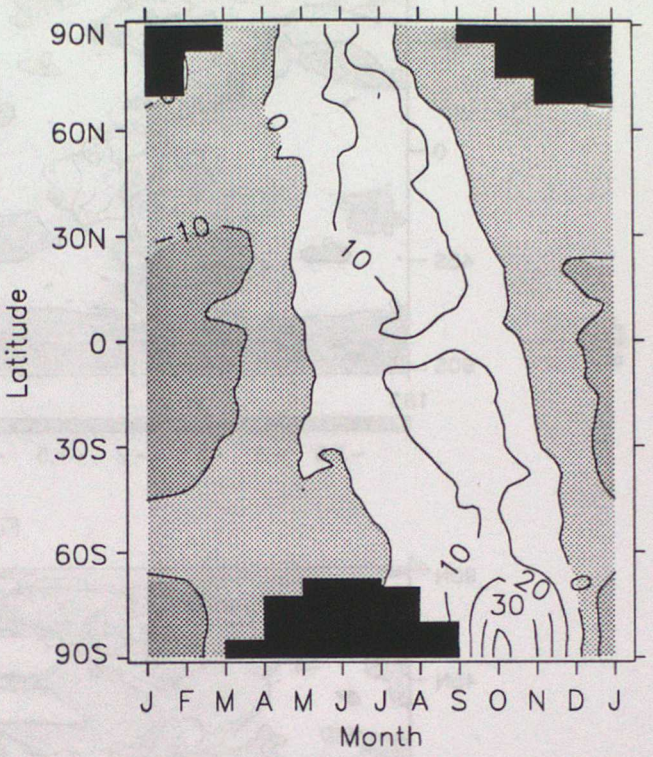

Figure 5c

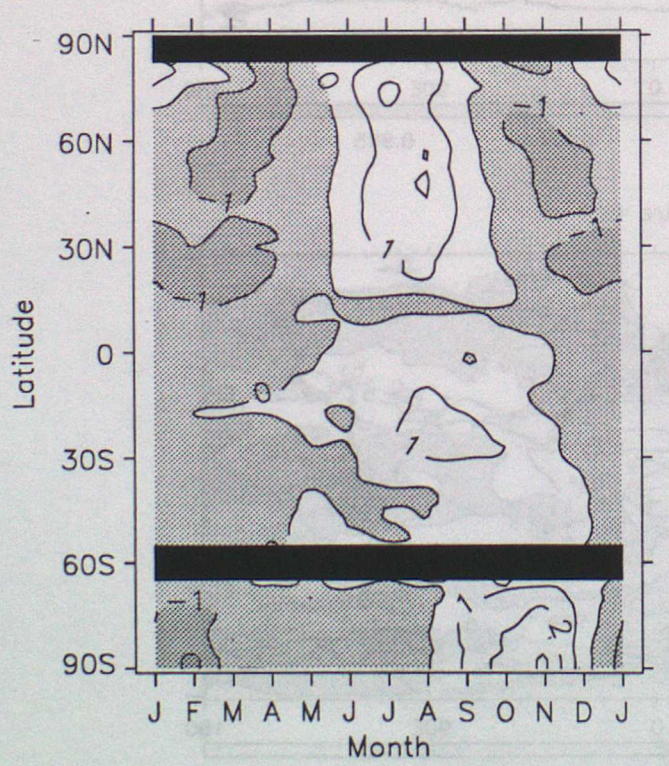

Figure 5d

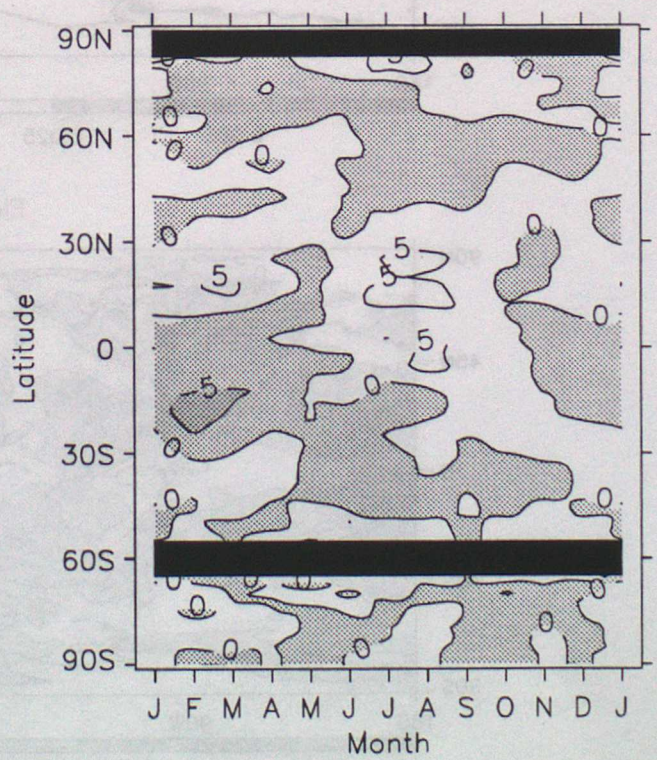

Figure 6a

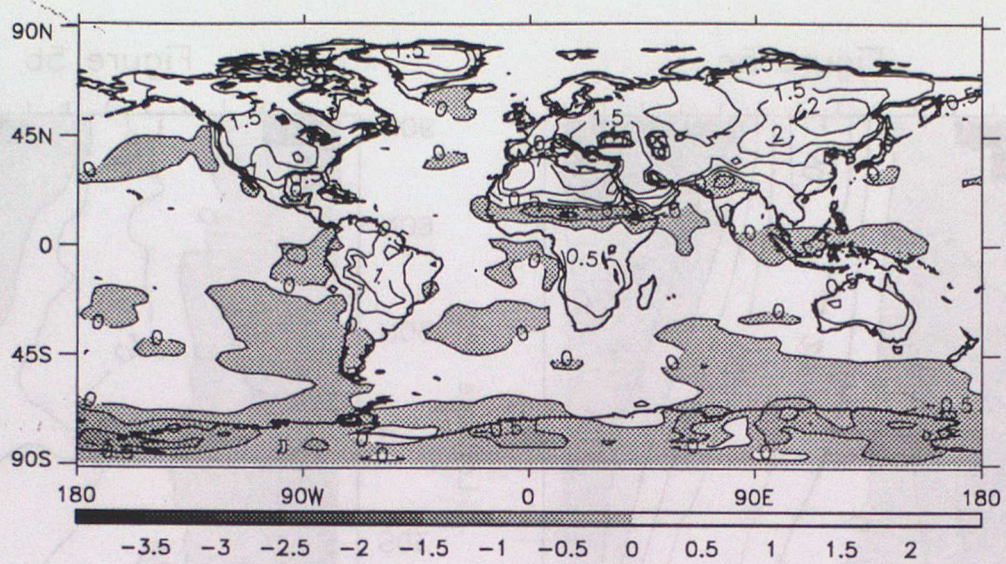

Figure 6b

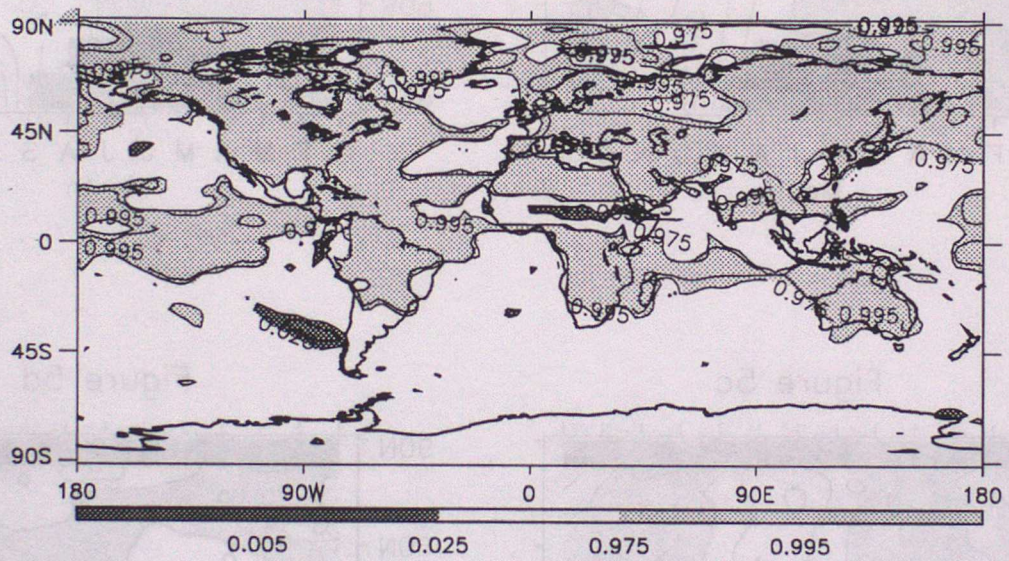

Figure 6c

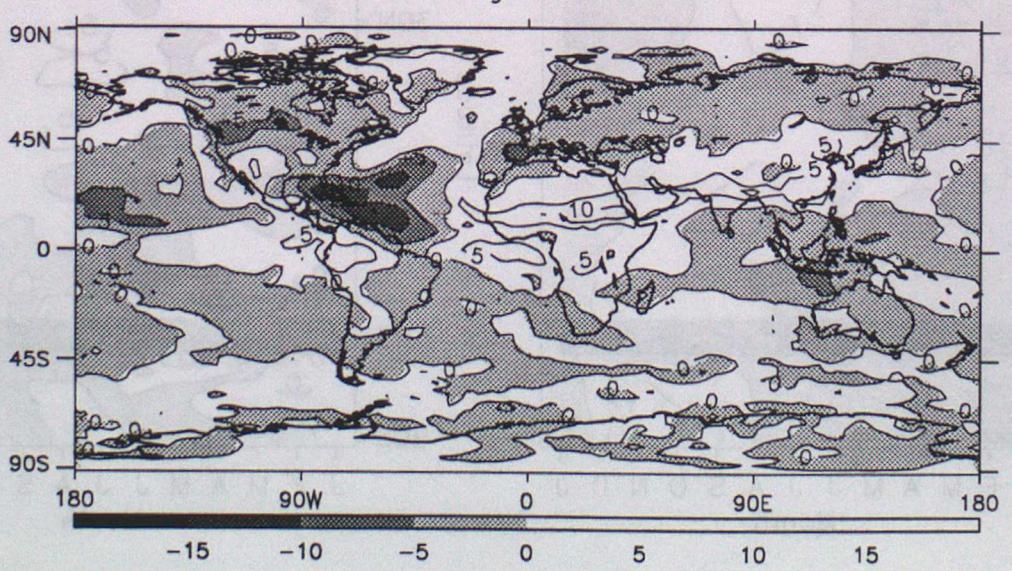

Figure 6d

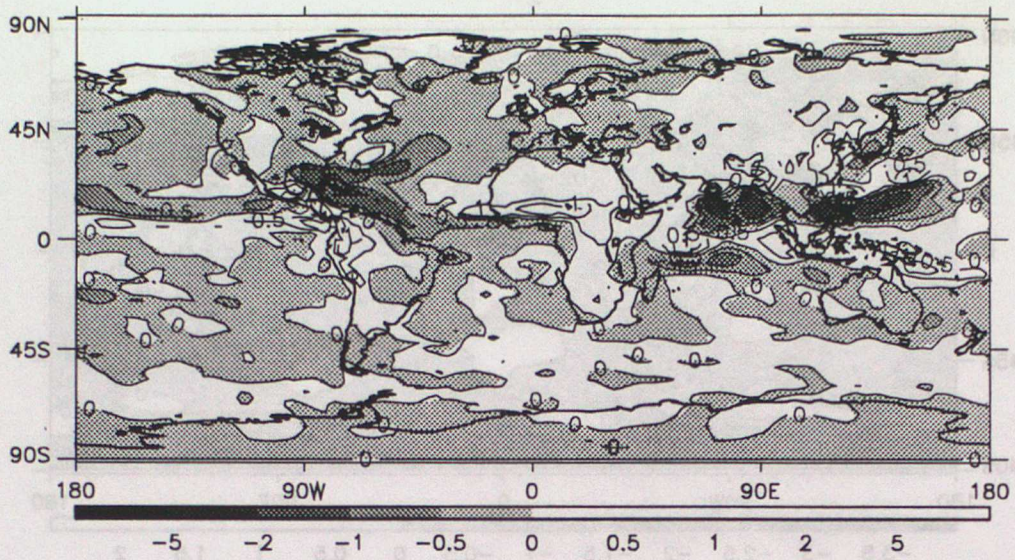

Figure 6e

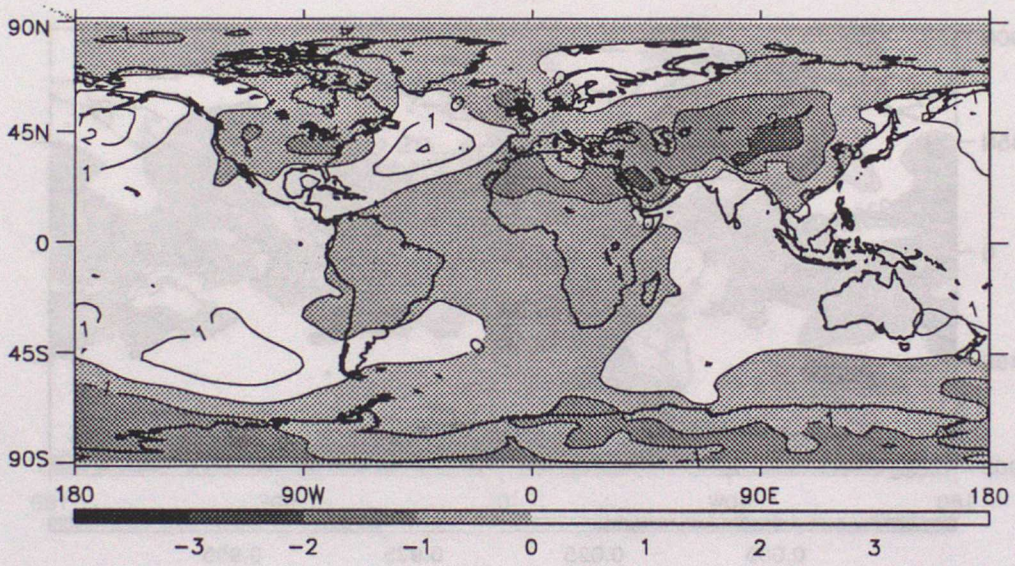

Figure 6f

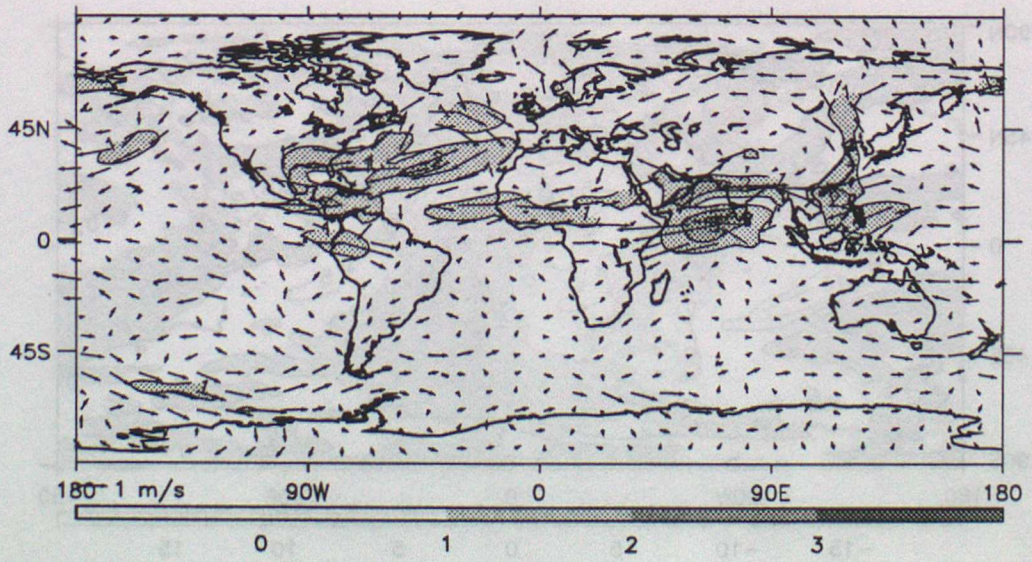

Figure 7a

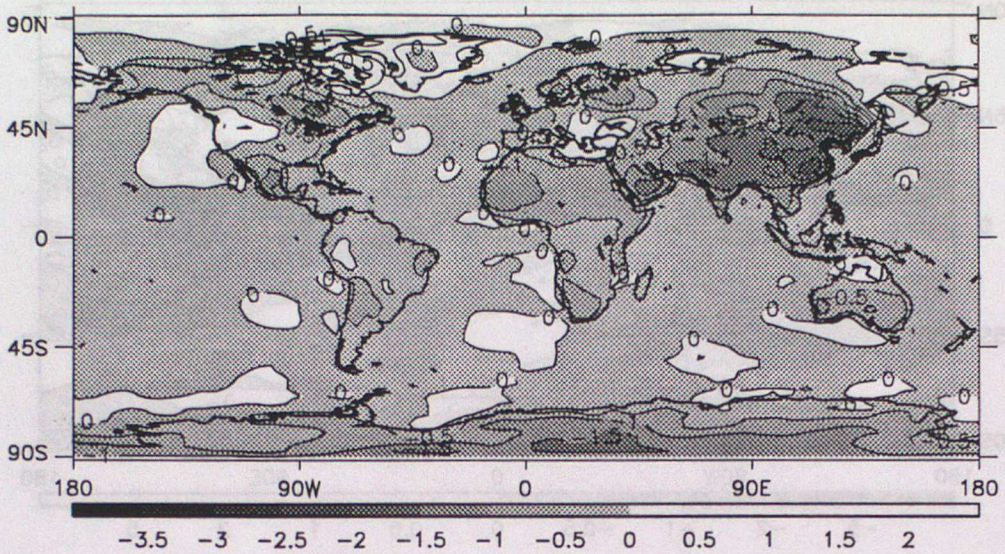

Figure 7b

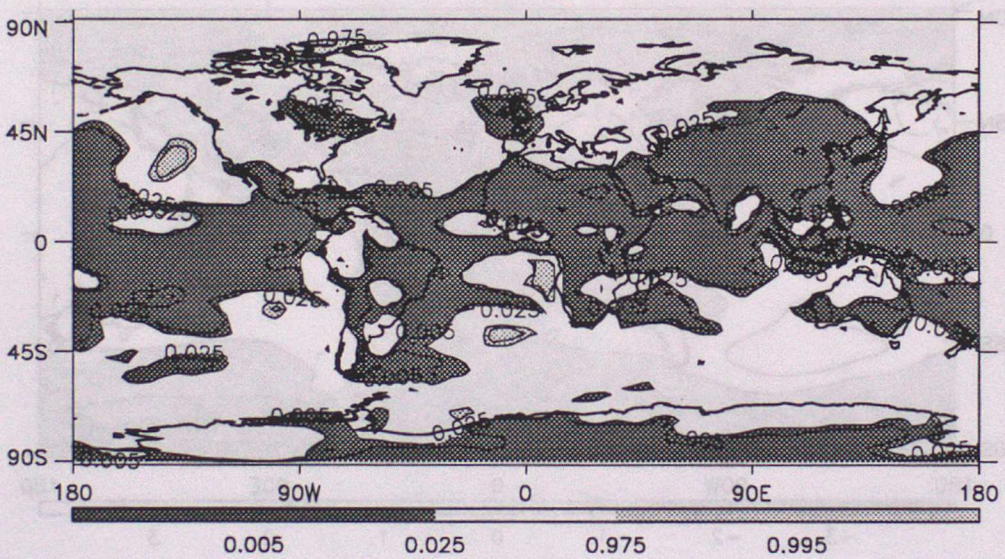

Figure 7c

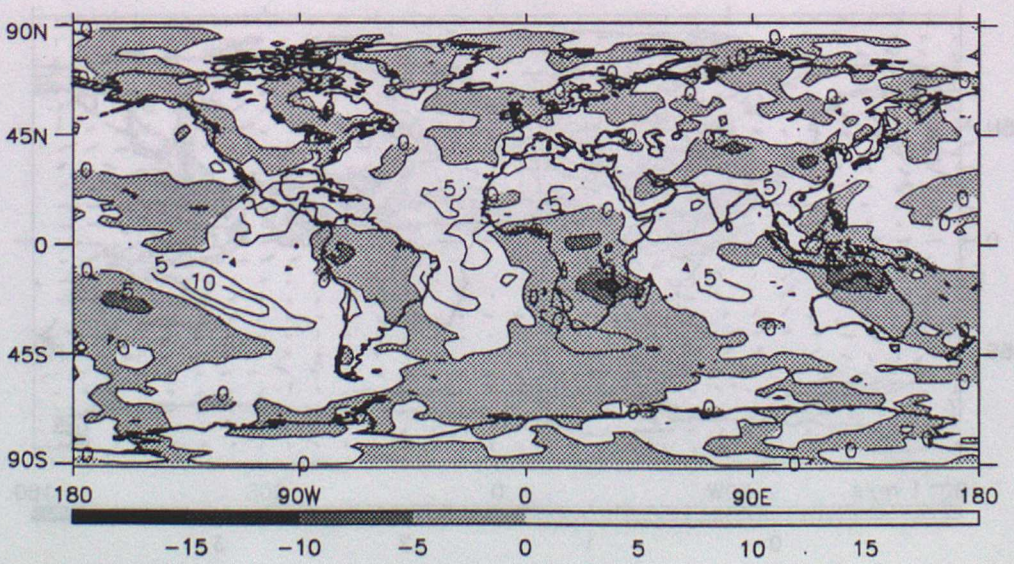

Figure 7d

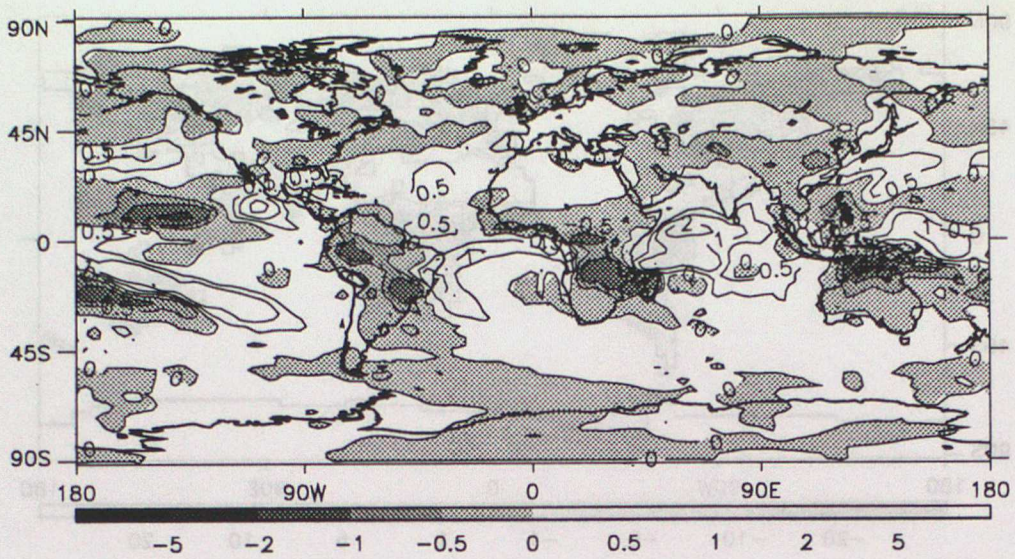

Figure 7e

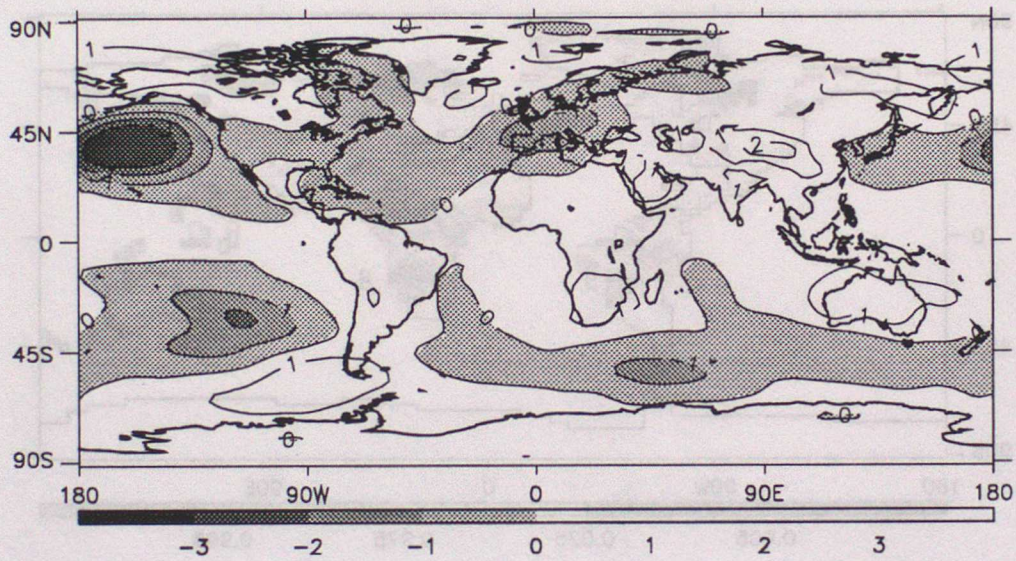

Figure 7f

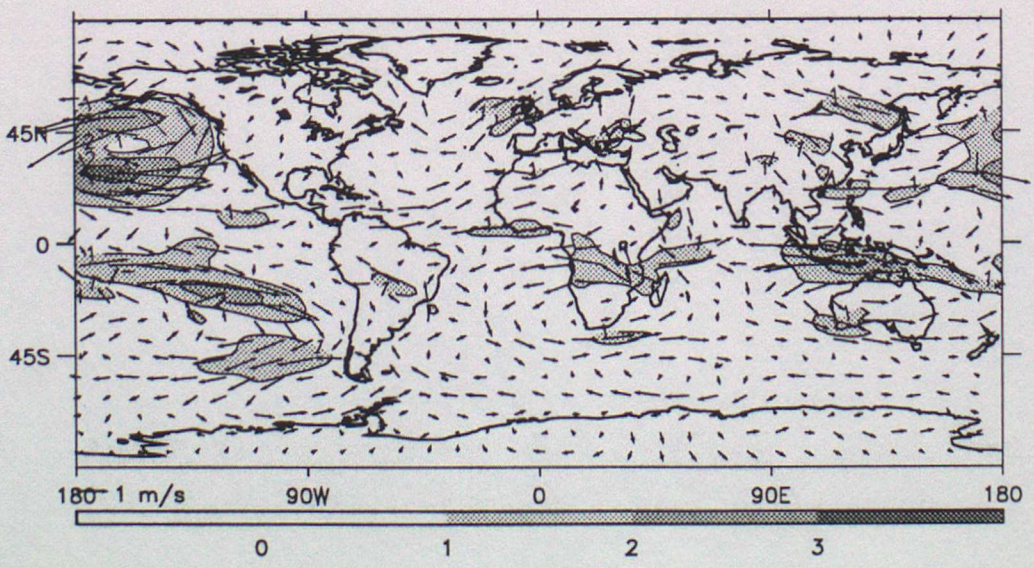

Figure 8a

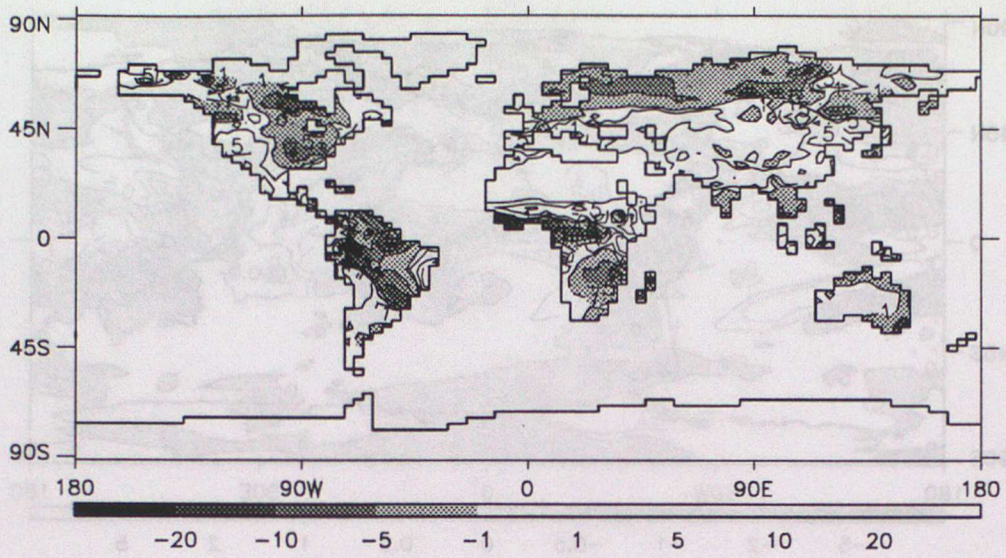

Figure 8b

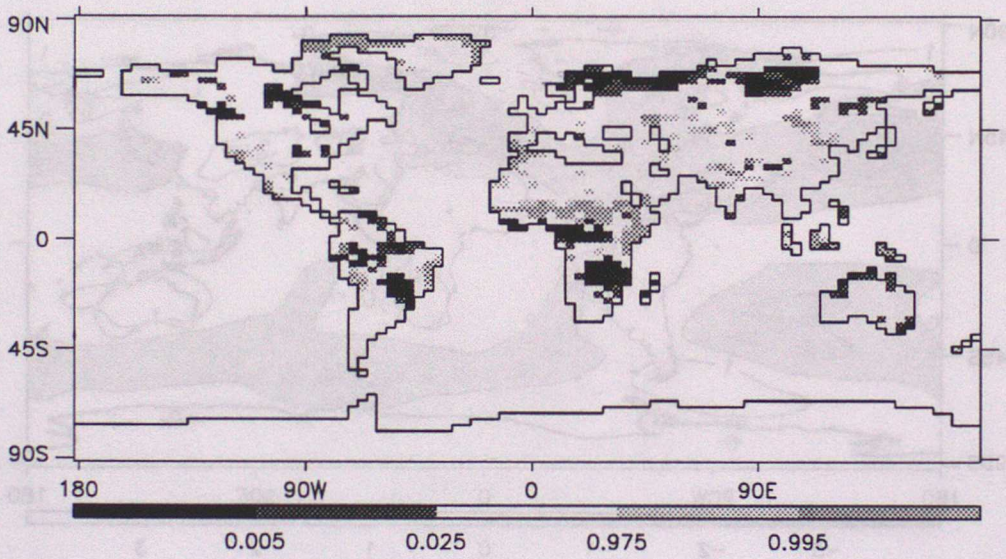

Figure 9a

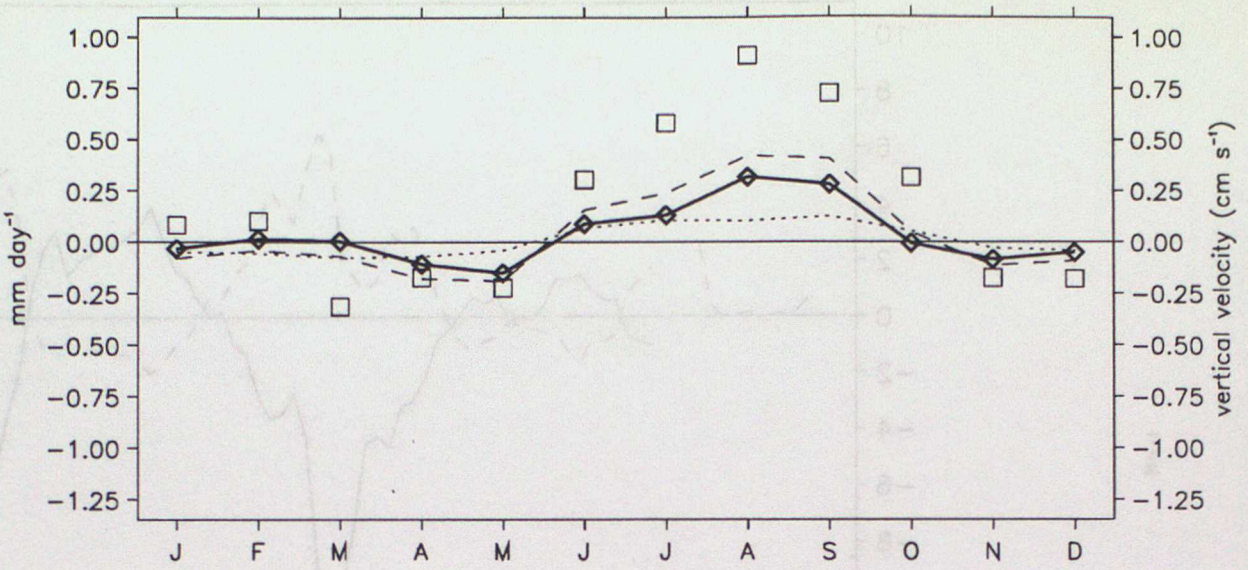

Figure 9b

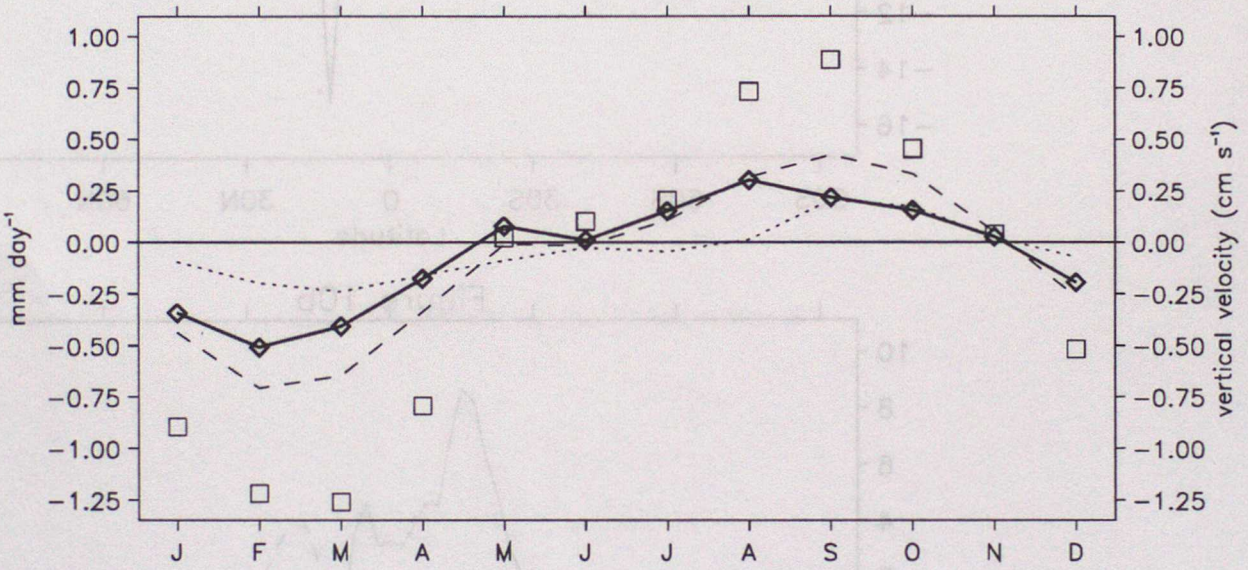

Figure 9c

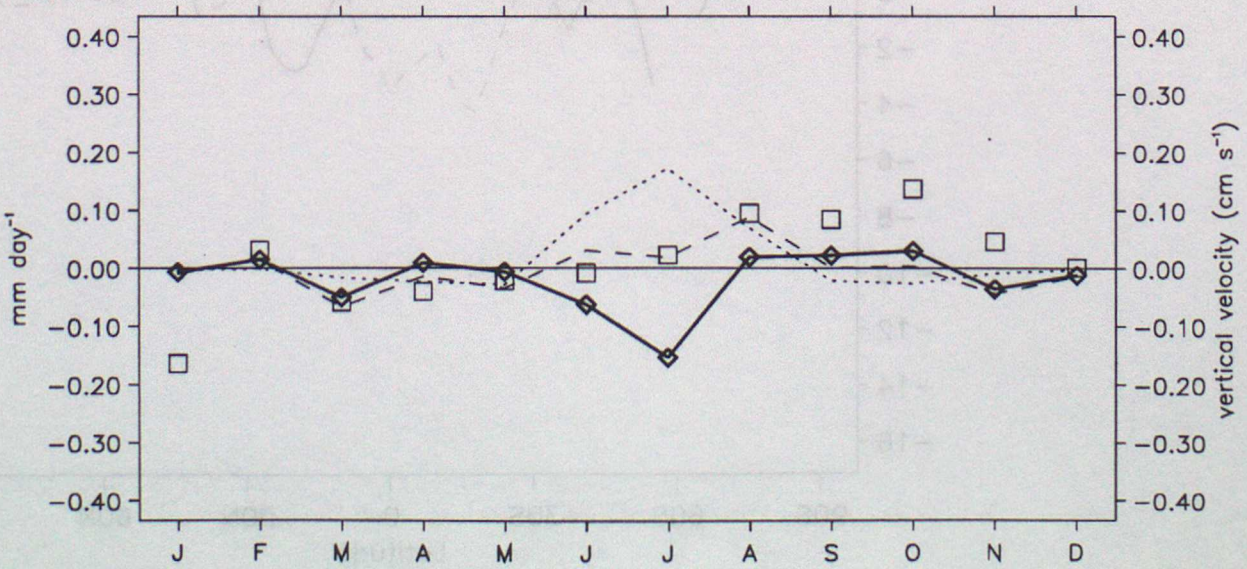

Figure 10a

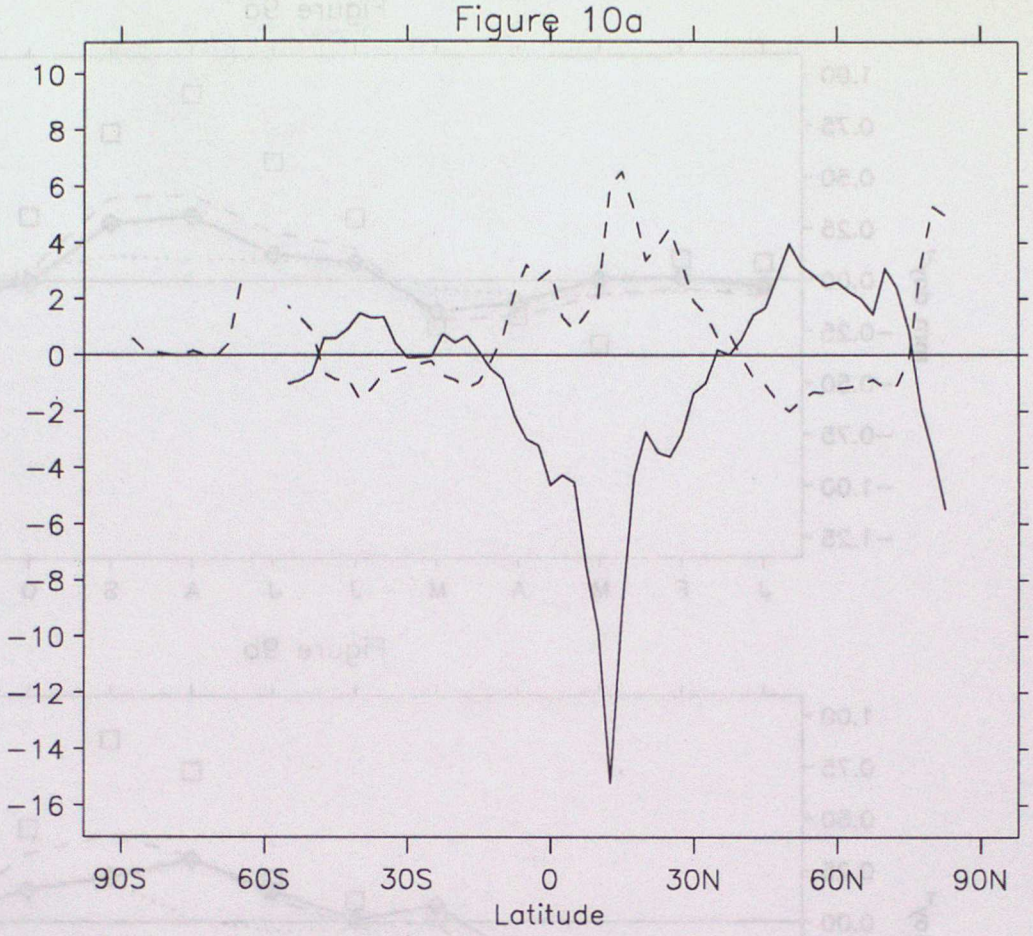

Figure 10b

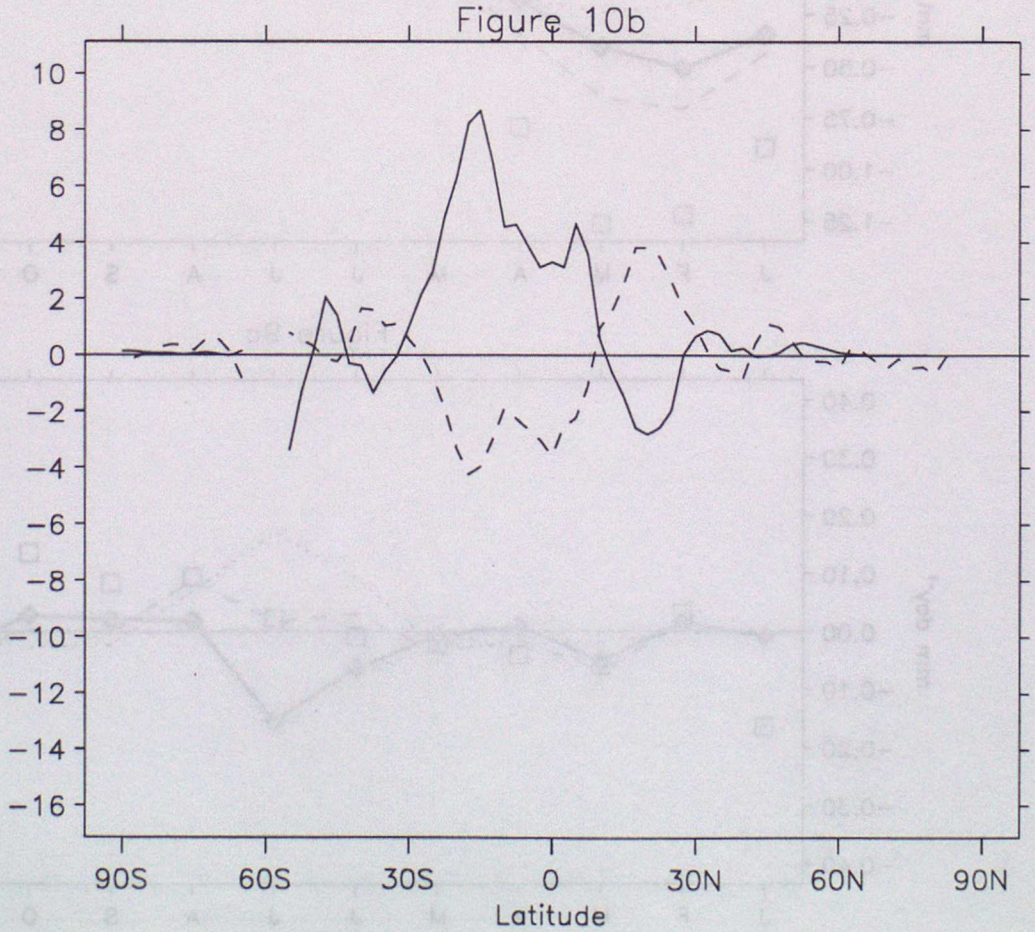

Figure 11a

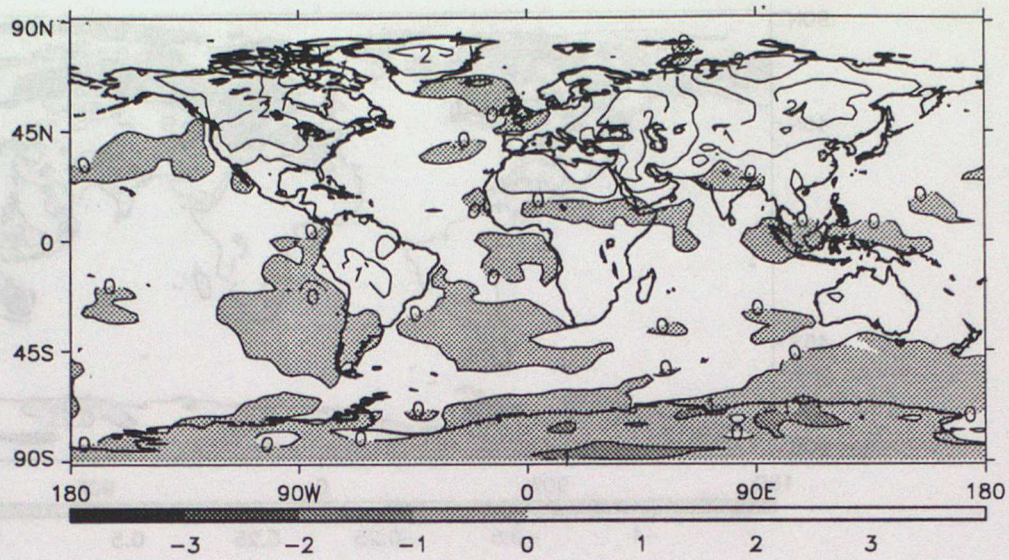

Figure 11b

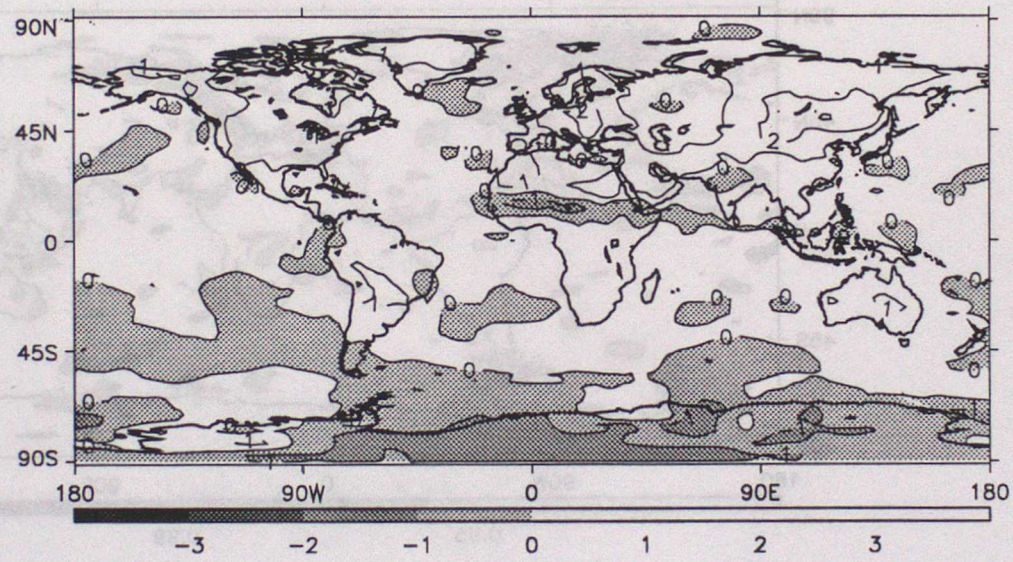

Figure 11c

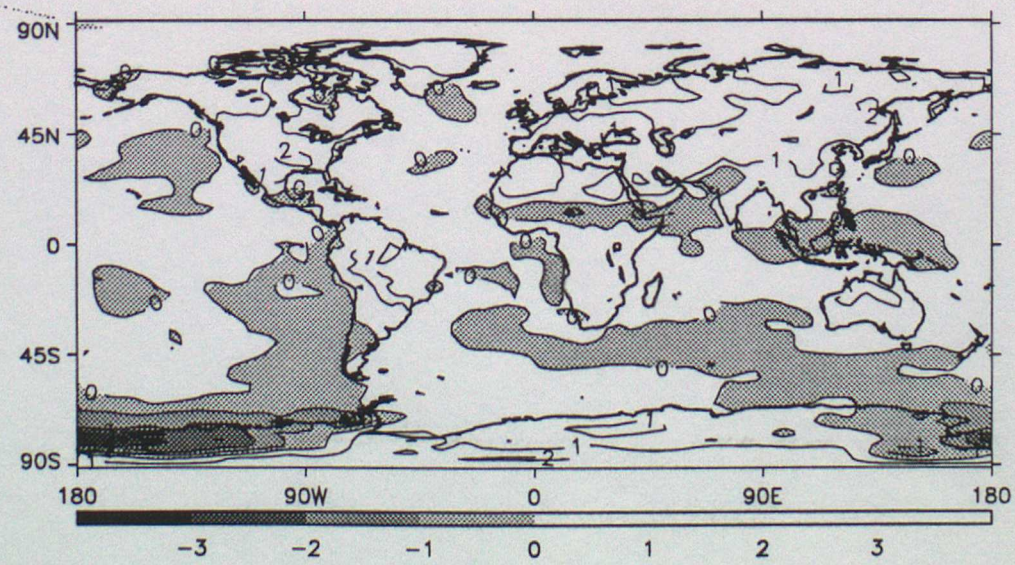

Figure 12a

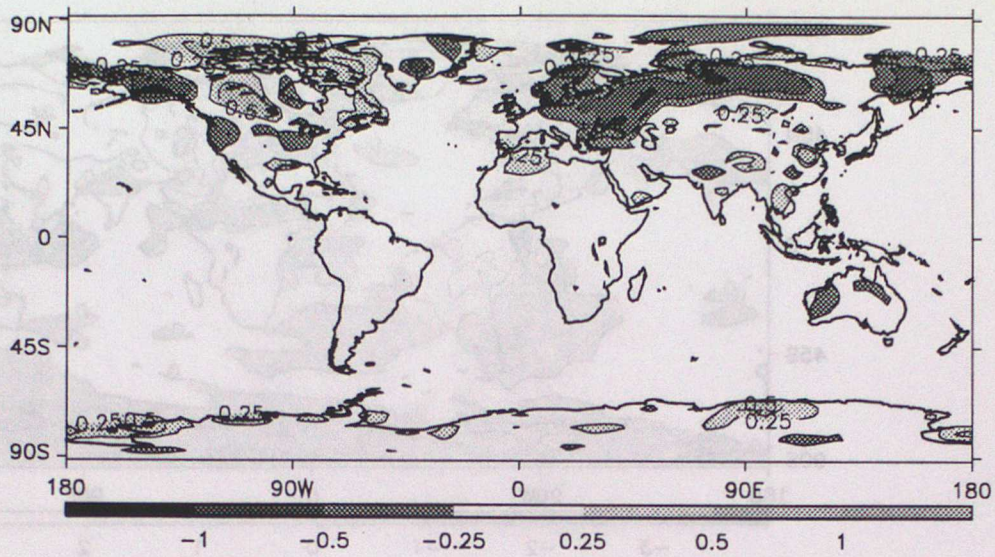

Figure 12b

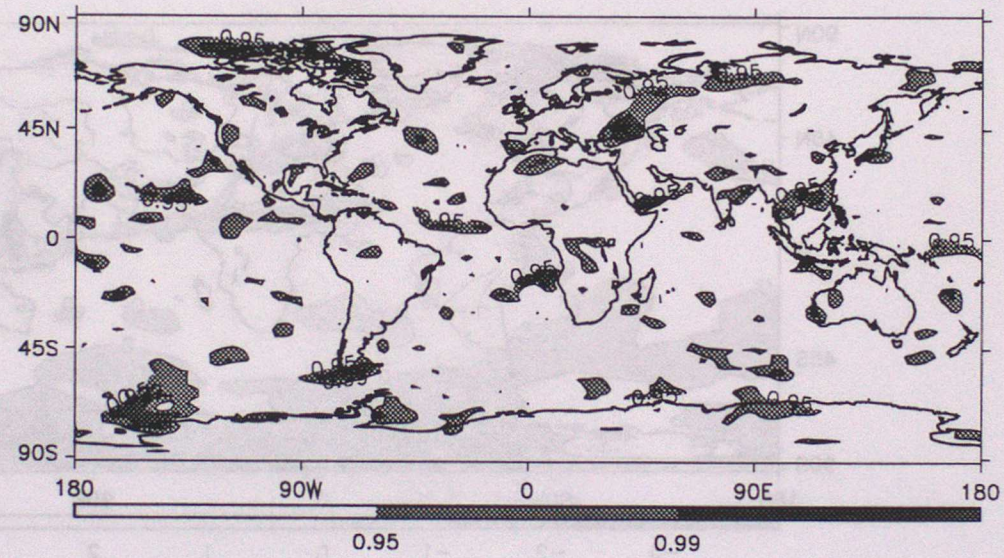

Figure 13

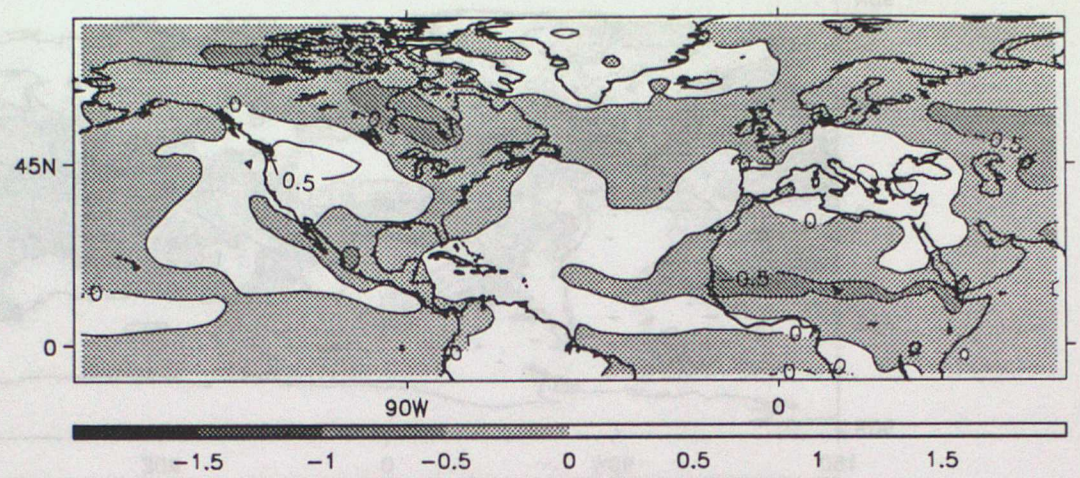

Figure 14

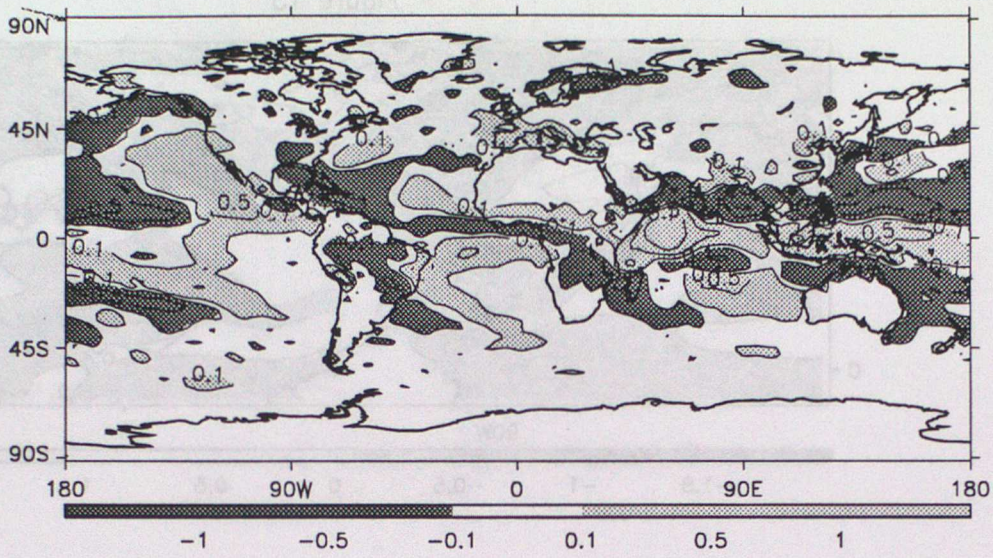

Chapter 3

Simulation of the climate of the Last Glacial Maximum at 21kBP using the UKMO coupled atmosphere - mixed layer ocean model

C. D. Hewitt

1. Introduction

This report describes results from the UK Met. Office (UKMO) simulation of the climate of the Last Glacial Maximum (LGM) 21,000 years before present (21kBP). This experiment is part of the Paleoclimate Modelling Intercomparison Project (PMIP, Joussaume and Taylor, 1995).

The following section (§2) describes the UKMO general circulation model (GCM) and the PMIP experimental design used in the model experiment. Section 3 then presents results from the UKMO model simulation, and includes a comparison with the sea surface temperature (SST) reconstruction of the Climate: Long-Range Investigation, Mapping, and Prediction (CLIMAP) Project (CLIMAP Project Members, 1981), as well as a model-model intercomparison of annual mean temperature response from four European GCMs which are described elsewhere in the EC report -

- the UKMO Unified Model,
- the UK Universities Global Atmospheric Modelling Programme model (UGAMP),
- the Laboratoire de Météorologie Dynamique model versions 4 and 5 (LMD4 and LMD5) used at the Laboratoire de Modélisation du Climat et de l'Environment,
- and the ECMWF model modified for climate studies by the University of Hamburg and the Max-Planck Institute (ECHAM) used for palaeoclimate simulations by the University of Bremen.

2. The Model and Experimental Design

a. The Model

The UKMO atmospheric climate model is coupled to a mixed layer ocean model and a sea-ice model, all at a horizontal grid-resolution of 2.5° by 3.75° . The atmospheric model is version HADAM2b of the unified forecast and climate model (Cullen, 1993) and is similar to version HADAM2 described in Hewitt and Mitchell (1996). The changes made to the model physics between these two versions are described in Hall *et al* (1995). The main differences are a modification of the temperature range of partitioning of mixed-phase clouds, the gravity wave drag scheme includes anisotropy of the orography, trapped lee waves, and a better representation of flow blocking from high drag states,

negative humidities are corrected by borrowing moisture from neighbouring grid-points, and altered coefficients for horizontal diffusion which is used to remove unwanted grid-scale noise and to represent dissipation by unresolved eddies.

The mixed layer ocean model represents the ocean as a 50 m well-mixed layer of water, with a prescribed seasonally varying heat flux C. The rate of change of temperature T of the mixed layer at each grid-point is given by

$$\rho C_P h \partial T/\partial t = C + S \qquad (1)$$

where ρ and C_P are the density and specific heat capacity of sea water respectively, and h is the depth of the mixed layer (50 m). S is the net heat flux from the atmosphere, and C accounts for the transfer of heat in the ocean due to ocean dynamics. C is derived from (1) by diagnosing S from an atmospheric integration where the sea surface temperatures (SSTs) and sea-ice depth are prescribed using climatological values. Note that the heat flux C is the same in the control and anomaly simulations which means that any changes in computed SST are due to changes in S only.

The sea ice model incorporates both the dynamics and thermodynamics of sea-ice, and is a simplified version of that used in the full ocean GCM described in Johns *et al* (1996). The thermodynamic properties are based on the zero-dimensional model of Semtner (1976), and leads are represented based on Hibler (1979). Sea ice forms when the ocean temperature falls below 271.35 K; the top surface temperature of the ice is calculated by the atmosphere model and the temperature of the mixed-layer under the ice is fixed at 271.35 K. A simple parameterization of sea ice dynamics is included, based on Bryan (1969), with the ice thickness, concentration and snow depth advected using a climatology of ocean surface currents.

b. Experimental Design

The model's land distribution and topography, as set up in the control simulation for the present day climate, need to be modified at 21kBP to take into account the lower sea-level and the large continental ice sheets that existed at the Last Glacial Maximum. Peltier's ICE-3G ice sheet reconstruction (Tushingham and Peltier, 1991) has been interpolated to the model grid-points as part of the Paleoclimate Modelling Intercomparison Project (PMIP). This data provides the extra land points exposed as a result of the sea-level lowering, and the orographic heights of the ice sheets. CO_2 concentrations have been lowered at 21kBP by about 29% from their present day concentrations, and the orbital parameters have been calculated from Berger (1978), fixing the Vernal equinox at noon on March 21st , and are listed in table 1. The solar constant is kept fixed at 1365 W m^{-2} .

Table 1: orbital parameters for the control (0kBP) and LGM (21kBP) experiments derived from Berger (1978)

	0kBP	21kBP
Longitude of perihelion (relative to the vernal equinox)	102.5°	114.4°
Obliquity	23.44°	22.95°
Eccentricity	0.0167	0.0190

A "spin up" experiment was performed with the 21kBP forcing described above and initial atmospheric conditions and sea surface temperatures taken from the control simulation. The simulation was run for 16 years to allow the atmosphere-mixed layer ocean-sea ice coupled climate system to reach some sort of equilibrium. A 20 year experiment for 21kBP was then started from the end of the spin up phase. The results presented in the following sections are averages constructed from 20 years of the control and anomaly simulation.

3. Response simulated at Last Glacial Maximum

a) Sea surface temperature

The global mean annual average SST changes simulated by the GCM at the LGM agree reasonably well with the CLIMAP reconstruction (figure 1). The largest regional changes are in the North Atlantic in February and August, which the model successfully qualitatively reproduces. The model also successfully produces a cooling in the North Pacific, and relatively small changes in the Tropics. However, the CLIMAP reconstruction shows a marked warming of the subtropical gyres of the North and South Pacific Ocean, which the model completely fails to produce. Broccoli and Marciniak (1996) found similar disagreement using the GFDL model, but they point out that the SST reconstruction in these regions was made from relatively few sediment cores leaving large areas of the Pacific sparse of data. The CLIMAP reconstruction also shows a warming of the western Indian Ocean. while the GCM shows a cooling. These warm waters may be a result of a change in the ocean currents during the Ice Age (Prell and Kutzbach, 1987) which the simple mixed layer ocean model can not represent. Another major region of model-data discrepancy is the Southern Ocean where the CLIMAP reconstruction shows a cooling

which is not as large in the model, but this may be explained by the possibility that CLIMAP overestimated the extent of glacial age sea ice (Burckle *et al*, 1982).

Finally, the CLIMAP low-latitude SSTs have been the subject of much speculation, with some indicators implying a much larger cooling, for example a 5°C cooling inferred from Barbados corals (Guilderson *et al*, 1995), which is more in line with GCM simulations.

b) Surface air temperature

The global mean warming simulated on doubling CO_2 using this atmosphere/mixed layer ocean model is 2.8 K (Senior, pers. comm.), which would imply that the lowering of CO_2 at 21kBP would be expected to produce a cooling of about -1.4 K compared to the control simulation. The global mean annual average change in insolation at 21kBP compared to 0kBP is close to 0 W m^{-2} , with relatively small regional and seasonal insolation anomalies, and so would not have a large influence on the annual mean temperature change.

The global mean cooling simulated by this model at the LGM is 4.4 K (table 2). The lowering of CO_2 would therefore account for about one-third of this cooling, and the inclusion of the continental ice sheets with their high albedo and high orography produces most of the remainder of the surface cooling. This can readily be seen in figure 2 with the largest cooling in the Northern hemisphere, over land, around the ice sheets. It is worth noting that there is a large sensitivity at high latitudes, which is also seen in $2\times CO_2$ experiments.

The large-scale changes are comparable to the findings from experiments performed with the other GCMs in this project with both computed SSTs and SSTs prescribed from the reconstruction of the CLIMAP Project. All the models produce a larger cooling in the Northern hemisphere than the Southern hemisphere (table 2), and a larger cooling over land than over the ocean. However, the computed SST experiments produce a greater inter-hemispheric difference with an enhanced Northern hemisphere cooling compared to the fixed SST experiments but similar temperature change in the Southern hemisphere, except for the LMD4 model which produces a relatively small cooling of the Northern hemisphere, over both the Northern hemisphere land and Northern hemisphere ocean compared to the other GCMs (not shown in the table. Pinot, pers. comm.), and very small changes over the ocean of both hemispheres. The changes over the Southern hemisphere land, however, are comparable to the other GCMs (not shown in the table). As discussed above, the UKMO GCM simulated SSTs are cooler than the CLIMAP SSTs in

large regions of the North Pacific, and warmer in the Southern Ocean where the sea-ice changes are not as great as CLIMAP indicates - this is also evident in the UGAMP computed SST experiment. The computed SST experiments also produce a greater global mean land-sea contrast, mainly resulting from increased cooling over the Northern hemisphere continents in response to the lower SSTs.

Table 2: annual mean surface air temperature changes between 21kBP and 0kBP, in Kelvin. fix refers to experiments that have prescribed SSTs, and cal refers to computed SST experiments.

	SST	Global	N.Hem.	S.Hem.	Land	Ocean
UKMO	cal	-4.4	-6.5	-2.3	-8.1	-1.7
UGAMP	cal	-3.9	-6.6	-1.3	-7.7	-1.5
LMD4	cal	-2.1	-3.0	-1.2	-4.6	-0.6
UGAMP	fix	-3.9	-5.6	-2.3	-7.7	-1.5
LMD4	fix	-3.3	-3.9	-2.7	-5.4	-1.9
LMD5	fix	-3.4	-4.5	-2.4	-5.2	-2.2
ECHAM	fix	-4.1	-4.6	-3.6	-7.4	-1.7

c) Sea-ice

The high-latitude surface air temperature changes described above produce dramatic changes in the thickness (figure 3) and extent (figure 4) of sea-ice. The Southern hemisphere sea-ice becomes thicker (of the order of 1 m), with the sea-ice edge extending further equatorward, particularly in winter, although the increases are not as large as indicated by the CLIMAP data. The Northern hemisphere sea-ice changes simulated at the LGM are much larger.

Much of the Arctic becomes permanently covered even in summer with sea-ice depths exceeding 15 m, an increase of typically 10 m. A large region of the north-western Pacific becomes partially ice covered in winter, extending equatorwards to about 45°N, as does the Norwegian Sea and most of the north-western sector of the North Atlantic, extending equatorwards along the American coast to about 45°N. Permanent winter sea-ice is evident over the Labrador Sea and north of Iceland. In summer the permanent sea-ice boundary retreats back to the Davis Strait and the Greenland Sea, although the Norwegian Sea and Labrador Sea remain partially ice covered.

The CLIMAP reconstruction and the UGAMP model have more extensive seasonal

sea-ice cover in the North Atlantic, although the CLIMAP reconstruction is a subject of debate in this region. The UGAMP model only attempts to represent the thermodynamics of sea-ice, while the UKMO model has a representation of the thermodynamics and simplified dynamics of sea-ice. The impact of dynamic sea-ice on climate sensitivity has been investigated by using the UKMO atmosphere/mixed-layer ocean model coupled to two different sea-ice models (Senior, pers. comm.) - one model only includes the thermodynamics, and the other is the one used in this study incorporating the dynamics as well. The findings of this study were that the inclusion of sea-ice dynamics improves the present day simulation of sea-ice, and the climate sensitivity to a doubling of CO_2 is reduced. Qualitatively similar results were found in a similar study using the GENESIS model from NCAR (Pollard and Thompson, 1994). This may help to explain the smaller sea-ice response seen in the UKMO results.

The annual cycle of fractional coverage in the Northern hemisphere is shifted forward by about one month with the maximum occurring in February rather than March (figure 5). The fractional coverage is larger over the annual cycle, although the amplitude remains similar. In the Southern hemisphere expansion in Autumn is more rapid and the maximum coverage is larger, but the annual cycle remains largely in phase with the present cycle.

d) Low-level circulation changes

The large-scale mean sea level pressure changes are driven by the surface temperature changes with increases over most of the Northern hemisphere (figure 6), and a compensatory decrease in pressure over the oceanic regions, and large parts of the Southern hemisphere.

In DJF the Icelandic Low is displaced eastwards beyond the sea-ice edge, and the Azores High extends westwards across the entire Atlantic resulting in an increase in the pressure gradient over the North Atlantic, producing stronger flow across the ocean into western Europe (figure 7). The overall effect is to concentrate the North Atlantic winter storm tracks in a narrower band (figure 8), limited in the poleward direction by the baroclinic effects of the temperature gradient associated with the equatorward extension of the sea-ice, and the displacement of the low produces an eastward extension of the storm tracks.

The Azores High is also intensified in JJA which produces a tighter pressure gradient over the equatorial Atlantic, strengthening the north-east trade winds in the region of northern South America and Central America throughout the year (figure 9).

Conversely, the subtropical anticyclone in the South Atlantic is weakened, producing weaker south-east trade winds, the net result being that the convergence zone (the ITCZ) in this region is displaced southwards and weakened, as is the Hadley Circulation. Over the highest parts of the Laurentide and Scandinavian ice sheets there is a strong westerly/north-northwesterly flow.

e) surface hydrology

The annual mean total precipitation averaged over the whole globe decreases by about 10% from 3.19 to 2.89 mm day^{-1} , consistent with the other GCMs in this project which produce reductions ranging from 4% to 9%. Most of this decrease is due to a reduction in convective precipitation along the ITCZ (figure 10a), mainly concentrated over the Amazon Basin (discussed above). The large-scale precipitation changes are dominated by decreases in the regions of the large continental ice sheets (figure 10b).

The weakening and displacement of the ITCZ produce large changes in precipitation minus evaporation (P–E, figure 11), with decreases along the ITCZ and a southeastwards displacement of moisture over the Amazon basin. The end result is a decrease in the model's soil moisture in the Tropics, where convective precipitation dominates over large-scale precipitation, and a large increase in soil moisture content in central South America. In the mid- and high-latitudes, where large-scale precipitation is more important, the P–E decreases, especially on the eastern side of the Laurentide ice sheet and the southern half of Greenland.

Summary

The UKMO GCM produces a global average temperature change of -4.4 K at the LGM, which is comparable to the other GCM simulations in this project. The SST changes are largest in the North Atlantic, consistent with the CLIMAP reconstruction, but the changes in the subtropical Pacific are not consistent with CLIMAP. Sea ice changes are largest in the Arctic with a southward expansion, but the changes are not as large as suggested by CLIMAP.

An intercomparison of annual average temperature changes from the different GCMs reveals that computed SST experiments generally produce larger decreases in the Northern hemisphere and a larger cooling over land than experiments forced with CLIMAP SSTs.

References

Berger, A.L., 1978: Long-term variations of daily insolation and Quaternary climatic changes. *J. Atmos. Sci.*, **35**, 2362-2367.

Broccoli, A.J., and E.P. Marciniak, 1996: Comparing simulated glacial climate and paleodata: A reexamination. *Paleoceanography*, **11**, 3-14.

Bryan, K., 1969: Climate and the ocean circulation. III The ocean model. *Mon. Wea. Rev.*, **97**, 806-827.

Burckle, L.H., D. Robinson, and D. Cooke, 1982: Reappraisal of sea-ice distribution in Atlantic and Pacific sectors of the Southern Ocean at 18,000 yr B.P. *Nature*, **299**, 435-437.

CLIMAP Project Members, 1981: Seasonal reconstruction of the earth's surface at the last glacial maximum. Geological Society of America Map and Chart Series, **MC-36**.

Cullen, M.J.P., 1993: The Unified Forecast/Climate Model. *Met. Mag.*, **122**, 81-94.

Guilderson, T.P., R.G. Fairbanks, and J.L. Rubenstone, 1995: Tropical temperature variations since 20,000 years ago: Modulating interhemispheric climate change. *Science*, **263**, 663-665.

Hall, C.D., R.A. Stratton, and M.L. Gallani, 1995: Climate simulations with the unified model: AMIP runs. *Climate Research Technical Note* **61**, Meteorological Office, Bracknell, U.K.

Hewitt, C.D., and J.F.B. Mitchell, 1996: GCM simulations of the climate of 6kBP: mean changes and inter-decadal variability. *J. Climate* (accepted).

Hibler, W.D., 1979: A dynamic-thermodynamic sea ice model. *Journal of Physical Oceanography*, **9**, 815-846.

Johns, T.C., R.E. Carnell, J.F. Crossley, J.M. Gregory, J.F.B. Mitchell, C.A. Senior, S.F.B. Tett, and R.A. Wood, 1996: The Second Hadley Centre Coupled Ocean-Atmosphere GCM: Model Description, Spinup and Validation. Submitted to *Climate Dyn.*

Joussaume, S., and K.E. Taylor, 1995: Status of the Paleoclimate Modeling Intercomparison Project. *Proceedings of the first international AMIP scientific conference*, Monterrey, USA, **WCRP-92**, 425-430.

Pollard, D. and S.L. Thompson, 1994: Sea-ice dynamics and CO_2 sensitivity in a global climate model. *Atmosphere-Ocean*, **32**, 449-467.

Prell, W.L., and J.E. Kutzbach, 1987. Monsoon variability over the past 150,000 years. *J. Geophys. Res.*, **92**, 8411-8425.

Semtner, A.J., 1976: A model for the thermodynamic growth of sea ice in numerical investigations of climate. *Journal of Physical Oceanography*, **6**, 379-389.

Tushingham, A.M., and W.R. Peltier, 1991: ICE-3G: a new global model of late Pleistocene glaciation based upon geophysical predictions of post-glacial relative sea level change. *J. Geophys. Res.*, **96**, 4497-4523.

Figure Legends

Figure 1: change in SST between 21kBP and 0kBP. Contours every 2.5 K. (a) UKMO GCM February, (b) CLIMAP February, (c) UKMO GCM August, (d) CLIMAP August.

Figure 2: change in annual mean 1.5m temperature between 21kBP and 0kBP simulated by the UKMO GCM. Contours at 0, -1, -2.5, -5, -10, -20, -30 K. LGM model coastlines in black, thick white lines show LGM land-ice, thin white lines show where simulated LGM annual mean sea-ice concentration exceeds 10%.

Figure 3: change in thickness of sea ice between 21kBP and 0kBP simulated by the UKMO GCM. Contours at -1, 0, 0.5, 1, 5, 10 m. (a) DJF, (b) JJA.

Figure 4: fractional coverage of sea-ice simulated by the UKMO GCM. Contours at 0.1, 0.2, 0.5, 0.7, 0.9 %. (a) DJF 0kBP, (b) DJF 21kBP, (c) JJA 0kBP, (d) JJA 21kBP.

Figure 5: monthly mean fractional coverage of sea-ice simulated by the UKMO GCM, averaged over non-land points from (a) 45°N to 90°N, (b) 45°S to 90°S.

Figure 6: pressure at mean sea level simulated by the UKMO GCM. Contours every 4 mb (hPa), heavy shading above 1020 mb, light shading below 1000 mb. Thick black outline shows land-ice, medium black outline shows sea-ice, and thin black outline shows coastlines. (a) DJF 0kBP, (b) DJF 21kBP, (c) JJA 0kBP, (d) JJA 21kBP.

Figure 7: low-level wind (model level 4, $\sigma = 0.8698$) in DJF, contours every 5 m s^{-1}, shaded above 10 m s^{-1}. (a) 0kBP, (b) 21kBP.

Figure 8: band pass filtered 500 mb (hPa) geopotential height simulated by the UKMO GCM in DJF. Contours every 1 dm, shaded above 4 dm. (a) 0kBP, (b) 21kBP.

Figure 9: as figure 7 but for JJA.

Figure 10: changes in components of precipitation between 21kBP and 0kBP simulated by the UKMO GCM. Decreases shaded. (a) Convective precipitation, contours at 0, $\pm$1, 2, 5 mm day^{-1}, (b) large-scale precipitation, contours at 0, $\pm$0.5, 1, 2 mm day^{-1}.

Figure 11: change in precipitation-evaporation between 21kBP and 0kBP simulated by the UKMO GCM. Contours at 0, $\pm$ 0.5, 1, 2, 5 mm day^{-1}, decreases shaded.

Figure 1a

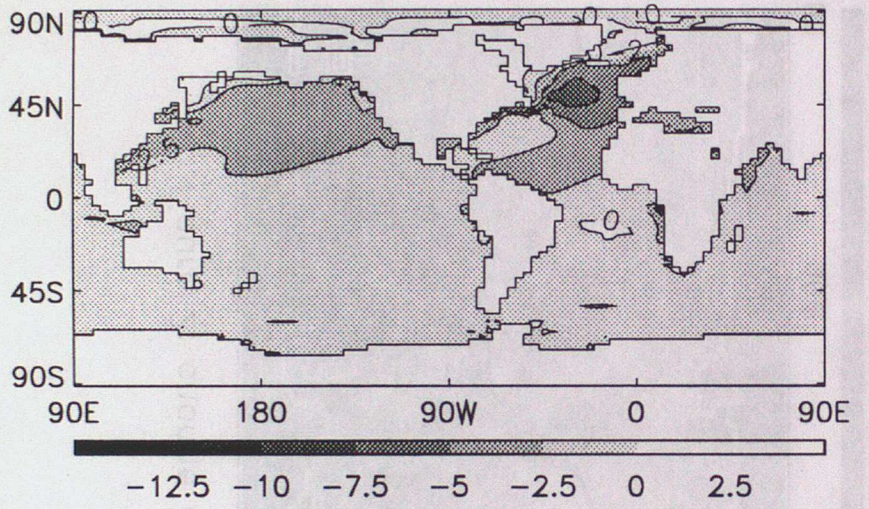

Figure 1b

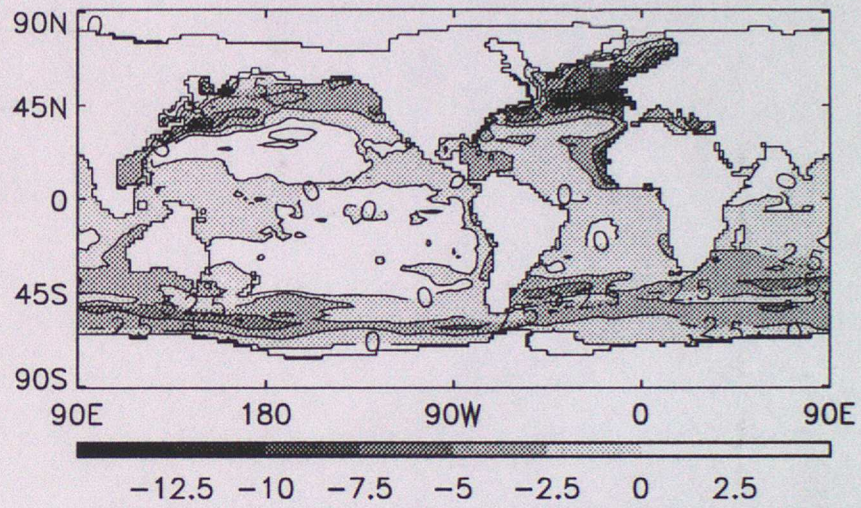

Figure 1c

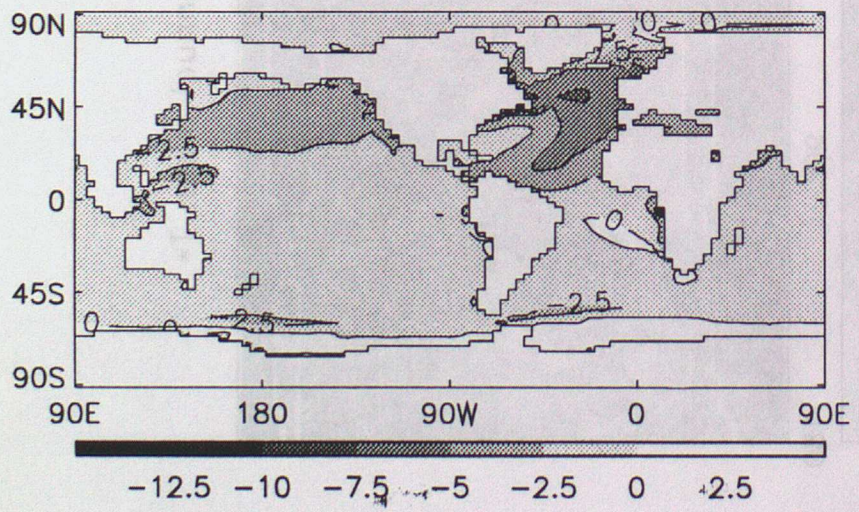

Figure 1d

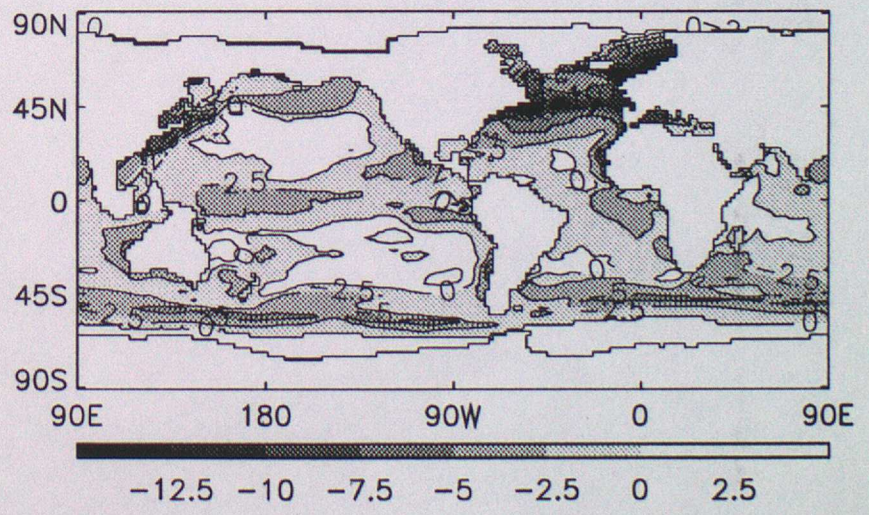

Figure 2: change in UKMO annual mean T*

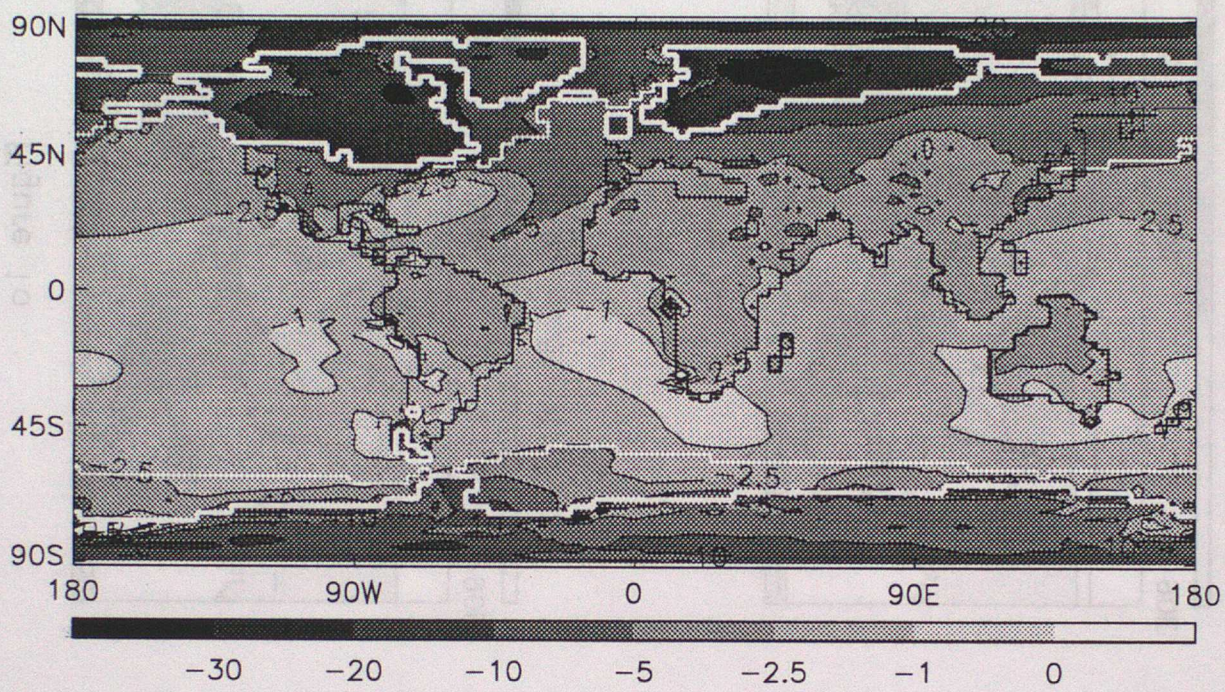

Figure 3a: change in sea–ice depth for DJF

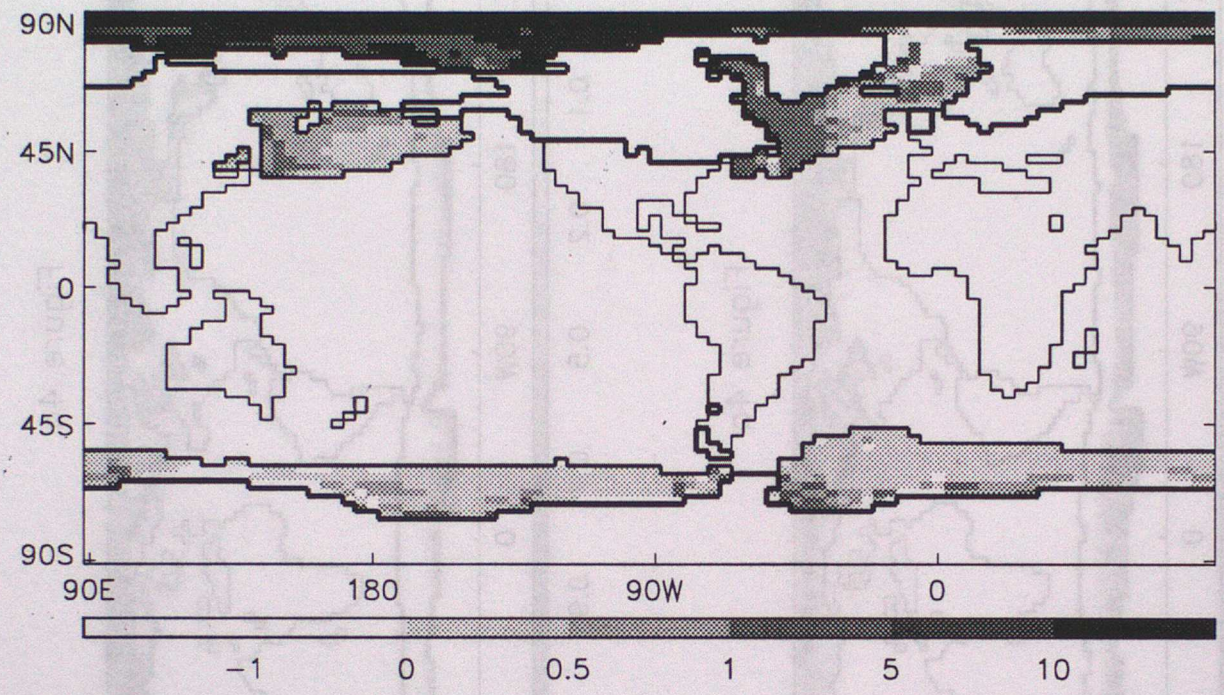

Figure 3b: change in sea–ice depth for JJA

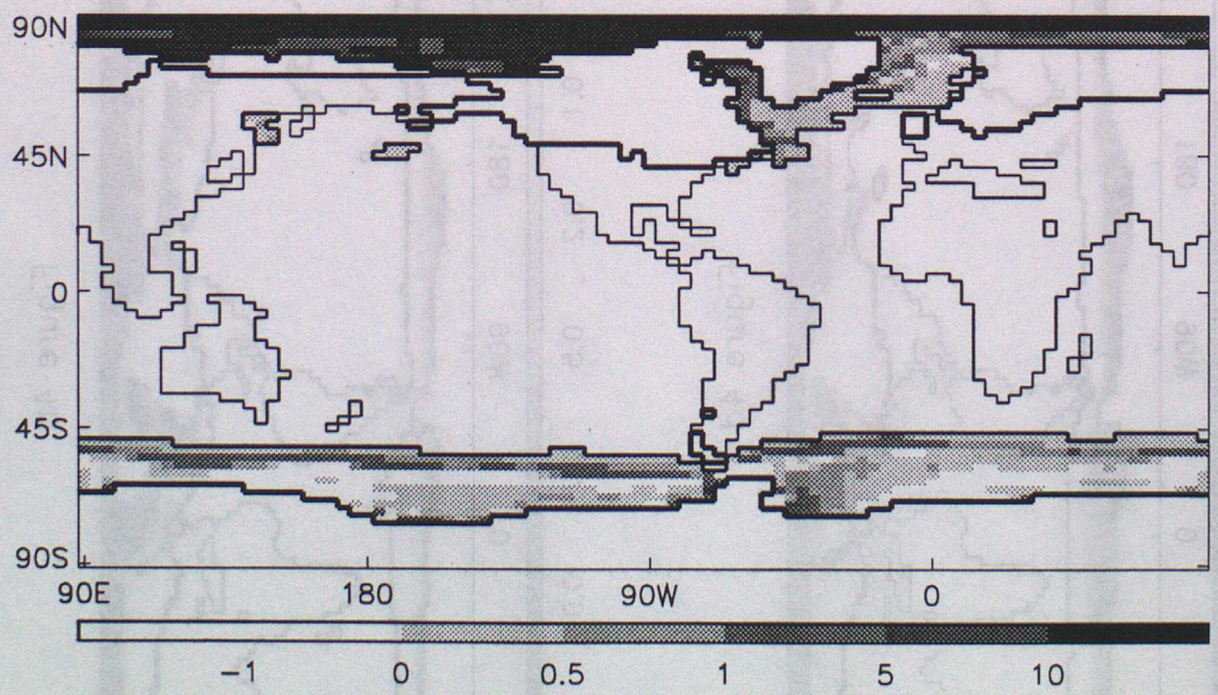

Figure 4a

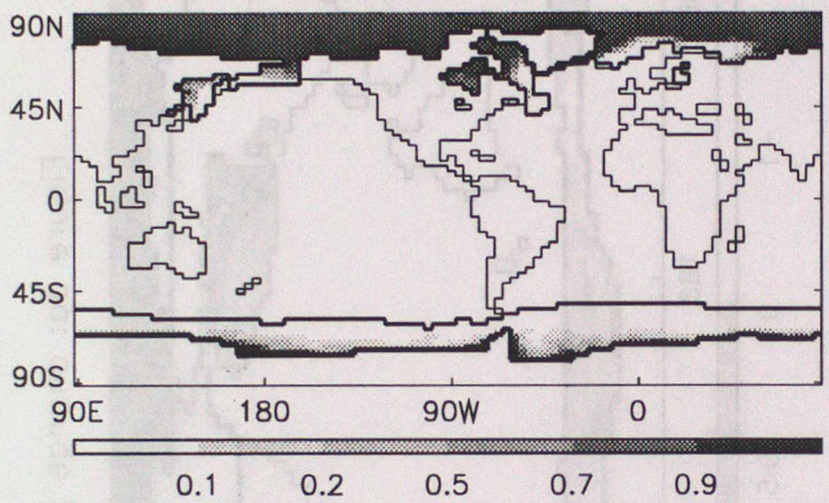

Figure 4b

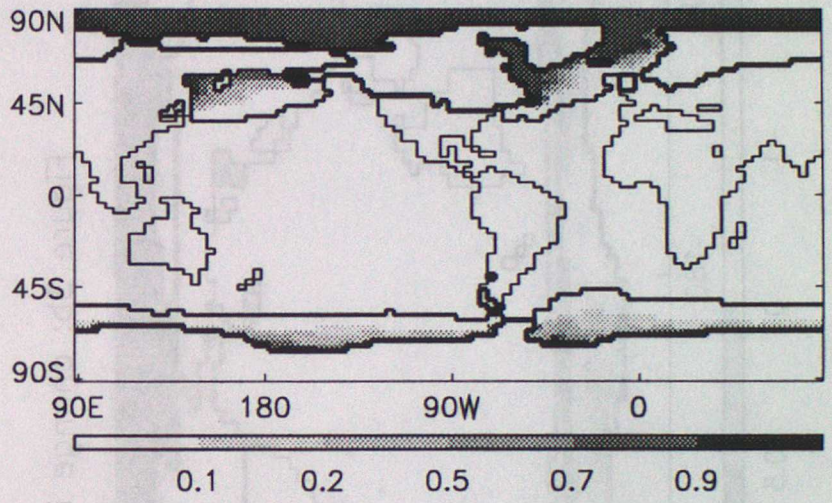

Figure 4c

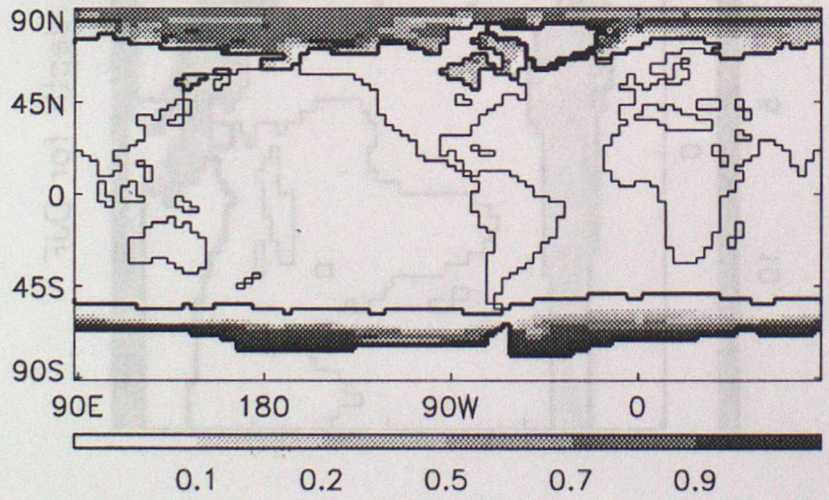

Figure 4d

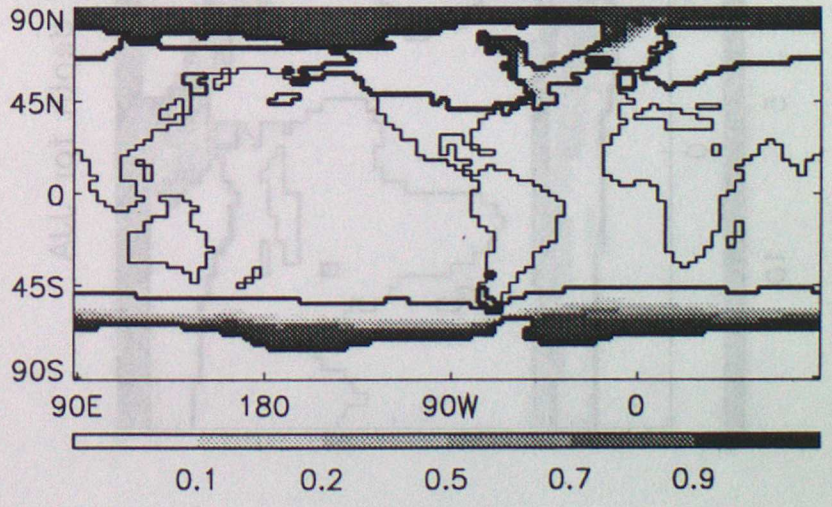

Figure 5a: Sea Ice Fraction averaged from 45N to 90N

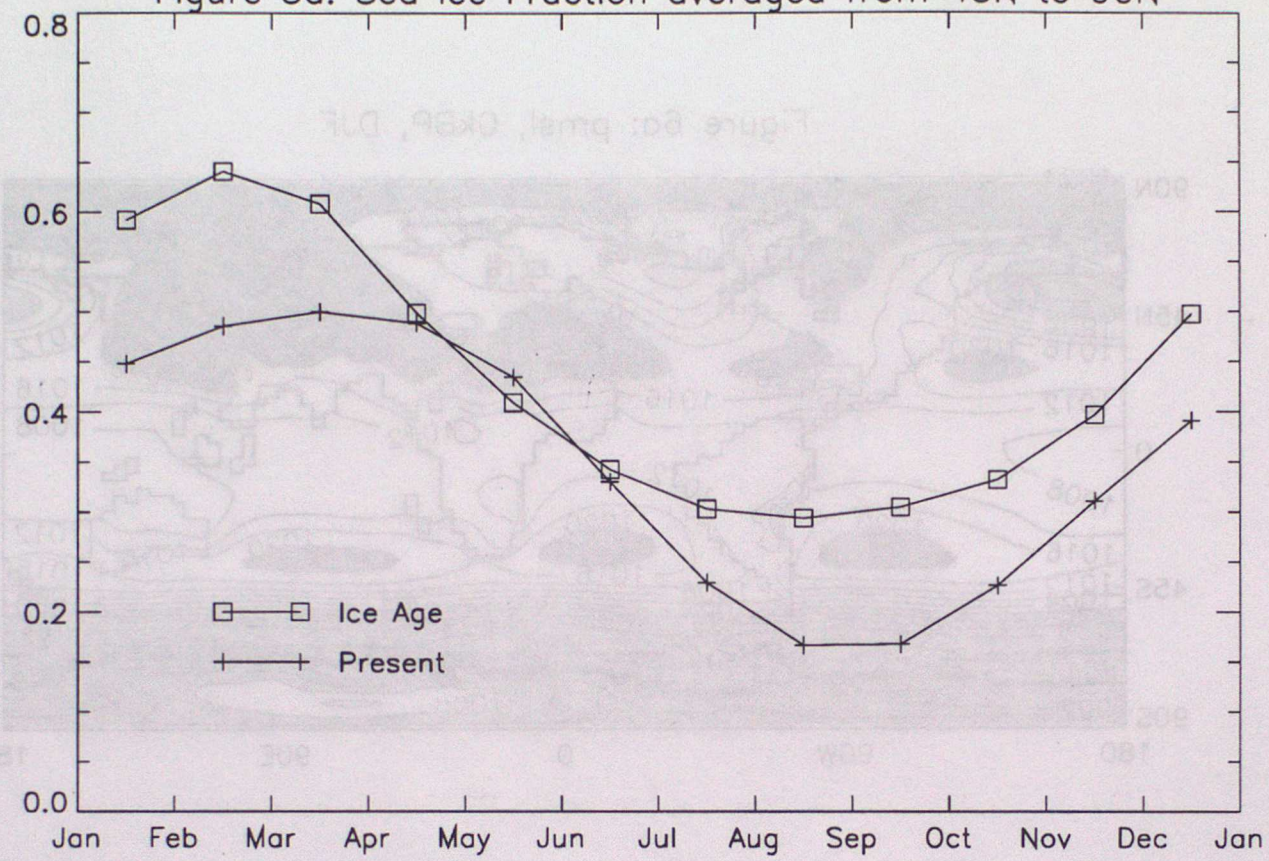

Figure 5b: Sea Ice Fraction averaged from 45S to 90S

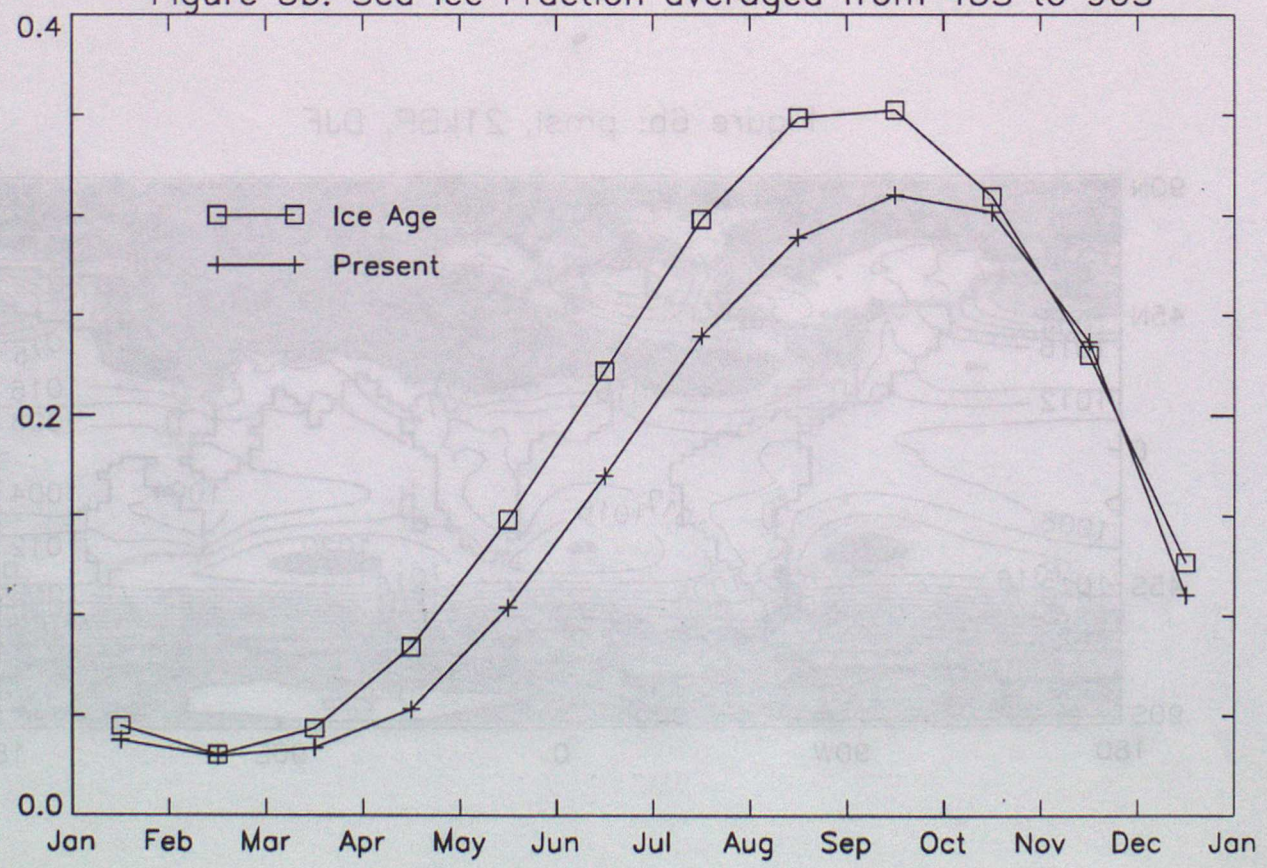

Figure 6a: pmsl, 0kBP, DJF

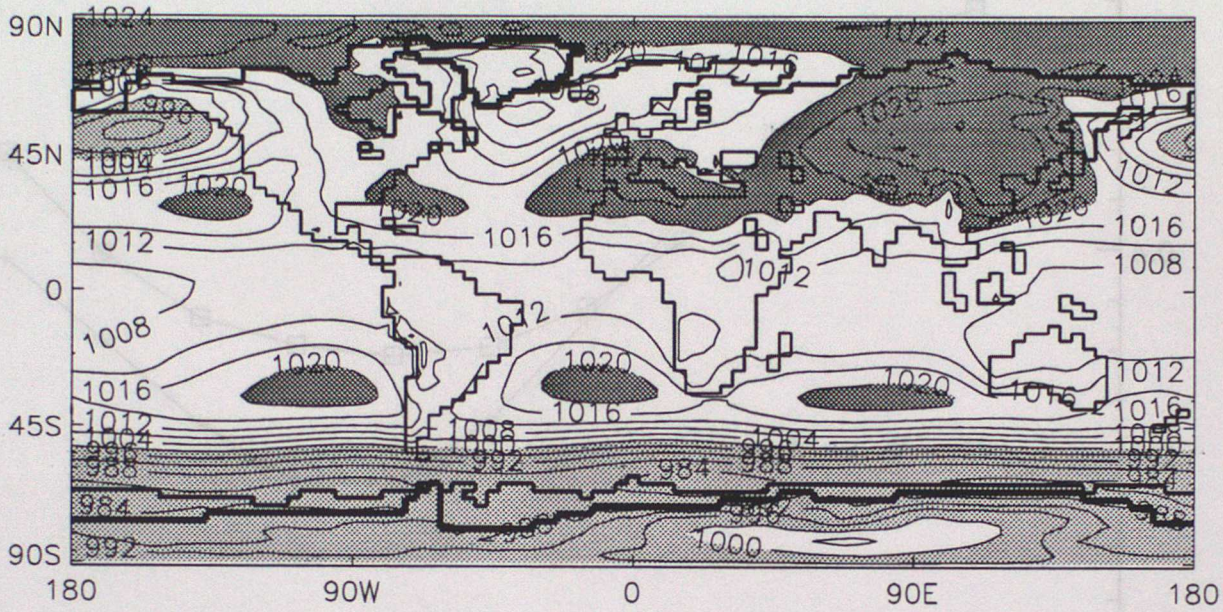

Figure 6b: pmsl, 21kBP, DJF

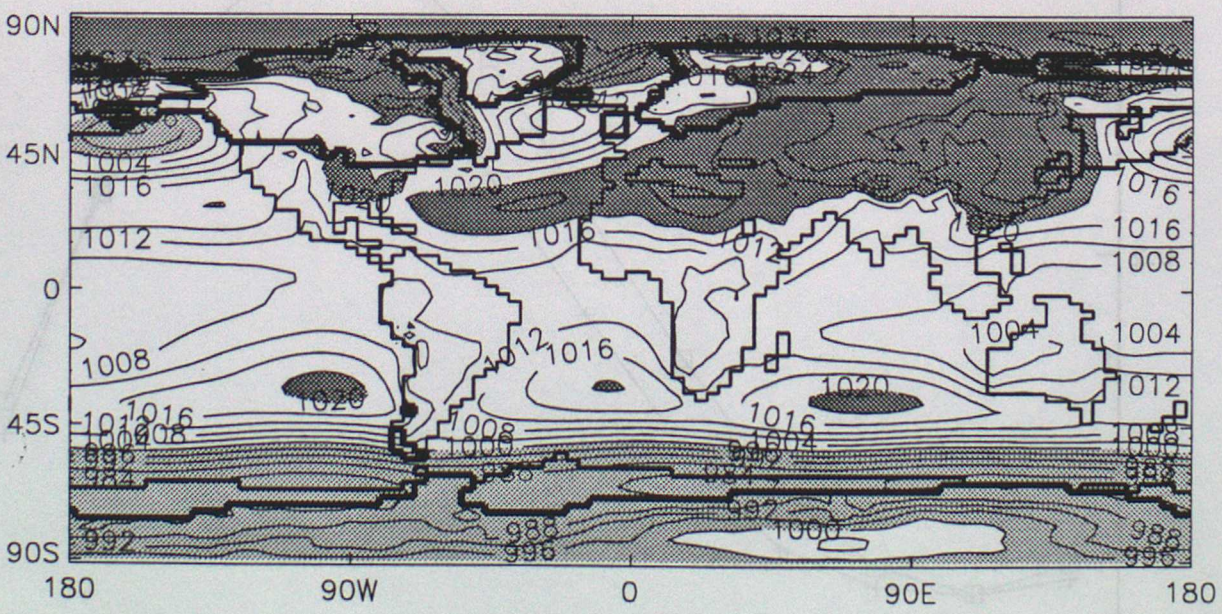

Figure 6c: pmsl, 0kBP, JJA

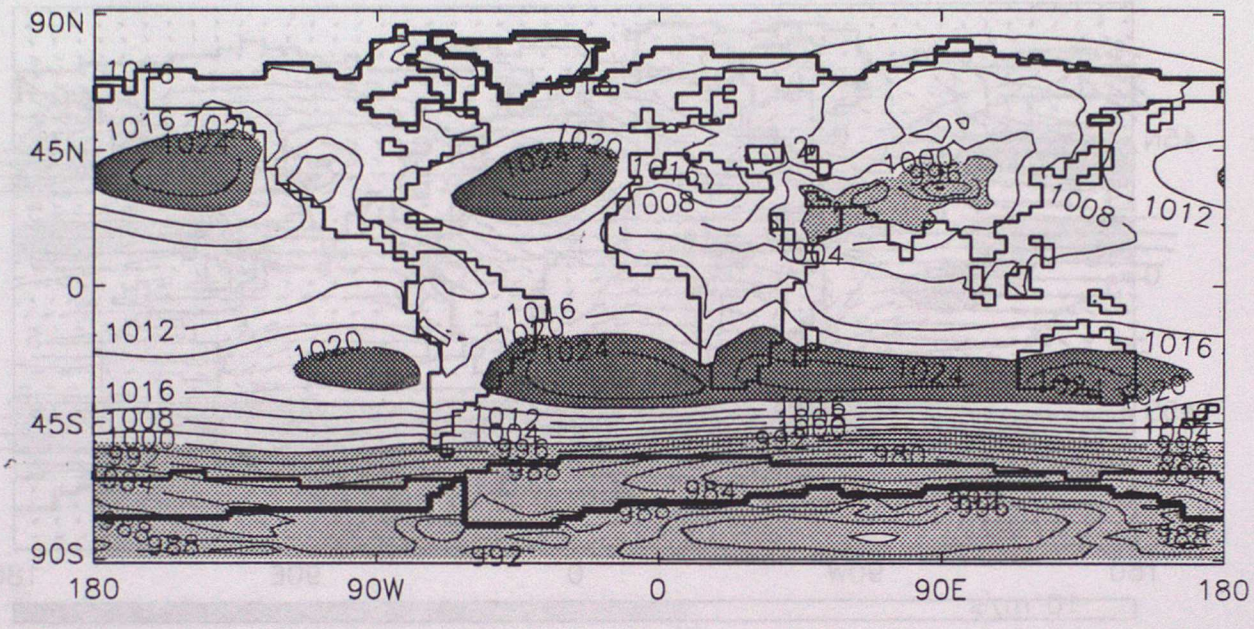

Figure 6d: pmsl, 21kBP, JJA

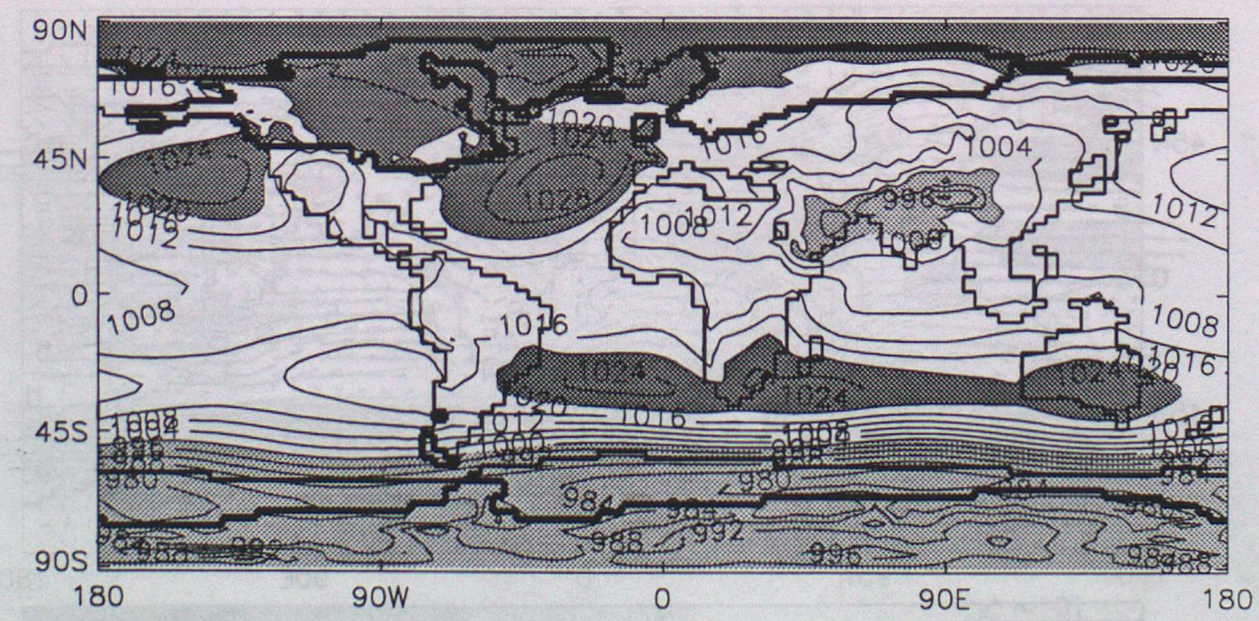

Figure 7a: wind, 0kBP, DJF

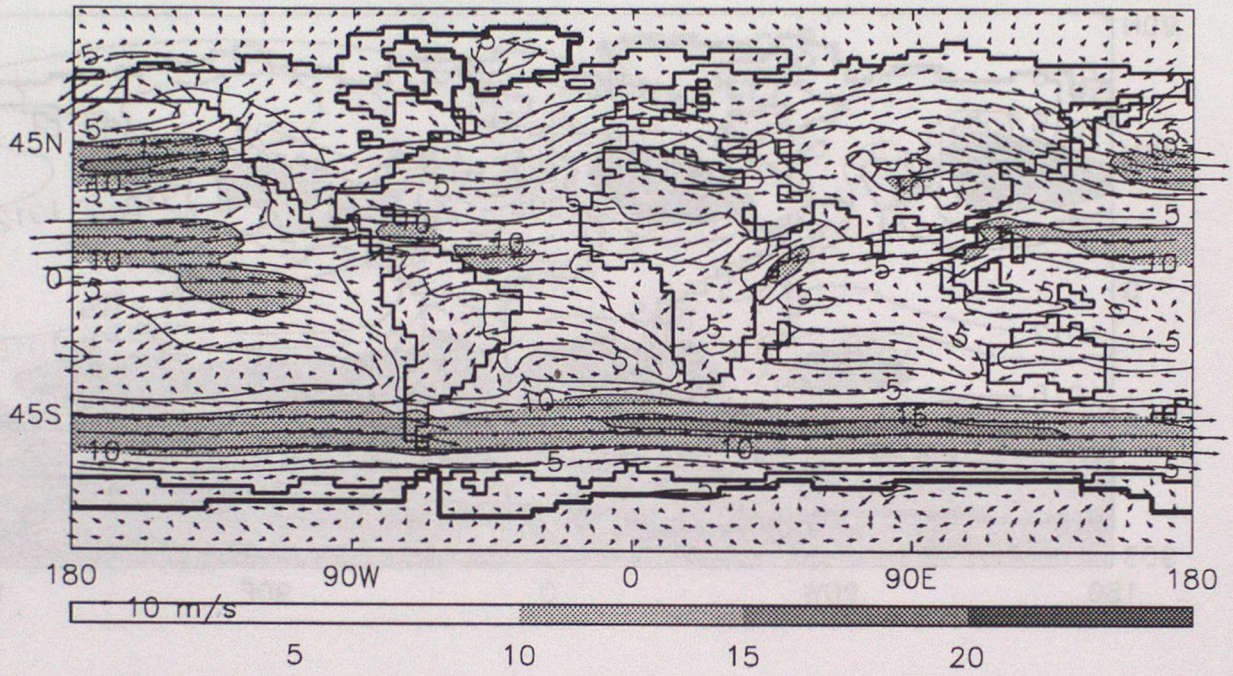

Figure 7b: wind, 21kBP, DJF

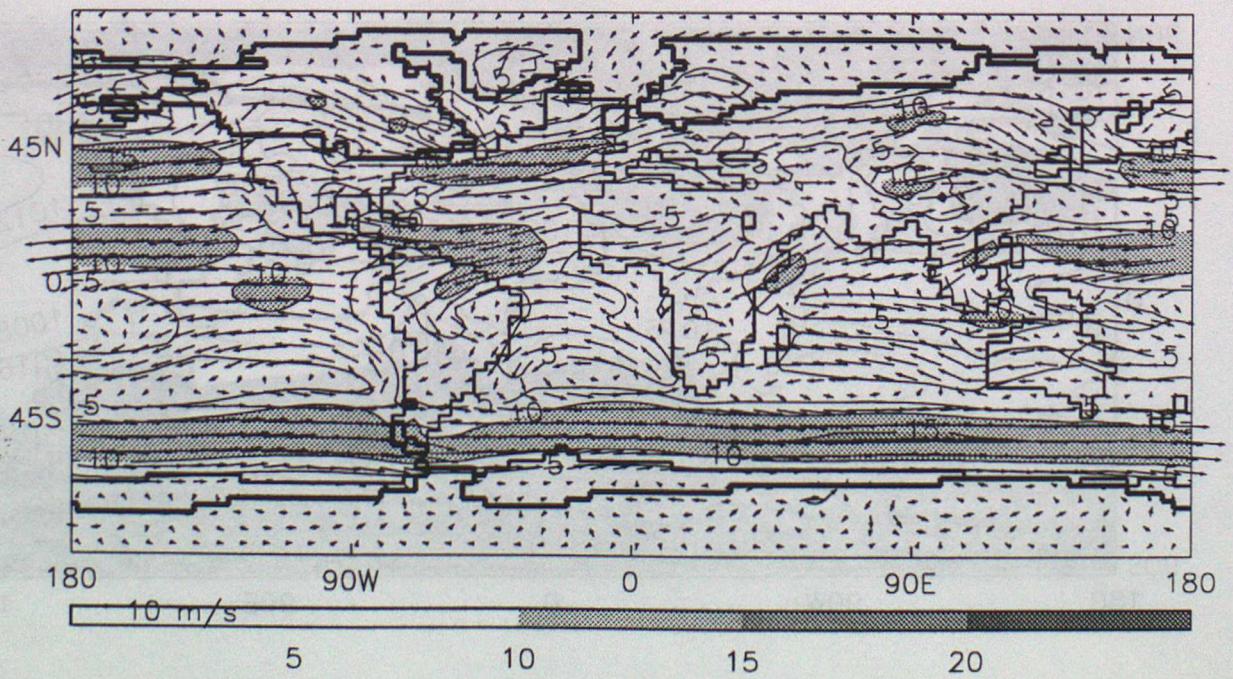

Figure 8a: 0kBP DJF

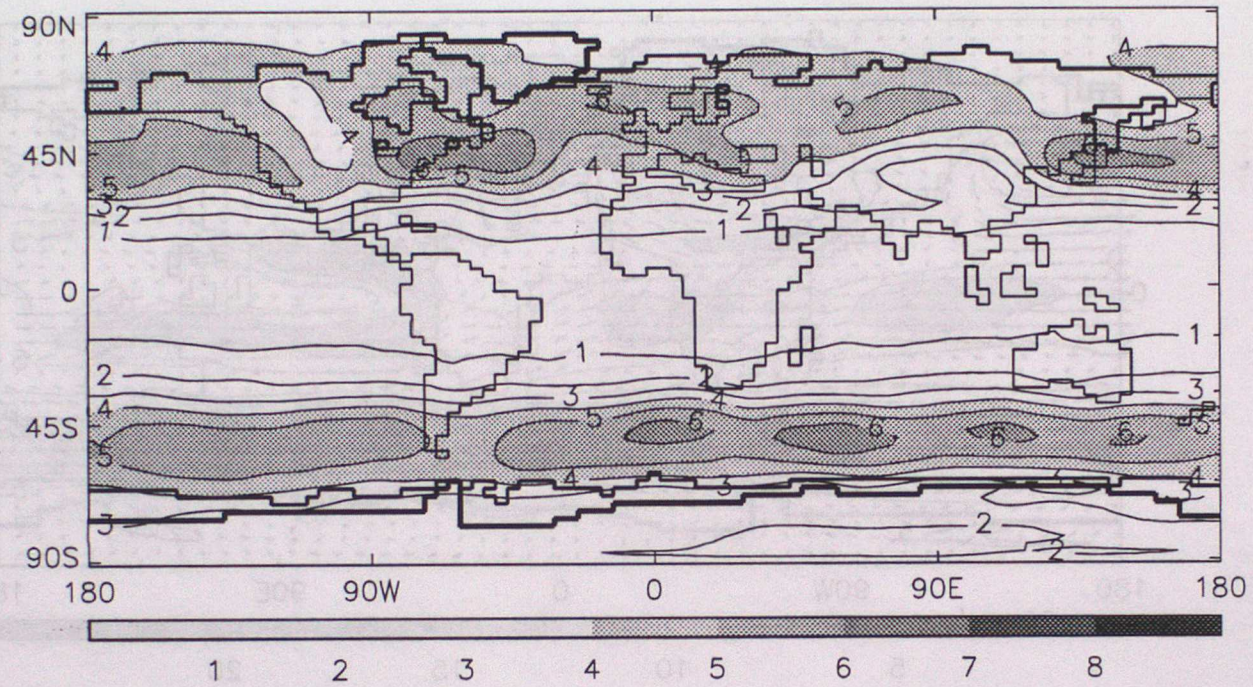

Figure 8b: 21kBP DJF

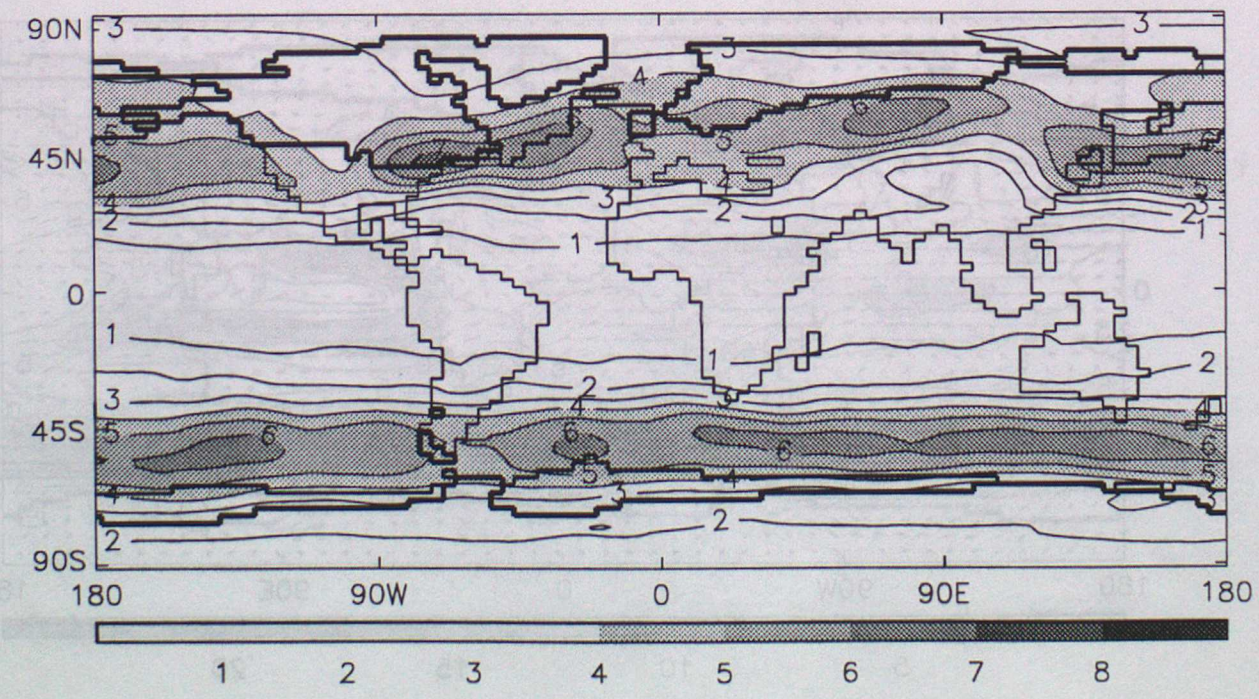

Figure 9a: wind, 0kBP, JJA

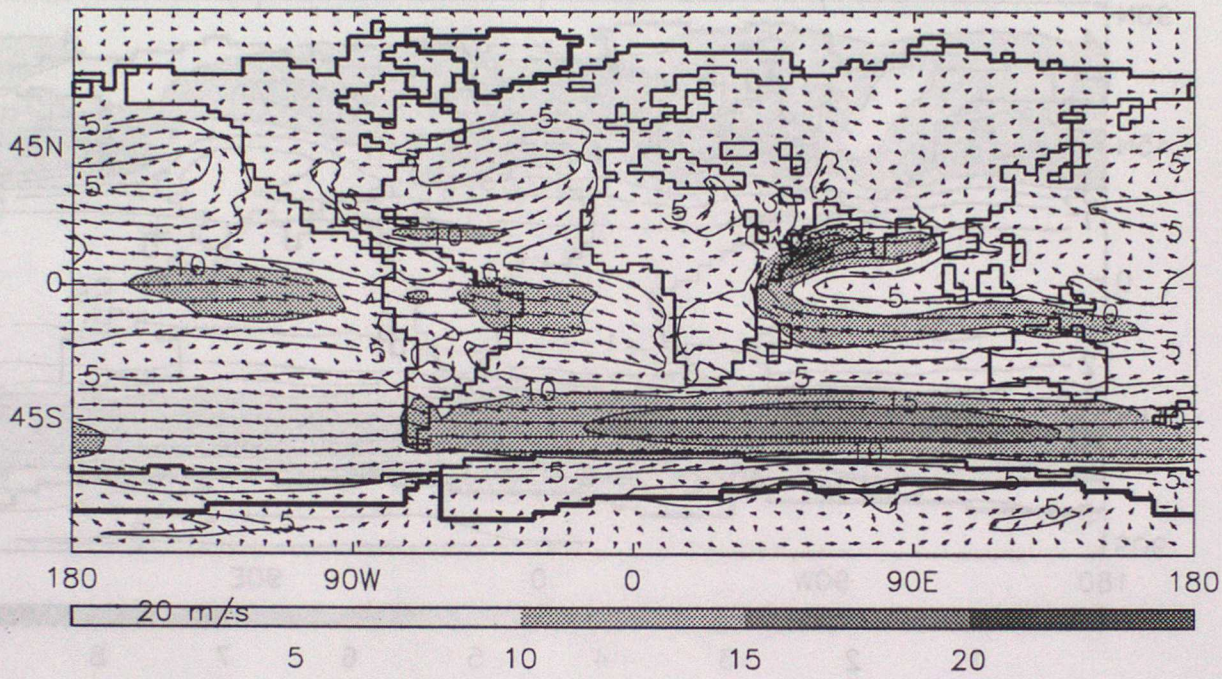

Figure 9b: wind, 21kBP, JJA

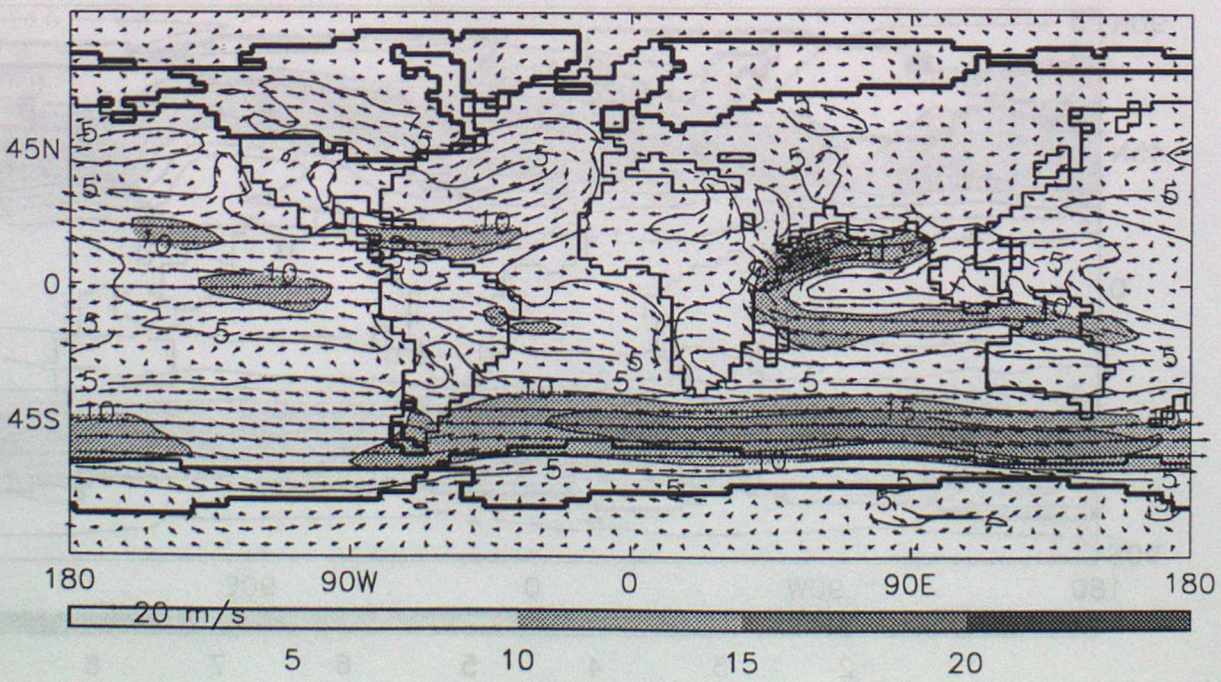

Figure 10a: change in convective precipitation

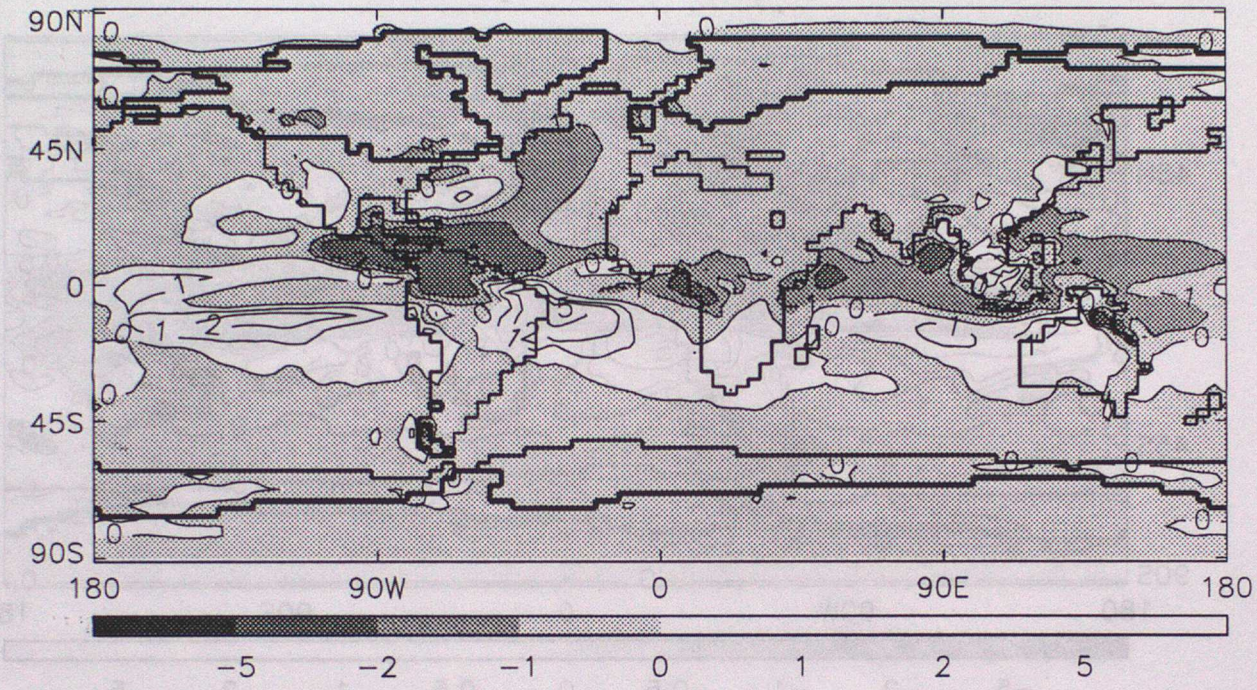

Figure 10b: change in large−scale precipitation

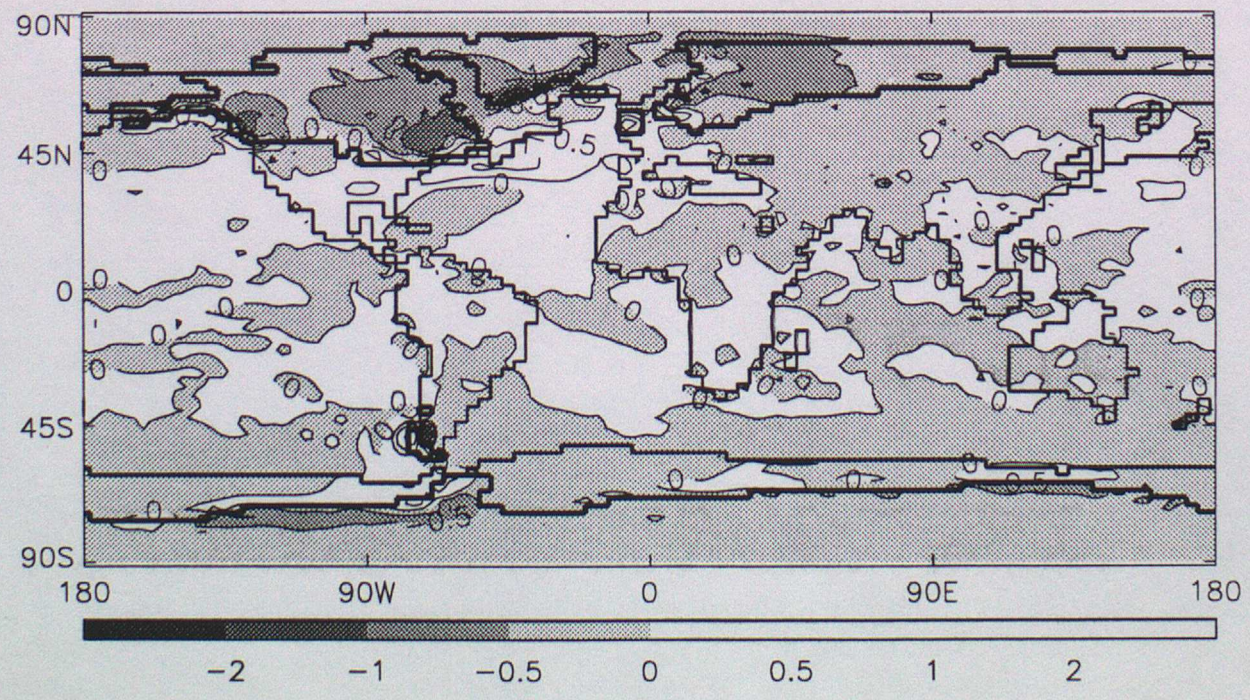

Figure 11: change in P−E

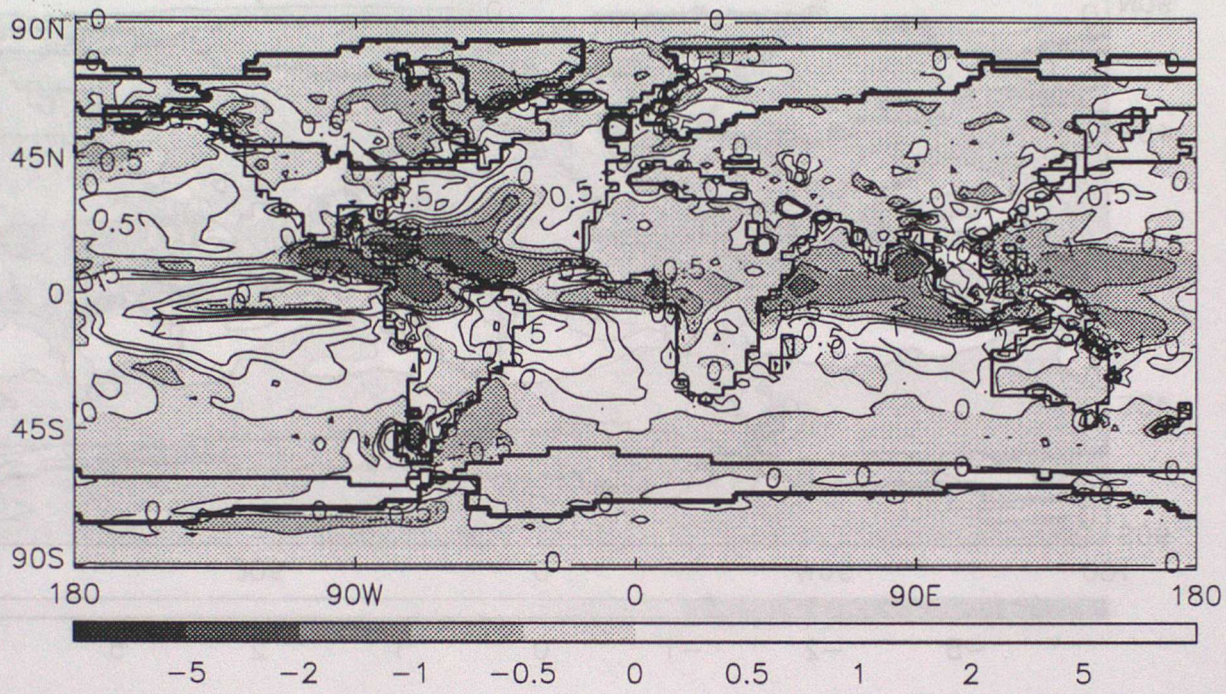

CLIMATE RESEARCH TECHNICAL NOTES

CRTN 1	Oct 1990	Estimates of the sensitivity of climate to vegetation changes using the Penman-Monteith equation. P R Rowntree
CRTN 2	Oct 1990	An ocean general circulation model of the Indian Ocean for hindcasting studies. D J Carrington
CRTN 3	Oct 1990	Simulation of the tropical diurnal cycle in a climate model. D P Rowell
CRTN 4	Oct 1990	Low frequency variability of the oceans. C K Folland, A Colman, D E Parker and A Bevan
CRTN 5	Dec 1990	A comparison of 11-level General Circulation Model Simulations with observations in the East Sahel. K Maskell
CRTN 6	Dec 1990	Climate Change Prediction. J F B Mitchell and Qing-cun Zeng
CRTN 7	Jan 1991	Deforestation of Amazonia - modelling the effects of albedo change. M F Mylne and P R Rowntree
CRTN 8	Jan 1991	The role of observations in climate prediction and research. D J Carson
CRTN 9	Mar 1991	The greenhouse effect and its likely consequences for climate change. D J Carson
CRTN 10	Apr 1991	Use of wind stresses from operational N.W.P. models to force an O.G.C.M. of the Indian Ocean. D J Carrington
CRTN 11	Jun 1991	A new daily Central England Temperature series, 1772-1991. D E Parker, T P Legg and C K Folland
CRTN 12	Jul 1991	Causes and predictability of Sahel rainfall variability. D P Rowell, C K Folland, K Maskell, J A Owen, M N Ward

CLIMATE RESEARCH TECHNICAL NOTES

CRTN 13	Jul 1991	Modelling changes in climate due to enhanced CO2, the role of atmospheric dynamics, cloud and moisture. C A Senior, J F B Mitchell, H Le Treut and Z-X Li
CRTN 14	Sep 1991	Sea temperature bucket models used to correct historical SST data in the Meteorological Office. C K Folland
CRTN 15	Aug 1991	Modelling climate change, and some potential effects on agriculture in the U.K. P R Rowntree, B A Callander and J Cochrane
CRTN 16	Aug 1991	The Boreal Forests and Climate G Thomas and P R Rowntree
CRTN 17	Aug 1991	Development of a Stratosphere-Troposphere Data Assimilation System. R Swinbank.
CRTN 18	Sep 1991	A study of asynchronous coupling using a simple climate model. M K Davey.
CRTN 19	Sep 1991	The Oceanic Carbon Cycle. N K Taylor
CRTN 20	Nov 1991	Worldwide ocean-atmosphere surface fields in Sahel wet and dry years using provisionally corrected surface wind data. M N Ward
CRTN 21	Dec 1991	Coupled tropical ocean global atmosphere models at the UKMO. M K Davey, C Gordon, S Ineson and S Lawrence
CRTN 22	Dec 1991	Empirical parameterisation of tropical ocean-atmosphere coupling. M Allen, M K Davey, D L T Anderson and P D Killworth
CRTN 23	Feb 1992	The temporal evolution of Equatorial Currents in the Indian Ocean D L T Anderson, D J Carrington, R A Corry and C Gordon
CRTN 24	Feb 1992	Stratospheric analyses provided by the U.K. Meteorological Office M J Bailey, A O'Neill and V D Pope

CLIMATE RESEARCH TECHNICAL NOTES

CRTN 25	Feb 1992	Modelling interannual variability in the Indian Ocean using momentum fluxes from the UKMO and ECMWF operational weather analyses. D L T Anderson and D J Carrington
CRTN 26	Mar 1992	A GCM simulation of the impact of Amazonian deforestation on climate using an improved canopy representation J Lean and P R Rowntree
CRTN 27	Mar 1992	The parameterization of rainfall interception in GCMs A J Dolman and D Gregory
CRTN 28	Jun 1992	Development of worldwide marine data eigenvectors since 1985 A W Colman
CRTN 29	Jun 1992	A tropical ocean model with reduced physics M K Davey
CRTN 30	Jun 1992	International Temperature Workshop, Boulder, Colorado, USA, 16 January 1992 Edited by D E Parker
CRTN 31	Jul 1992	Simulation of clear-sky outgoing longwave radiation over the oceans using operational analyses A Slingo and M J Webb
CRTN 32	Sep 1992	A prediction of the transient response of climate J M Murphy
CRTN 33	Nov 1992	LEPS scores for assessing climate model simulations and long-range forecasts. C K Folland
CRTN 34	Jan 1993	Stratospheric Data Assimilation System Guide Editer: R Swinbank
CRTN 35	Mar 1993	A Stratosphere-Troposphere Data Assimilation System R Swinbank and A O'Neill
CRTN 36	Mar 1993	Validation of hydrological schemes for climate models against catchment data. P R Rowntree and J Lean

CLIMATE RESEARCH TECHNICAL NOTES

CRTN 37	Apr 1993	Modelling of palaeoclimates: Examples from the recent past J F B Mitchell
CRTN 38	May 1993	A simulation of seasonality in ENSO forecast skill M K Davey, D L T Anderson and S Lawrence
CRTN 39	Jul 1993	ENSO Prediction experiments using a simple ocean-atmosphere model D-H Wu, D L T Anderson and M K Davey
CRTN 40	Sep 1993	Diagnosis of dynamic sea-surface and sea-level changes from the Cox ocean model J M Gregory
CRTN 41	Sep 1993	Seasonal variations of the clear-sky greenhouse effect: the role of changes in atmospheric temperatures and humidities M J Webb, A Slingo and G L Stephens
CRTN 42	Nov 1993	Sea-level changes under increasing atmospheric CO_2 in a transient coupled ocean-atmosphere GCM experiment. J M Gregory
CRTN 43	Dec 1993	Global and regional patterns of climate change: recent predictions for the Arctic P R Rowntree
CRTN 44	Feb 1994	The effect of changing horizontal diffusion in the atmospheric version of the unified climate model C D Hall and R A Stratton
CRTN 45	Mar 1994	Simulation of El-Niño/Southern Oscillation like variability in a global AOGCM and its response to CO_2 increase. S F B Tett
CRTN 46	Apr 1994	Global data required for monitoring climate change. D E Parker and C K Folland
CRTN 47	May 1994	Seasonal uptake of anthropogenic CO_2 in an ocean general circulation model. N K Taylor

CLIMATE RESEARCH TECHNICAL NOTES

CRTN 48	Jun 1994	A tropic-wide oscillation of boreal summer rainfall and patterns of sea-surface temperature. M N Ward, K Maskell, C K Folland, D P Rowell and R Washington
CRTN 49	Jun 1994	Simulation of the tropical Pacific using a simplified ocean model M A Balmaseda, D L T Anderson and M K Davey
CRTN 50	Sep 1994	Simulation of global mean temperature using a box-diffusion climate model P R Rowntree
CRTN 51	Sep 1994	Seasonal dependence of ENSO prediction skill M A Balmaseda, M K Davey and D L T Anderson
CRTN 52	Nov 1994	Simulation of the Indian Monsoon and Tropical Intraseasonal Variability by a General Circulation Model P M Inness and D Gregory
CRTN 53	Mar 1995	A comparison of modelled surface fluxes with climatological estimates. C Gordon and D K Wright
CRTN 54	Mar 1995	The representation of moist convection in atmospheric models. D Gregory
CRTN 55	Mar 1995	A consistent treatment of the evaporation of rain and snow for use in large-scale models D Gregory
CRTN 56	Apr 1995	Workshop on simulations of the Climate of the Twentieth Century using GISST, 28-30 November 1994, Hadley Centre, Bracknell, UK Edited by C K Folland and D P Rowell
CRTN 57	May 1995	Enhanced shortwave cloud radiative forcing due to anthropogenic aerosols. S E Swartz and A Slingo
CRTN 58	May 1995	The simulation of the tropical oceans in models of different horizontal resolution. C Gordon, D K Wright and C M Roberts
CRTN 59	Sep 1995	The water budget of middle latitude continental regions - a modelling and observational study P R Rowntree
CRTN 60	Sep 1995	Intraseasonal variability of the Indian summer monsoon simulated by the Hadley Centre climate model K Ashok, D Gregory and P M Inness

CLIMATE RESEARCH TECHNICAL NOTES

CRTN 61	Sep 1995	Climate simulations with the Unified Model: AMIP runs C D Hall, R A Stratton and M L Gallani
CRTN 62	Nov 1995	Validation of surface parameters over the oceans in climate simulations with the unified model. C D Hall
CRTN 63	Dec 1995	The GISST2.2 sea surface temperature and sea-ice climatology D E Parker, M Jackson and E B Horton
CRTN 64	Dec 1995	Parametrization of momentum transport by convection. II: Tests in single column and general circulation models. D Gregory, R Kershaw and P M Inness
CRTN 65	Jan 1996	Understanding the sensitivity of a GCM simulation of Amazonian deforestation to the specification of vegetation and soil characteristics. J Lean and P R Rowntree
CRTN 66	Jan 1996	On the efficient calculation of infra-red fluxes and cooling rates using the two-stream equations. J M Edwards
CRTN 67	Jan 1996	The second Hadley Centre coupled ocean-atmosphere GCM: Model description, spinup and validation. TC Johns,RE Carnell,JF Crossley,JM Gregory, JFB Mitchell,CA Senior,SFB Tett and RA Wood
CRTN 68	Feb 1996	The sensitivity of climate simulations to the specification of mixed phase clouds D Gregory and D Morris
CRTN 69	Apr 1996	Using an ensemble of Multi-Decadal GCM simulations ro assess potential seasonal predictability D P Rowell
CRTN 70	May 1996	North Atlantic and European Seasonal Predictability using an Ensemble of Multi-Decadal AGCM Simulations J R Davies, D P Rowell and C K Folland
CRTN 71	Jun 1996	A description of the Second Hadley Centre Coupled Model (HADCM2) T C Johns
CRTN 72	Jul 1996	Palaeoclimate Modelling Intercomparison: UKMO GCM simulations for 6kBP and 21kBP C D Hewitt and J F B Mitchell